University of Naples “Federico II”

Department of Chemical Sciences

Doctoral Thesis

Investigation on protein aggregation in natural and artificial models

Federica Donnarumma

Tutor: Prof. Delia Picone

Advisor: Prof. Renata Piccoli

XXIX cycle - 2014/2017

Contents

List of Abbreviations

3D-DS: 3-dimensional domain swapping

AFM: Atomic Force Microscopy

AMP: ampicillin

carboPt: carboplatin

cisPt: cisplatin

CD: circular dichroism

CDDP: *cis*-diamminedichloroplatinum(II)

DSS: 2,2-dimethyl-2-silapentene- 5-sulfonate sodium

DTT: dithiothreitol

FPLC: Fast Performance Liquid Chromatography

FT-IR: Fourier-Trasform Infrared *(spectroscopy)*

H/D: Hydrogen/Deuterium *(exchange)*

HSQC: Heteronuclear Single Quantum Correlation

IPTG: isopropil-β-D-1-tiogalattopiranoside

KAN: kanamicine

LB: Luria-Bertani medium

NMR: Nuclear Magnetic Resonance *(spectroscopy)*

oxaPt: oxaliplatin

PAGE: poly-acrylamide gel electrophoresis

RNase A: bovine pancreatic ribonuclease

RNase A-Onc: bovine pancreatic ribonuclease-onconase

SDS: sodium dodecyl sulphate

Tm: Temperature of melting

Preface

Protein aggregation is a very fascinating topic concerning the behaviour of proteins that can form high molecular structures either spontaneously or artificially, when the environmental conditions are modified. The smallest structural unit from which take origin an aggregate, called protomer, can assemble in supramolecular structures, which are sometimes selected by nature *ab initio*, or often built up as a response to natural or non-natural events. Anyway, in both cases oligomers can follow different fates. They can be highly stable, mainly when formed by irreversible phenomena, or can represent metastable or even transient events, thus undergoing fast or slow dissociation. Covalently linked oligomers are the most stable supra-molecular protein structures. The majority of protein oligomers forms through non-covalent associations, which can often lead to metastable dimers or oligomers. Their lability is essentially related to the nature of the interaction between the subunits, and to the extent of interface area. H-bonds are weaker than electrostatic interactions, but they can be crucial in anchoring a domain into a specific orientation that can be further stabilized by hydrophobic or electrostatic interactions.

Proteins accomplish several cellular functions required to live and their folding/unfolding are constantly checked in cells. Since the biosynthesis on ribosome, the protein chains adopt a definite three-dimensional structure known as native conformation, thanks to an efficient control-system. When the native state is neither achieved either maintained, the proteins can self-assemble forming insoluble deposits. The accumulation of these aggregates causes the loss of function of the protein and the saturation of the protein control systems (chaperones and proteases); this process can causes toxicity and pathogenicity [1-2]. Researchers have been aware since the early days of protein studies that, under stress conditions, proteins may aggregate, often in an irreversible way. What is new in modern Protein

Chemistry is the realization that aggregation is the first etiologic event in an increasing number of pathologies and that aggregation often occurs through misfolding rather than just unfolding [2,3]. Dramatic examples of pathologies associated with misfolding include Alzheimer's and Parkinson's diseases, the Huntington's chorea, prion diseases and amyloid lateral sclerosis [4,5]. The common feature in all these devasting pathologies is the accumulation of amorphous or more often fibrillar protein aggregates, called amyloid fibres, that causes neuronal toxicity [6]. The growing interest in protein aggregation is not exclusively restricted to its medical implications and to a relatively small number of proteins involved in diseases. Oligomeric proteins are prevalent in nature more than we suppose. Several proteins have been found to lead to higher oligomers and fibres, suggesting the hypothesis that most, if not all, amino acid sequences might be able to misfold in a similar ordered way [7]. This evidence places protein misfolding into a much wider perspective. It has also been shown more recently that protein aggregation is not always toxic but it is an advantageous feature for a number of reasons, including new opportunities for functional control, such as allosteric regulation and the establishment of higher-order complexity [7]. Oligomerization represents a very important phenomenon in the formation of molecular machines, like for motor proteins (kinesin, microtubules) that are indispensable to confer cellular integrity, intra/intercellular communication and movement. The formation of essential "cellular bodies" such as melanosomes, dendritic cell aggresome-like structures, P-bodies and stress granules depends on protein aggregation [8]. It is also well established that some cellular functions involve the formation of amyloid-like structures, as occurs for CPEB (cytoplasmic polyadenylation element-binding protein) fibres that improve the intraneuronal communications and the consolidation of long term memory when they accumulate on the synapsis [9]. The aggregation propensity have been exploited by a large number of organism. Even viruses, that are not completely "organized" as a cell, are able to infect and destroy the host-cell thanks to the capability of the proteins on their envelope to self-assembly [10].

In vivo, protein aggregation occurs in response to a wide range of "stimuli" that could be:

- genetic, i.e. a modifications in DNA and or RNA encoding for a monomeric precursor;
- biochemical, i.e. a modifications during the protein anabolism and/or catabolism;
- physicochemical, i.e. changes in pH, temperature, protein concentration, ionic strength.

As described, such environmental conditions can have negative or positive effects on aggregation propensity and protein functionality. Understanding how proteins aggregate has therefore become an important goal of modern Structural Biology.
Protein aggregates can have very different morphologies which may range from amorphous to well ordered fibrillar structures. In the latter case, the aggregated species are usually named amyloid fibres from the original idea of Rudolph Virchow who, around 1854, thought sugars as important components of the aggregates [11]. The current accepted definition is 'an unbranched protein fibre whose repeating substructure consists of β-strands that run perpendicular to the fibre axis, forming a cross-β sheet of indefinite length' [12]. This structure would be a universal fold that most if not all proteins may be able to adopt in given conditions [13] It is known that the repeating cross-β sheet motif is characterised by an X-ray diffraction pattern with a meridional reflection at around 4.7 Å corresponding to the inter-β strand spacing and an equatorial reflection at around 6–11 Å corresponding to the distance between stacked β-sheets [13,14]. Since these structural features have been observed in several aggregates both in vitro than in vivo, the amyloid fold seems to be a very stable structure [7]. Another important property of the amyloid deposits is that they have inherent birefringence that increases intensely after staining, for instance, with the Congo red dye. They are also very resistant to proteolytic degradation. However,

there are other mechanisms by which proteins can form ordered aggregates without raising the cross-β motif. These include domain-swapping and end-to-end stacking [15-17].

The medical [18], biological [19] and fundamental [20] interest associated with protein aggregation and fibrillogenesis raises the important question of which characteristics promote oligomerization and how it is possible to predict and modulate this behaviour. A set of principles has been identified. First of all, it is assumed that the information is stored linearly along the amino acid sequence [21]. Regions with high propensity to aggregate are rich in hydrophobic amino acids and poor in charged residues. π–stacking of aromatic residues has also been implicated to play an important role [22,23]. Second, the sequence must have some tendency to adopt structural features compatible with the semi-ordered structure observed in the repetitive assembly proper of fibres [17,24]. This observation may be easily rationalized by considering that essential elements in stabilizing β structures are not only the inter-strand hydrogen bonds but also packing of the side chains. Therefore, while polyproline is unlikely to form fibres since its conformation is hardly compatible with a β-structure, sequences with β-propensity could easily form amyloids. Sequences which adopt an α-helical structure in a globular protein can act as chameleons and form packed fibrillar β-structures [25-28].

Finally, the last aspect that seems to be important in fibre formation is that aggregation prone regions need to be at least partially if not completely accessible. This is easily obtained in peptides and intrinsically unstructured proteins but can be more difficult in globular proteins, in which potential β-prone sequences are usually well buried in the protein core. Under given conditions it is possible to affect the solvent accessibility and the proteins self-assemble.

Much of what it is known about protein aggregation and misfolding, derives from biophysical studies in vitro. Proteins can be grouped into two main families: the intrinsically unfolded proteins [29,30], and globular proteins or domains [2]. There is a distinct difference between the two families. How the disordered proteins

aggregate is quite easy to understand: regions in the linear sequence more aggregation prone start the event when their concentration in the cell is above their solubility [31,32]. Conversely, it is more difficult to understand how globular proteins aggregate. In fact, they generally do not unless exposed to environmental perturbations [33]. High temperature [34, 35], high pressure [36,37], low pH [38], alcohols [39], chaotropic solvents and sample shaking [40] have widely been used for this purpose to study aggregation in vitro. Under these conditions, proteins that have evolved to protect their buried hydrophobic core from the solvent accessibility, may misfold and aggregate [5,41]. More recently, a subfamily of globular proteins was identified whose members have the tendency to aggregate spontaneously without the involvment of highly denaturing conditions [42]. To explain this behaviour it was hypothesized that local structural fluctuations, rather than global changes, could promote conformational transitions which would then initiate aggregation. This hypothesis may well explain, for instance, the fibrillation of acylphosphatase from S. solfataricus, which retains its global fold and enzymatic function under mildly destabilizing conditions [43].

The molecular mechanisms leading to aggregation are still unclear. For this reason, small globular proteins may serve as useful models to study aggregation. They are simple systems and it is easier to follow the behaviour by changing few parameters systematically. Additionally, thanks to their small size, are amenable to computational analysis. Finally, it is straightforward to design and produce mutants aimed to rigorously investigation on a feature of interest.

References

[1] Knowles TP, Vendruscolo M, Dobson CM. (2014) The amyloid state and its association with protein misfolding diseases. *Nat Rev Mol Cell Biol.* 15(6):384-96.

[2] Chiti F., Dobson C.M. (2006) Protein misfolding, functional amyloid, and human disease *Annu. Rev. Biochem.* 75:333–366.

[3] Luheshi L M and Dobson C M. Bridging the gap: From protein misfolding to protein misfolding diseases (2009) *FEBS Lett.* 583 2581–6

[4] Bellotti V, Mangione P and Stoppini M (1999) Biological activity and pathological implications of misfolded proteins *Cell. Mol. Life Sci.*55 977–91

[5] Dobson C M (1999) Protein misfolding, evolution and disease.*Trends Biochem. Sci.* 24 329–32

[6] Stefani M and Dobson C M (2003) Protein aggregation and aggregate toxicity: new insights into protein folding, misfolding diseases and biological evolution *J. Mol. Med.* 81 678–99

[7] Pastore A, Temussi PA. (2012) Protein aggregation and misfolding: good or evil? *J. Phys.: Condens. Matter* 24 244101-244110

[8] Huff M E, Balch W E and Kelly J W (2003) Pathological and functional amyloid formation orchestrated by the secretory pathway *Curr. Opin. Struct. Biol.* 13 674–82

[9] Kausik S and Kandel ER. (2016) The Role of Functional Prion-Like Proteins in the Persistence of Memory. *Cold Spring Harbor Laboratory Press.* 8:a021774

[10] Marreiros R, Müller-Schiffmann A, Bader V, Selvarajah S, Dey D, Lingappa VR and Korth C. (2015) Viral capsid assembly as a model for protein aggregation

diseases: Active processes catalyzed by cellular assembly machines comprising novel drug targets. *Virus Res* 207:155-64

[11] Sipe JD and Cohen AS (2000) Review: History of the Amyloid Fibril. *J. Struct. Biol.* 130 88–98

[12] Greenwald J and Riek R (2010) Biology of amyloid: structure, function, and regulation. *Structure* 18 1244–60

[13] Astbury WT. (1935) X-Ray Studies of Protein Structure. *Nature* 137, 803-805

[14] Sunde M, Serpell LC, Bartlam M, Fraser PE, Pepys MB and Blake CC (1997) Common core structure of amyloid fibrils by synchrotron X-ray diffraction. *J. Mol. Biol.* 273 729–39

[15] Bennett MJ, Sawaya M R and Eisenberg D. (2006) Deposition diseases and 3D domain swapping. *Structure* 14 811–24

[16] Eisenberg D, Nelson R, Sawaya MR, Balbirnie M, Sambashivan S, Ivanova M I, Madsen AØ and Riekel C (2006) The Structural Biology of Protein Aggregation Diseases: Fundamental Questions and Some Answers. *Acc. Chem. Res.*39 568–75

[17] Nelson R and Eisenberg D (2006) Structural models of amyloid-like fibrils. *Adv. Protein Chem.* 73 235–82

[18] Powers ET, Morimoto RI, Dillin A, Kelly JW and Balch WE (2009) Biological and chemical approaches to diseases of proteostasis deficiency. *Annu. Rev. Biochem.* 78 959–91

[19] Fowler DM, Koulov AV, Balch WE and Kelly JW (2007) Functional amyloid--from bacteria to humans. *Trends Biochem. Sci*. 32 217–24

[20] Zhang S (2003) *Nature Biotechnol.* Fabrication of novel biomaterials through molecular self-assembly21 1171–8

[21] Chiti F, Stefani M, Taddei N, Ramponi G and Dobson CM (2003) Rationalization of the effects of mutations on peptide andprotein aggregation rates *Nature* 424 805–8

[22] Tartaglia, G.G., Cavalli, A., Pellarin, R. & Caflisch, A. (2004). The role of aromaticity, exposed surface, and dipole moment in determining protein aggregation rates. *Protein Sci* 13(7), 1939-41.

[23] Gazit, E. (2002). A possible role for π-stacking in the self-assembly of amyloid fibrils. *Faseb J* 16(1), 77-83.

[24] Marshall KE and Serpell LC 2(009) Structural integrity of β-sheet assembly *Biochem. Soc. Trans.* 37 671–6

[25] Zou W Q and Gambetti P (2007) Prion: the chameleon protein *Cell. Mol. Life Sci.* 64 3266–70

[26] Atwood CS, Obrenovich ME, Liu T, Chan H, Perry G, Smith MA and Martins RN (2003) Amyloid-β: a chameleon walking in two worlds: a review of the trophic and toxic properties of amyloid-β *Brain Res. Brain Res. Rev*. 43 1–16

[27] Uversky VN (2003) A Protein-Chameleon: Conformational Plasticity of α-Synuclein, a Disordered Protein Involved in Neurodegenerative Disorders. *J. Biomol. Struct. Dyn.* 21 211–34

[28] de Chiara C and Pastore A (2011) Supramolecular Structure and Function vol 10, ed J Brnjas-Kraljevi´c and G Pifat-Mrzljak (Dordrecht: Springer) pp 87–100

[29] Huang A and Stultz CM (2009) Finding order within disorder: elucidating the structure of proteins associated with neurodegenerative disease. *Future Med. Chem.* 1 467–82

[30] Babu MM, van der Lee R, de Groot NS and Gsponer J (2011) Intrinsically disordered proteins: regulation and disease. *Curr.Opin. Struct. Biol*. 21 432–40

[31] Gsponer J, Futschik ME, Teichmann A and Babu M M (2008) Tight Regulation of Unstructured Proteins: From Transcript Synthesis to Protein Degradation.*Science* 322 1365–8

[32] Jain N, Bhattacharya M and Mukhopadhyay S (2011) Chain Collapse of an Amyloidogenic Intrinsically Disordered Protein. *Biophys. J.* 101 1720–9

[33] Chiti F, Webster P, Taddei N, Clark A, Stefani M, Ramponi G and Dobson CM (1999) Designing conditions for in vitro formation of amyloid protofilaments and fibrils. *Proc. Natl Acad. Sci. USA* 96 3590–4

[34] Litvinovich SV, Brew SA, Aota S, Akiyama SK, Haudenschild C and Ingham KC (1998) Formation of amyloid-like fibrils by self-association of a partially unfolded fibronectin type III module. *J. Mol. Biol*. 280 245–58

[35] F¨andrich M, Fletcher MA and Dobson CM (2001) Amyloid fibrils from muscle myoglobin. *Nature* 410 165–6

[36] Ferr˜ao-Gonzales AD, Souto SO, Silva JL and Foguel D (2000) The preaggregated state of an amyloidogenic protein: Hydrostatic pressure converts native transthyretin into the amyloidogenic state. *Proc. Natl Acad. Sci. USA* 97 6445–50

[37] De Felice FG, Vieira MN, Meirelles MN, Morozova-Roche LA,Dobson CM and Ferreira ST (2004) Targeting the neurotoxic species in Alzheimer's disease: inhibitors of Aβ oligomerization *FASEB J.* 18 1099–101

[38] McParland VJ, Kad NM, Kalverda AP, Brown A, Kirwin-Jones P, Hunter MG, Sunde M and Radford SE (2000) Partially Unfolded States of β2-Microglobulin and Amyloid Formation in Vitro. *Biochemistry* 39 8735–46

[39] Sassi P, Giugliarelli A, Paolantoni M, Morresi A and Onori G (2011) Unfolding and aggregation of lysozyme: A thermodynamic and kinetic study by FTIR spectroscopy. *Biophys. Chem.* 158 46–53

[40] Apetri AC and Surewicz WK (2003) Atypical Effect of Salts on the Thermodynamic Stability of Human Prion Protein. *J. Biol. Chem*. 278 22187–92

[41] Kelly JW (1996) Alternative conformations of amyloidogenic proteins govern their behaviour. *Curr. Opin. Struct. Biol*. 6 11–7

[42] Chiti F and Dobson CM. (2009) Amyloid formation by globular proteins under native conditions. *Nature Chem. Biol*. 5 15–22

[43] Plakoutsi G, Bemporad F, Monti M, Pagnozzi D, Pucci P and Chiti F. (2006) Exploring the Mechanism of Formation of Native-like and Precursor Amyloid Oligomers for the Native Acylphosphatase from Sulfolobus solfataricus.*Structure* 14 993–1001

Route map of this Thesis

In this Thesis, two proteins, RNase A and MNEI have been proposed as models for aggregation studies. Although different in structure and in function, they share common hallmarks. Both of them are:

a) aggregation prone: their aggregation propensity is well known;

b) small: their molecular weight, i.e 13.7 KDa for RNase A and 11 KDa for MNEI, make them suitable proteins to be studied by several physicochemical technics. Additionally it can be easier to produce them as recombinant proteins thanks to well optimized procedures;

c) Monomeric: their native monomeric fold make them useful systems to monitor the oligomerization pathways starting from a most simple protomeric subunit;

Through a multidisciplinary approach, an extensive investigation on the relationship between environmental changes and aggregation propensity has been performed. Wide attention has been focused on the most common physicochemical agents, such as pH, temperature, ionic strength, metalation on stability and aggregation. At the same time genetic mutations in “hot- regions” were also investigated.
The Thesis is divided into three big sections. The Part A, is completely dedicated to RNaseA, the natural model. In the Chapter 1 an extensive study on the influence of metalation on protein aggregation has been pursued. The following Chapter 2 is focused on a RNaseA-Onc mutant designed to investigate the role of hinge loop on protein stability and aggregation propensity.

The second part of this Thesis, Part B, is ruled by MNEI, the artificial model. In the Chapter 3, high attention is given on the characterization of the physicochemical properties of MNEI and the propensity to form insoluble, both ordered and disordered aggregates, in response to environmental parameters, i.e. pH, temperature and ionic strength. In the Chapter 4, the study is aimed to understand the molecular basis leading to fibrilization with insight on early steps of unfolding.

In the third section, Part C, a full description on the production procedures referred to the two proteins studied has been reported.

Each Chapter is a result of an extensive study supported by a wide range of technics and by precious collaborations with national and international groups who are greatly acknowledged.

Part A

Natural models

Ribonuclease A

State of art

Bovine pancreatic RNase A (ribonuclease A) is one of the most studied protein in structural biology. By lyophilization from 40% acetic acid solutions, it can oligomerize in form of dimers, trimers, tetramers, higher order oligomers [1,2]. RNase A can also form amyloid fibers [2]. Oligomerization of RNase A also occurs in solution at high substrate concentrations or high temperature [3]. The most accepted mechanism through RNase A oligomerizes is the so called 3D-domain swapping (3D-DS), i.e. the capability to reciprocally exchange protein domains [4]. In Fig. 1 a schematic overview is reported. In 3D domain swapping, one domain of a monomeric protein is replaced by the same domain from an identical protein chain. The result is an intertwined dimer or higher oligomer, with one domain of each subunit replaced by the identical domain from another subunit. A protein able to swap may interchange a large tertiary globular domain or a small secondary structure element as α-helix or a β-sheet [4]. RNase A can exchange both N-domain and the C-domain forming two dimeric isomers called as N-dimer and C-dimer, respectively. The structure of the more basic or minor trimer has also been solved [1,4]; it is formed by three monomers linked to each other by swapping their C-strands, thereby forming a circular structure that looks like a propeller. It was called C-trimer. A plausible linear model was proposed for the less basic, major trimer. In this linear model, two monomers are linked through swapping of their N-termini, and a third monomer is bound to one of them by a C-terminal domain swapping. It will be called the NC-trimer. According to modelling studies, only plausible models for tetramers and higher oligomers are reported. At the moment no X-ray or NMR structures for tetramers and oligomers are deposited on databank. In Fig. 2 the cartoon representations for N-dimer, C-dimer and C-trimer. All the model structures for RNase A oligomers are also reported. Oligomerization through 3D-DS, does not affect the enzymatic activity because the interchanging domains reconstitute the catalytic site. The conformers are enzymatically active and are endowed with

additional biological function such as the cytotoxicity and cytostaticity on cancer cells, a property completely absent into the monomeric species [4].

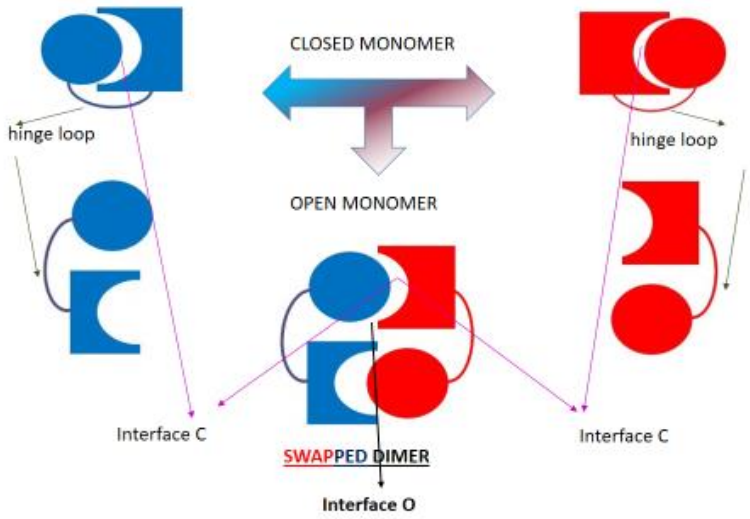

Fig. 1 - 3 D domain swapping scheme

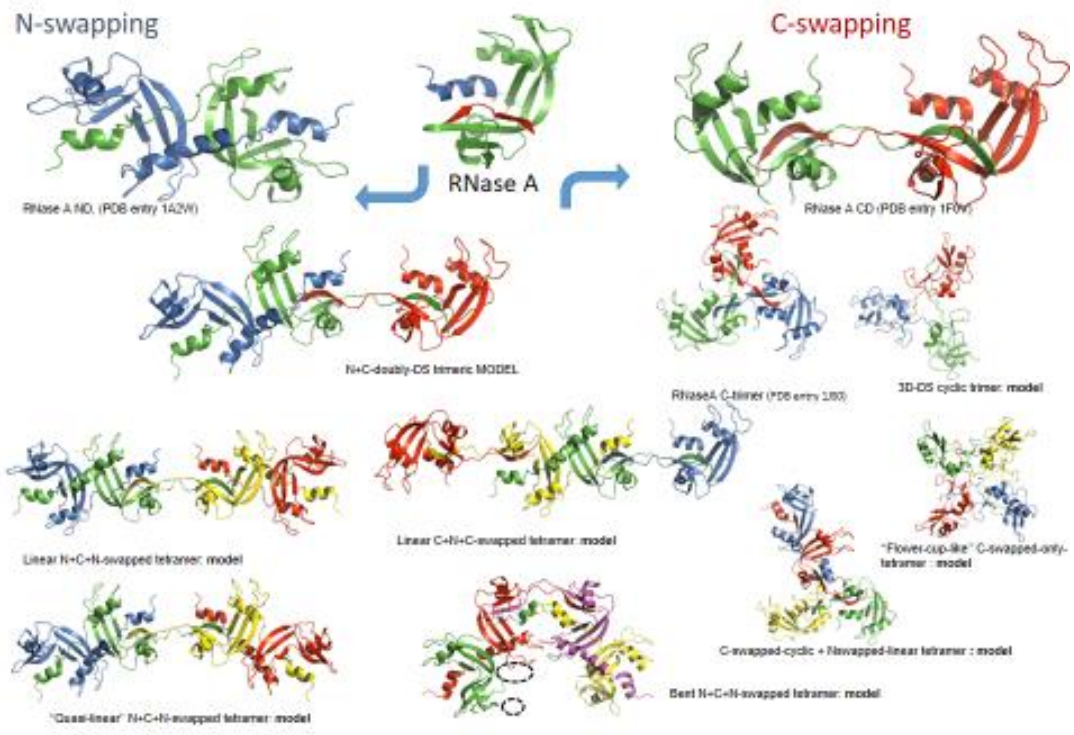

Fig. 2 RNase A oligomers. Structures and models

References

[1] Bennett MJ, Schlunegger MP, Eisenberg D. (1995) 3D domain swapping: a mechanism for oligomer assembly. *Protein Sci.* 4(12):2455-68

[2] Liu Y, Eisenberg D. (2002) 3D domain swapping: as domains continue to swap *Protein Sci.* 11(6):1285-99

[3] Teng PK,AndersonNJ,GoldschmidtL, Eisenberg D.(2012) Ribonuclease A suggests how proteins self-chaperone against amyloid fiber formation. *Protein Sci.* 21(1):26-37

CHAPTER

1

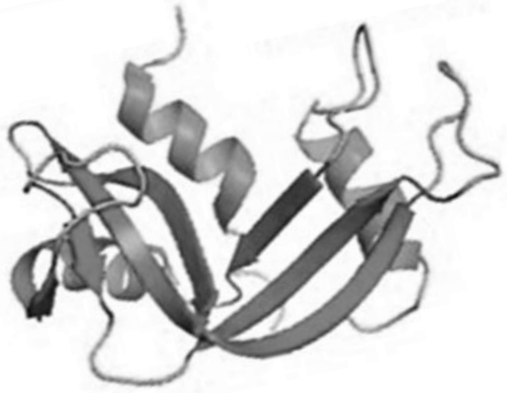

Bovine pancreatic ribonuclease metalation by Platinum-based drugs: insight on protein oligomerization

Abstract

Metalation can influence the oligomerization state of proteins, can alter their hydrodynamic properties and/or can cause fine structural variations. Platinum-complexes are the most successful families of compounds clinically effective and commercialized against malignant tumours. In this work, the reaction between RNase A and three Pt-complexes clinically effective (cis-platinum, carboplatinum and oxaliplatinum) has been analysed. They induce extensive protein aggregation leading to the formation of dimers, trimers and higher oligomers that were purified at homogeneity. Structural and functional properties of the platinated species, together with their spontaneous dissociation and thermally induced denaturation, have been characterised. The effects of platination on enzymatic activity and biological properties induced by Pt-complexes exposure have been assayed. X-ray structures of the Pt-monomeric adducts that RNase A forms provide a rational basis to explain the different effects of the three anticancer agents on protein aggregation and the relationship between structure and function. In this framework, RNase A showed high versatility to study protein-metal interactions that could be crucial for the biological (side) effects of several metallodrugs against malignant tumours.

1.1 Introduction

Platinum complexes (Fig.1) represent one of the most successful families of clinically used anticancer drugs [1]. Cisplatin (cis-Pt $Cl_2(NH_3)_2$, *cis*-diamminedichloroplatinum(II), CDDP) is the best known Pt-based anticancer agent. Carboplatin (*cis*-diammine(cyclobutane-1,1-dicarboxylate-O,O')platinum(II)) and oxaliplatin (ethane-dioate(1R,2R)-1,2-cyclohexanediamineplatinum(II)) are two CDDP analogues usually employed to treat tumours poorly responsive to cisplatin treatments [2].

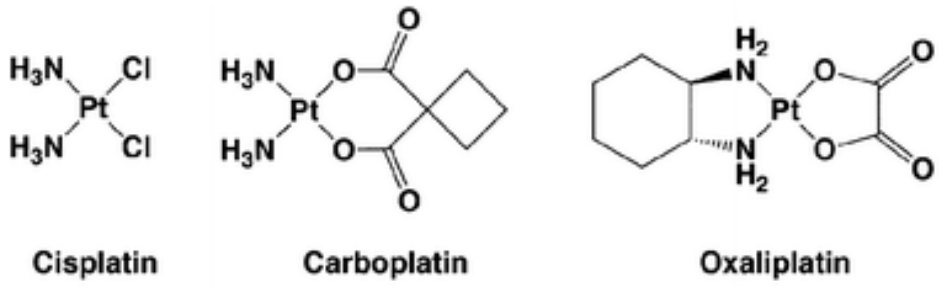

Fig. 1 Platinum complexes: structure of cisplatin, carboplatin and oxaliplatin

Pt-based drugs show their pharmacological action through the formation of stable DNA adducts [1-3]. The Pt-DNA adducts roll out and bend the DNA duplex, favouring the binding by high-mobility group (HMG) proteins that recognize these modifications as damage and trigger cell in apoptosis [4]. The formation of DNA adducts with CDDP, carboplatin and oxaliplatin has been extensively studied and the X-ray structures of these adducts have been solved [3-9]. Nevertheless, nucleobases are not the only biological targets of Pt-drugs [3]. Platinum can efficiently interact with sulphur atoms of cysteine [7] or methionine residues [8] or even with nitrogen

atom of histidine [9,10] or oxygen atoms of aspartic/glutamic side chain residues [11]. Actually, while the formation of Pt–DNA adducts has been extensively investigated, less attention has been bestowed to the interaction between platinum compounds and proteins. After injection into the bloodstream, most of the platinum (65 to 98%) is associated with proteins, mainly to serum albumin and hemoglobin. Moreover, a significant portion of Pt is bound to γ-glutamyl-cysteine-glycine (glutathione, GSH) [12] and/or other cysteine-rich proteins [13], like a few small proteins of the metallothionein family [14]. Platinum complexes entrance in cells is helped by proteins belonging to the so-called "copper trafficking" system [15]. Therefore, exploring how platinum-based drugs interact with proteins is worth of investigation for a deep understanding of the molecular basis of protein-drug recognition, for studying the inherent or acquired pharmacological resistance, for evaluating the bio-distribution and the clearance of Pt-based drugs, for the rational design of new therapeutic agents more effective against proliferating malignant cells. Furthermore, the interaction of these molecules with proteins has drawn increasing attention in the last few year, given the role that it plays in defining the toxicity profiles of the drugs [16, 17]. Previous studies have shown that Pt metalation can alter the hydrodynamic properties in a protein and/or cause fine structural variations resulting in oligomerization [18,19]. In order to clarify the relationship between platination and aggregation, a comparative study has been pursued by evaluating the behaviour of RNase A when incubated in presence of cisplatin, carboplatin and oxaliplatin, respectively. RNase A was elected for this study since a) it has been used as a model system in many fields of Protein Chemistry, including protein metalation [19,20] and protein aggregation [21]; b) it binds cisplatin and details of this binding are known [20]; c) it is able to form well characterized dimers and higher oligomers [21] which can be used as reference. In particular, RNase A forms a N-terminal swapped dimer, hereafter called N-Dimer [22], and a C-terminal swapped dimer, C-Dimer [23], two trimers characterized by swapping of both C- and N-termini and other oligomers [24-26], including tetramers, pentamers and hexamers [27]. Another

advantageous aspect is that it is an enzyme, therefore it possible to estimate the effect of platination on protein functionality. Interestingly, RNase A aggregates acquire selective cytotoxicity towards tumor cells [28]. This work reveals that cisplatin (CDDP) deeply induces RNase A oligomerization allowing the isolation of dimer, trimer and tetramers. The reaction with carboplatin and oxaliplatin equally produces oligomers even if the yield is lower than cisPt reaction. All the platinated species were isolated and carefully characterized from a biochemical and physicochemical point of view. This work reveals that 24 h incubation at 37 °C of RNase A in the presence of an excess of cisplatin, carboplatin and oxaliplatin (1:10 protein to metallodrug ratio) induces the formation of platinated monomers (Pt-M_{cis} ,Pt-M_{carbo} and Pt-M_{oxa}), dimers (Pt-D_{cis} ,Pt-D_{carbo} and Pt-D_{oxa}), trimers (Pt-T_{cis} ,Pt-T_{carbo} and Pt-T_{oxa}) and a small amount of higher oligomers. Denaturing and non-denaturing polyacrylamide gel electrophoresis and size-exclusion chromatography were used to characterize the formation of the oligomers. Circular dichroism and UV-Vis spectroscopy were used to investigate their structural stability and catalytic activity. In collaboration with the groups of Proffs. M.Donadelli and G.Gotte from the University of Verona, a functional characterisation on cytotoxic and cytostatic properties has been pursued.

1.2 Materials and methods

1.2.1 Production and purification of platinated species

Cisplatin and RNase A (type XII-A) were purchased from Sigma- Aldrich. RNase A was further purified as described in [29]. Carboplatin and oxaliplatin were purchased from Santa Cruz Biotechnology. Preliminary incubations for analytical purposes were pursued by incubating RNase A with cisplatin. Platinated species were obtained by incubating RNase A at a protein: metallodrug molar ratio of 1:10. RNase A was incubated at a concentration of 5 mg × ml^{-1} in 0.20 M sodium phosphate buffer pH 6.7 at 37° C for 24 hours with mild shaking. The platinated species were purified by size exclusion chromatography. The reaction mixture was loaded on a Sephadex G75 column (1.5 × 72 cm) previously equilibrated in 0.20 M sodium phosphate buffer pH 6.7, at a flow rate of 0.15 ml×min^{-1}. Concentration of all platinated species was spectrophotometrically measured at 280 nm, using the extinction coefficient of RNase A ($\varepsilon_{1\%}$ at 280 nm= 0.695). Sample homogeneity for all the platinated species was assessed by polyacrylamide gel electrophoresis under denaturing (SDS-PAGE 15%) [30] and non-denaturing conditions (12% native PAGE) [31].

1.2.2 Circular dichroism spectroscopy

The gel-filtered Pt-species were analyzed with far-UV CD spectroscopy, at the concentration of 0.1 mg × ml^{-1} in 0.20 M sodium phosphate buffer, pH 6.7. Circular dichroism (CD) experiments were performed on a Jasco J-810 spectropolarimeter (JASCO Corp., Milan, Italy) at 25 °C. Quartz cells with path length of 0.1 cm were used in the far-UV region from 200 to 250 nm. Each spectrum was obtained averaging three scans, subtracting contributions from the corresponding reference and converting the signal to mean residue ellipticity in units of deg × cm^2 × $dmol^{-1}$.

Other experimental settings were: 20 nm × min^{-1} scan speed, 2.0 nm band width, 0.2 nm resolution, 50 mdeg sensitivity, and 4 s response. Thermal unfolding profiles were obtained by monitoring the CD signal at 222 nm as function of temperature, in the range 20–100 °C, with a heating rate of 1.0 °C × min^{-1}.

1.2.3 Enzymatic activity

Ribonuclease activity of the purified RNase A platinated species was measured by using the spectrophotometric Kunitz method, i.e. monitoring the cleavage of yeast RNA via UV-Vis spectroscopy [32] at 25 °C in 0.050 M sodium acetate pH 5.0, using 0.5 mg × ml^{-1} of RNA and an enzyme concentration of 0.5 μg × ml^{-1}. The activity of the platinated proteins was also compared to that obtained under the same experimental conditions for RNase A.

1.2.4 Dissociation experiments

The stability of the gel filtered species was assessed by incubating at 4 and 37 °C aliquots of the fraction corresponding to the maximum of each form, without any further modification, in 0.20 M sodium phosphate buffer, pH 6.7, for time intervals settled between 1 and 35 days. The dissociation kinetics was monitored by cathodic polyacrylamide gel electrophoresis under non-denaturing conditions.

1.2.5 Crystallization and X-ray diffraction data collection

To obtain crystals, all the purified species were treated at 25 °C by Prof. A . Merlino and coworkers using the hanging drop vapor diffusion method, protein concentration of 15 mg × ml^{-1} and precipitant solution containing 30% ammonium sulfate and 0.30 M sodium chloride. Only crystals of purified cisplatin and carboplatin monomers

were obtained, within 7 days. Complete data sets for Pt-monomers wer collected at 100 K at the CNR Institute of Biostructures and Bioimages, Naples, Italy, using a Saturn 944 CCD detector equipped with CuKα X-ray radiation from a Rigaku Micromax 007 HF generator. The crystals diffract at 1.95 Å resolution. Coordinates and structure factors on cisplatin-monomer and carboplatin-monomer were deposited in the Protein Data Bank under the accession codes 4RTE and 5NA9, respectively.

1.2.6 Cell lines and cellular proliferation assay

Cytotoxic effect of each platinated species was assayed on tumoral cell lines Panc1 (deriving from pancreatic adenocarcinoma), A549 and SKBR3 (deriving from breast cancer). Cellular proliferation assays were performed by the group of Prof. M. Donadelli. Cells were seeded in 96-well plates ($5x10^3$ cells/well) at 37 °C with 5% CO_2 and 24 h later were treated with the various compounds and further incubated for 96 h. At the end of the treatments cells were stained with a Crystal Violet solution (Sigma, Milan, Italy) to determine cell growth photometrically at 595 nm**.** ANOVA (post hoc Bonferroni) analysis was performed by GraphPad Prism 5 software. P value < 0.05 was indicated as statistically significant. Values are the means of three independent experiments (± SD).

1.3 Results and Discussion

1.3.1 Platinum complexes influence the oligomerization state of RNase A

Previous studies have shown that Pt metalation of proteins can induce the formation of protein oligomers and/or cause subtle structural variations [18]. The first aim of this work was to monitor the formation of possible aggregates produced by incubation of RNase A with cisplatin, carboplatin and oxaliplatin. Preliminary studies have been pursued using cisplatin (CDDP), the simplest Pt-compound. RNase A was incubated at a concentration of 5 mg×ml^{-1} for 24 hours at 37 °C in the presence of cisplatin in a 1:10 protein:cisplatin molar ratio in 0.20 M sodium phosphate buffer, pH 6.7.. Additionally, another aliquot of RNase A was dissolved at a concentration of 5 mg×ml^{-1} in 40% V/V acetic acid/water solution, incubated for 1 hour at 37° C, lyophilized and then dissolved in 0.20 M sodium phosphate buffer according to the protocol described by Crestfield [34]. For further comparison, a third aliquot of RNase A was also incubated without cisplatin in sodium phosphate buffer. After incubation, the oligomerization was evaluated by cathodic PAGE under non-denaturing conditions. Two different amounts of protein were loaded on polyacrylamide gel, corresponding to 5 and 10 µg, respectively. The resulting electrophoretic patterns are shown in Fig. 2-A. Cisplatin incubation results in an appreciable oligomerization. Moreover, cisplatin induces structural modifications also on the native monomeric RNase A, influencing its electrophoretic mobility: as showed in Fig.2, the latter band in lanes 1-2 migrates more than the latter band in lanes 3-4 and 5, corresponding to the monomeric RNase A present in solution upon AcOH lyophilisation and the native RNase in pure buffer, respectively. In order to investigate the effects on RNase A oligomerization of two other Pt-drugs, i.e. carboplatin and oxaliplatin, the protein was incubated in the same experimental

conditions described for cisplatin. In the same way, a small amount of untreated RNase A was loaded on the native gel. Fig. 2-B reports that also carboplatin (lane 2) and oxaliplatin (lane 3) influence the oligomerization state of RNase A.

In all the cases analysed, the platinum complexes influence the oligomerization state of RNase A.

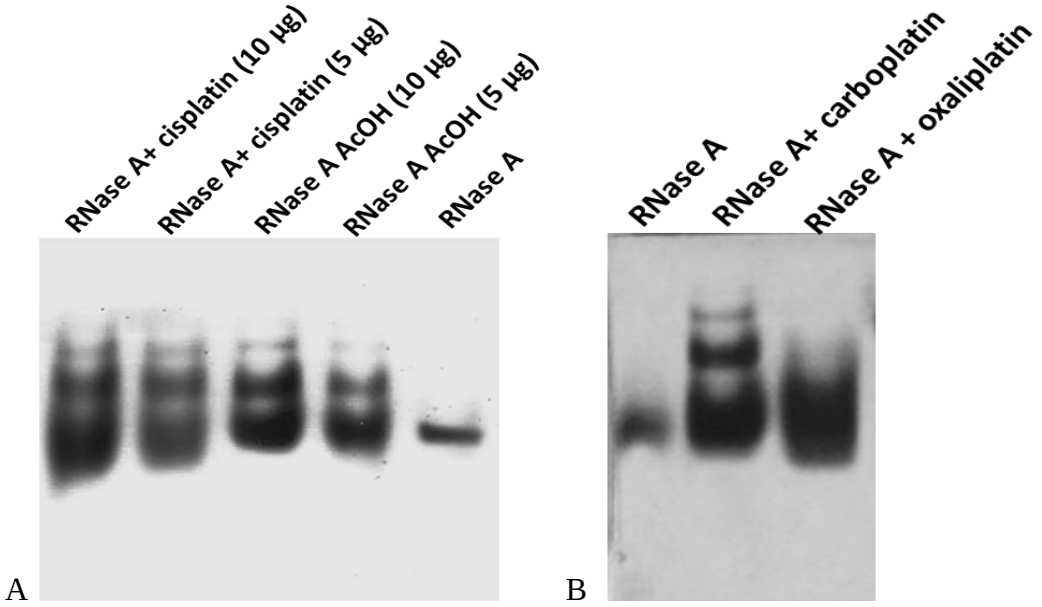

Fig. 2 Oligomerization patterns of RNase A: cathodic gel electrophoresis under native conditions (12% PAGE). A: incubation with cisplatin (lanes 1 and 2), lyophilization upon incubation in 40% acetic acid (lanes 3 and 4), and native RNase A incubated in 0.20 M sodium phosphate buffer, pH 6.7 (lane 5). B: incubation with carboplatin (lane 2), incubation with oxaliplatin (lane 3). RNase A dissolved in water is also reported as reference (lane 1).

1.3.2 Production and purification of platinated oligomers

Since analytical preparations show that cisplatin, carboplatin and oxaliplatin influence the oligomerization state of RNase A, a new set of incubations were putted on. Similar amounts of RNase A were incubated as described in "Materials and Methods" section. For each preparation, 15 mg of protein were dissolved in 3 ml of 0.20 M sodium phosphate buffer, pH 6.7. To each protein solution were added the following amounts of metallodrug: 3.3 mg of cisplatin, 4.1 mg of carboplatin and 4.3 mg of oxaliplatin to obtain the RNase A: Pt-drug molar ratio of 1:10. Each mixture was incubated at 37 °C for 24 hours under gentle shacking. Since the electrophoretic patterns (Fig. 2,panels A-B) suggest the presence of oligomers with different molecular weights, the platinated species were purified by size-exclusion chromatography. Thus, the protein-drug solutions were loaded on a Sephadex G75 (1.5 ×72 cm) column previously equilibrated in 0.20 M sodium phosphate buffer, pH 6.7. The elution was carried on at a flow rate of 0.15 $ml \times min^{-1}$. Fig. 3 reports the corresponding gel-filtration profiles obtained for the three metallodrugs. In accordance with the cathodic PAGE, high oligomerization occurs. A comparative analysis of the peak area suggests that the oligomerization yield increases in the direction oxaliplatin < carboplatin < CDDP. Cisplatin is the most effective giving rise to the formation of high amount of dimer, trimer, tetramer and traces of multimers of high molecular weight. Peak integration reveals that about 60% of the protein is eluted as monomer (indicated as M), whilst approximately 25 % is eluted as dimer (indicated as D), 8 % as trimer (indicated as T) and 4% as tetramer (indicated as Tt). A small amount, roughly equivalent to the remaining 3% of the total, corresponds to higher size aggregates (indicated as O). On the other hand, the profiles obtained upon incubation with carboplatin and oxaliplatin reveal that the amount of dimer, trimer and other oligomers decreases; in more detail, oxaliplatin incubation results in dimerization lower than carboplatin.

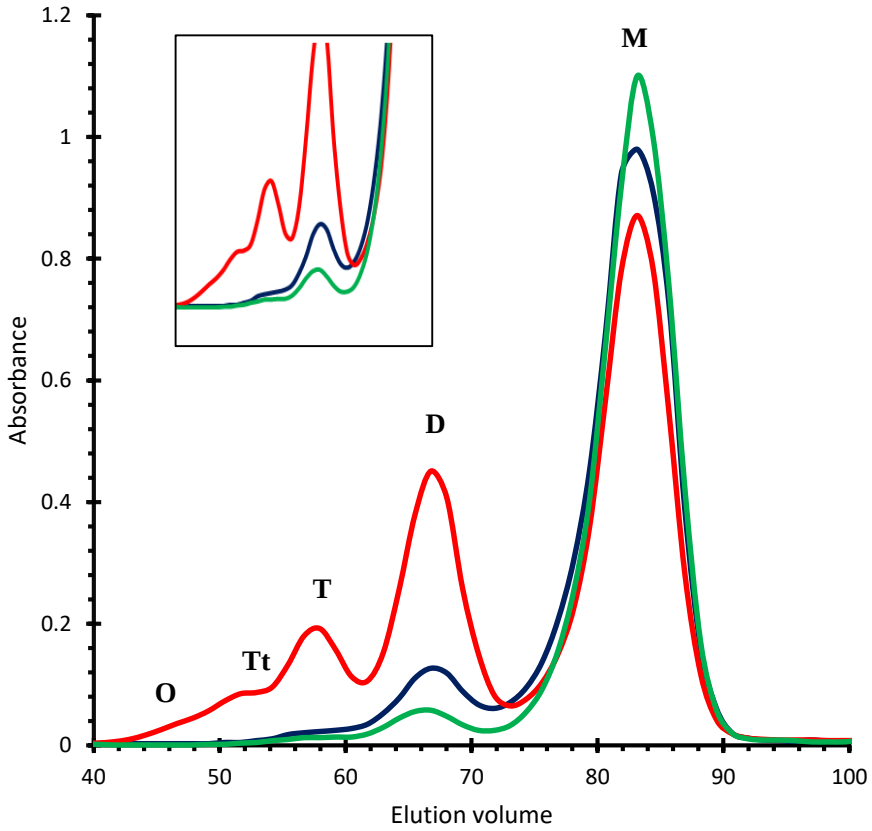

Fig. 3 Chromatographic profiles: Gel-filtration pattern on a Sephadex G75 (1.5 × 72 cm) column after 24 h of incubation at 37 °C in the presence of cisplatin (red line), carboplatin (blue line) and oxaliplatin (green line) in 1:10 protein:metallodrug molar ratio in x nM sodium phosphate buffer, pH 6.7 . The peaks corresponding to metalated monomer (M), metalated dimer (D), metalated trimer (T),metalated tetramer (Tt) and metalated oligomers (O) are highlighted. A zoomed section on dimer-trimer and higher oligomers is also reported.

1.3.3 Biochemical characterization: Pt-species are interestingly SDS resistant and strongly stable over time

All the platinated species purified were subjected to PAGE under native and denaturing conditions. The gel filtered fractions migrate as a single spot in non-denaturing conditions, suggesting the presence of a single conformer in each fraction (Fig 4, panels B-C-D). Moreover, RNase A incubated in phosphate buffer was also subjected to native PAGE as control, revealing that no oligomerization occurs if platinum is not present. For a further comparison, an aliquot of RNase A dissolved after lyophilization from 40% acetic acid was also loaded (panel A). Interesting differences among the oligomerization observed upon lyophilization from acetic acid solution and Pt-metalation are more evident on the denaturing SDS-PAGE (Fig.5, panels B-C-D). In fact, while oligomers formed by acetic acid lyophilisation dissociate thus migrating as a single spot corresponding to the monomeric protein (panel A), platinated species show a peculiar SDS resistance. This suggests that platinum allows interactions between subunits that are different from those occurring in the well-known swapped dimers and oligomers of RNase A. Besides the chemical resistance to denaturing SDS treatment, the resistance at two conditions of temperature was also monitored over time. Each Pt-species was incubated at the typical storage temperature of 4 °C and at the physiological temperature of 37 °C. The stability of the different aggregates was monitored until 35 days. Samples were analysed by native PAGE. The electrophoretic patterns after prolonged time is reported in Fig. 6. Both carboplatin and oxaliplatin oligomers show a weak dissociation at 4 °C and 37 °C. Differently, cisplatin species are resistant at least up to 35 days at 4 °C while a slow but constant dissociation occurs at 37 °C. Anyway, all the platinated species are more stable than the well-known swapped dimers in all the experimental conditions investigated.

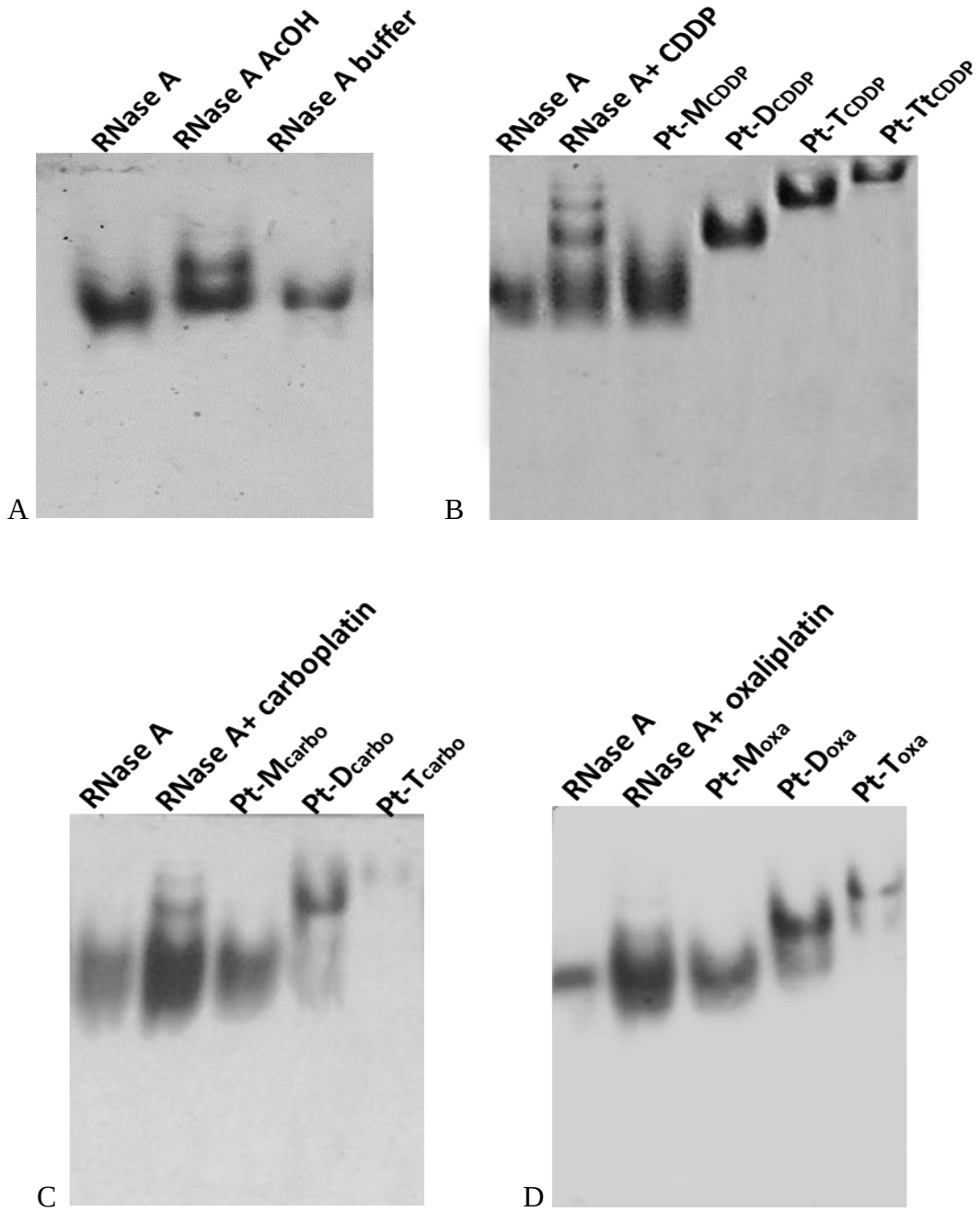

Fig. 4 Aggregation profiles: Gel-electrophoresis under native conditions (cathodic PAGE 12%) of purified platinated oligomers obtained incubating RNase A in the presence of cisplatin (B), carboplatin (C) and oxaliplatin (D). M: monomer, D: dimer; T: trimer; Tt: tetramer. RNase A dissolved in water and in phosphate buffer are also loaded as references togheter with a RNase A sample incubated in 40% acetic acid and liophylized.

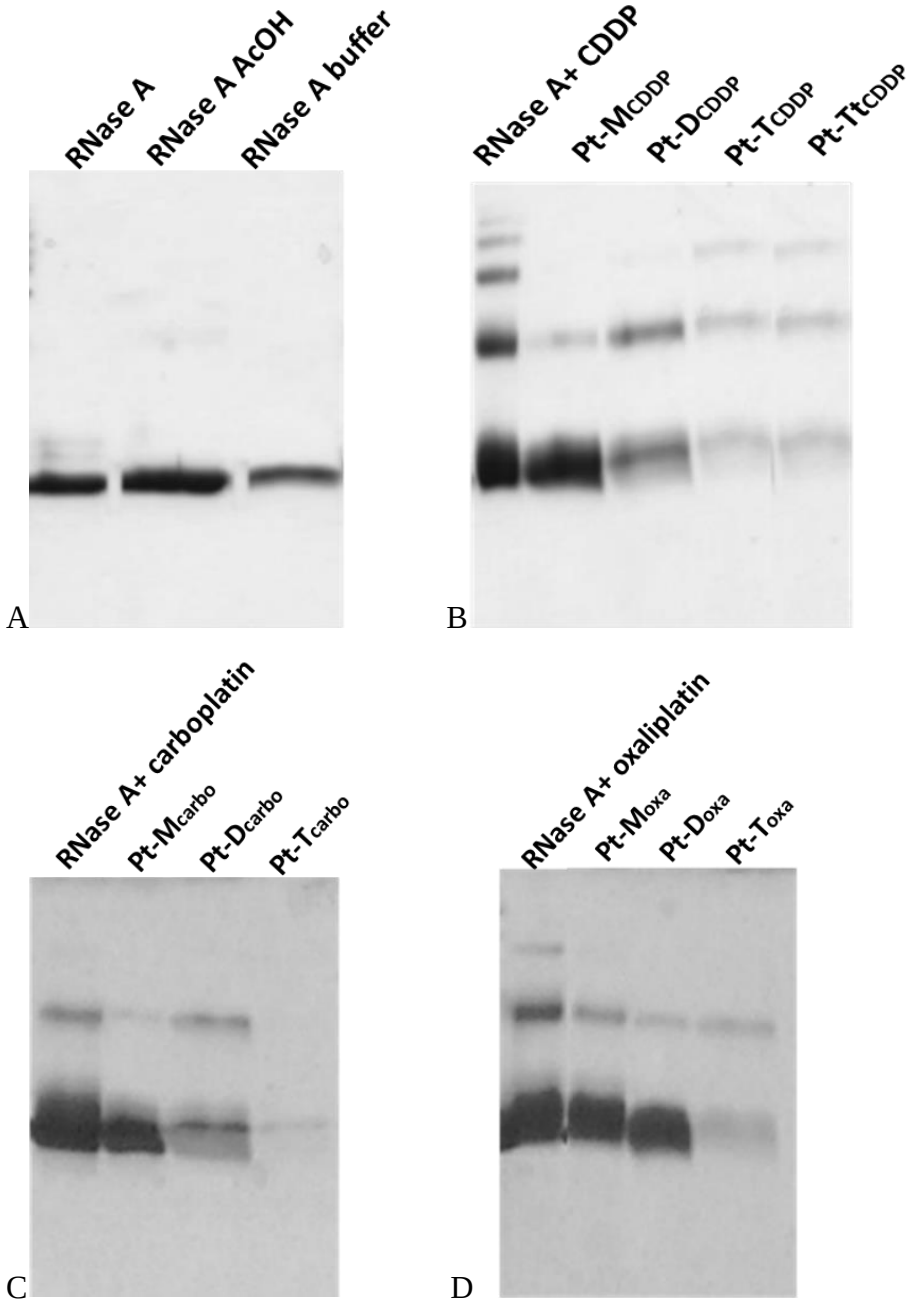

Fig. 5 Aggregation profiles: Gel-electrophoresis under denaturing conditions (SDS-PAGE 15%) of of purified platinated oligomers obtained incubating RNase A in the presence of cisplatin (B), carboplatin (C) and oxaliplatin (D). M: monomer, D: dimer; T: trimer; Tt: tetramer. RNase A dissolved in water and in phosphate buffer are also loaded as references togheter with a RNase A sample incubated in 40% acetic acid and liophylized.

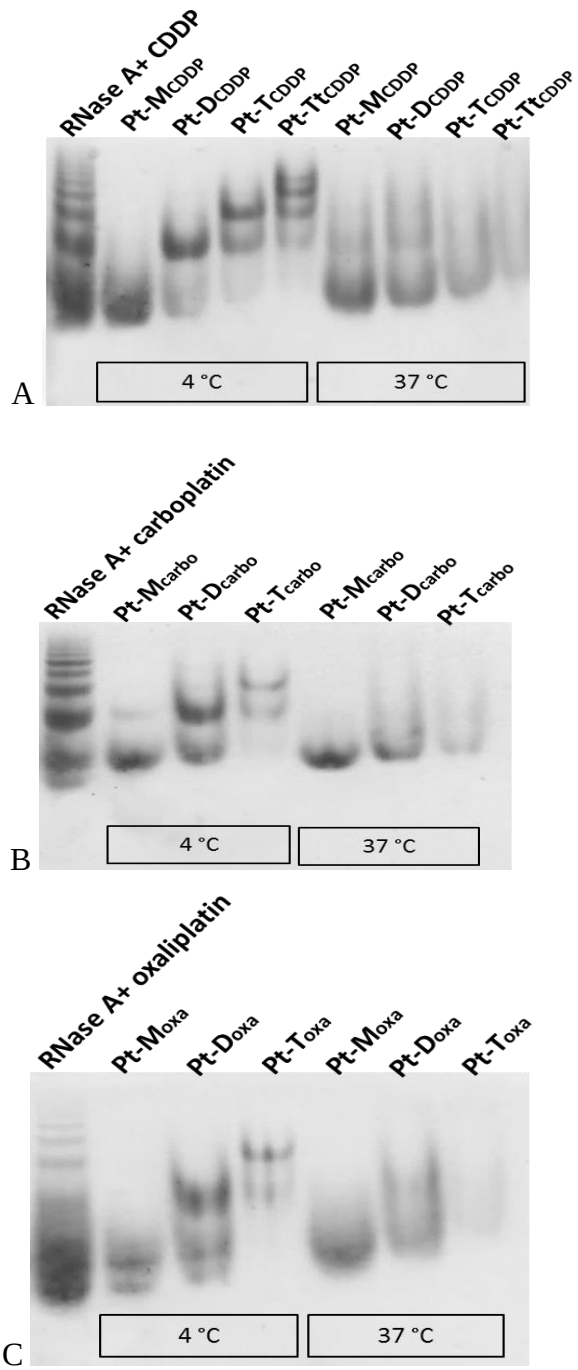

Fig. 6 Dissociation profiles. Gel-electrophoresis under native conditions (cathodic PAGE 12%) of purified platinated oligomers obtained by incubating RNase A in the presence of cisplatin (A), carboplatin (B) and oxaliplatin (C) upon 35 days of storage at 4 °C and 37 °C. M: monomer, D: dimer; T: trimer; Tt: tetramer.

1.3.4 Physicochemical characterization: Pt-species are folded and moderately thermostable

In order to characterize from a structural point of view the effect of cisplatin, carboplatin and oxaliplatin binding to RNase A in solution, the spectroscopic properties of the platinated monomeric, dimeric and trimeric species were studied by CD, which is a sensitive technique to monitor the secondary structure of proteins [34]. Far-UV CD spectra are shown in Fig. 7 (panel A, cisplatin; panel B, carboplatin; panel C, oxaliplatin). The spectra are almost indistinguishable from each other, revealing that all the platinated species, i.e. monomeric and oligomeric forms, are well-folded and suggest that they are assemblies of native RNase A monomers. This behavior demonstrates that drug complexation causes no denaturation of RNase A, supporting the idea that the formation of Pt adducts does not induce major conformational changes of the native protein structure.

With the aim to characterize the thermal stability of the platinated monomer, dimer and trimer, the CD signal at 222 nm was recorded as a function of temperature, in 0.20 M phosphate buffer at pH 6.7. These conditions are very similar to those used to characterize the stability of N-Dimer and C-Dimer, i.e. the N-terminal and C-terminal swapped dimers of RNase A (0.10 M phosphate buffer pH 6.8) [35]. The thermal denaturation profiles are reported in Fig. 8 (panel A, cisplatin; panel B, carboplatin; panel C, oxaliplatin). The curves of the Pt-species show a sharp sigmoidal transition that can be described using a two-state model. All the T_m alues obtained are summarized in Table 1. Cisplatinated species have the same T_m of the native RNase A. Carboplatin species are moderately thermostable but less than the native monomeric RNase A. Finally, oxaliplatin forms show T_m values highest than native RNase A and other platinated species. Interestingly, all the platinated dimers are more stable than the well known swapped dimers [35].

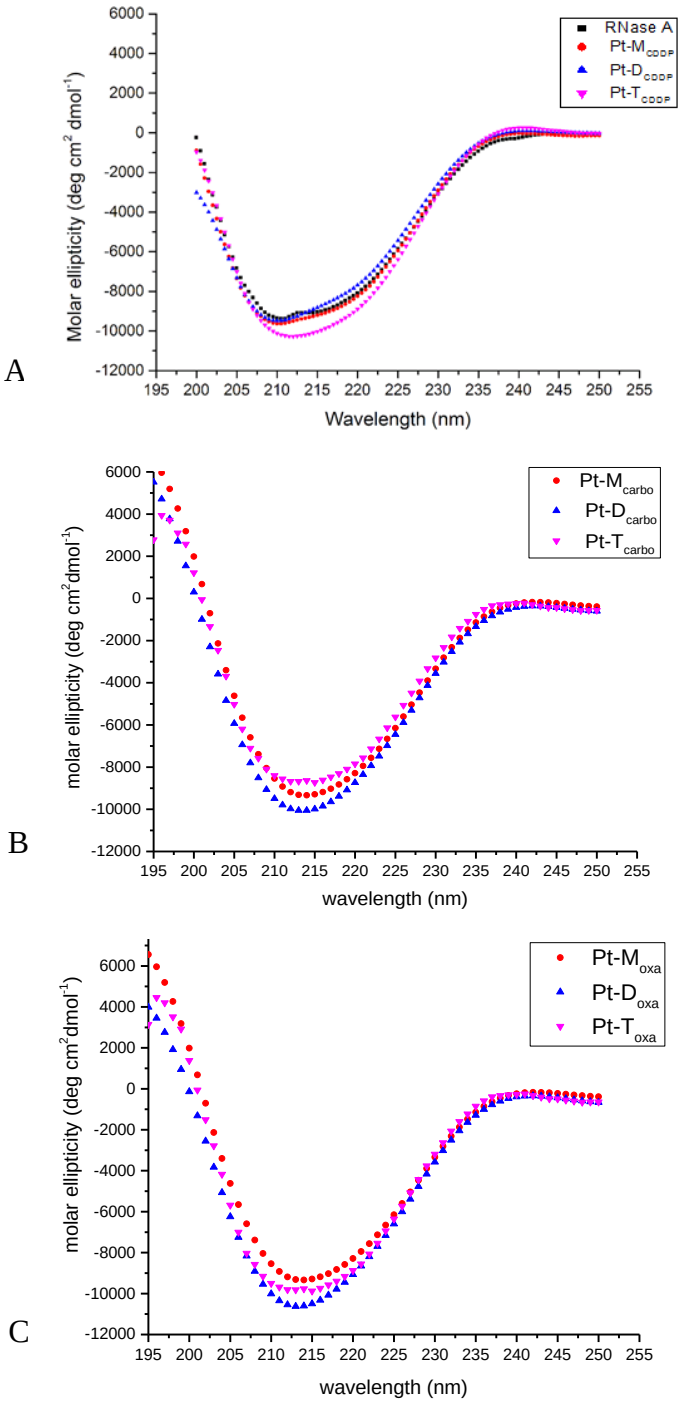

Fig. 7 Spectroscopic analysis on platinated species. CD spectra (25 °C) at a protein concentration of 0.1 mg×ml $^{-1}$in 0.20 M sodium phosphate buffer, pH 6.7. A: cisplatin; B: carboplatin; C: oxaliplatin. M: monomer (red) ;D:dimer (blu); T:trimer (magenta). The CD spectra recorded for RNase A (black) is also reported in panel A as reference.

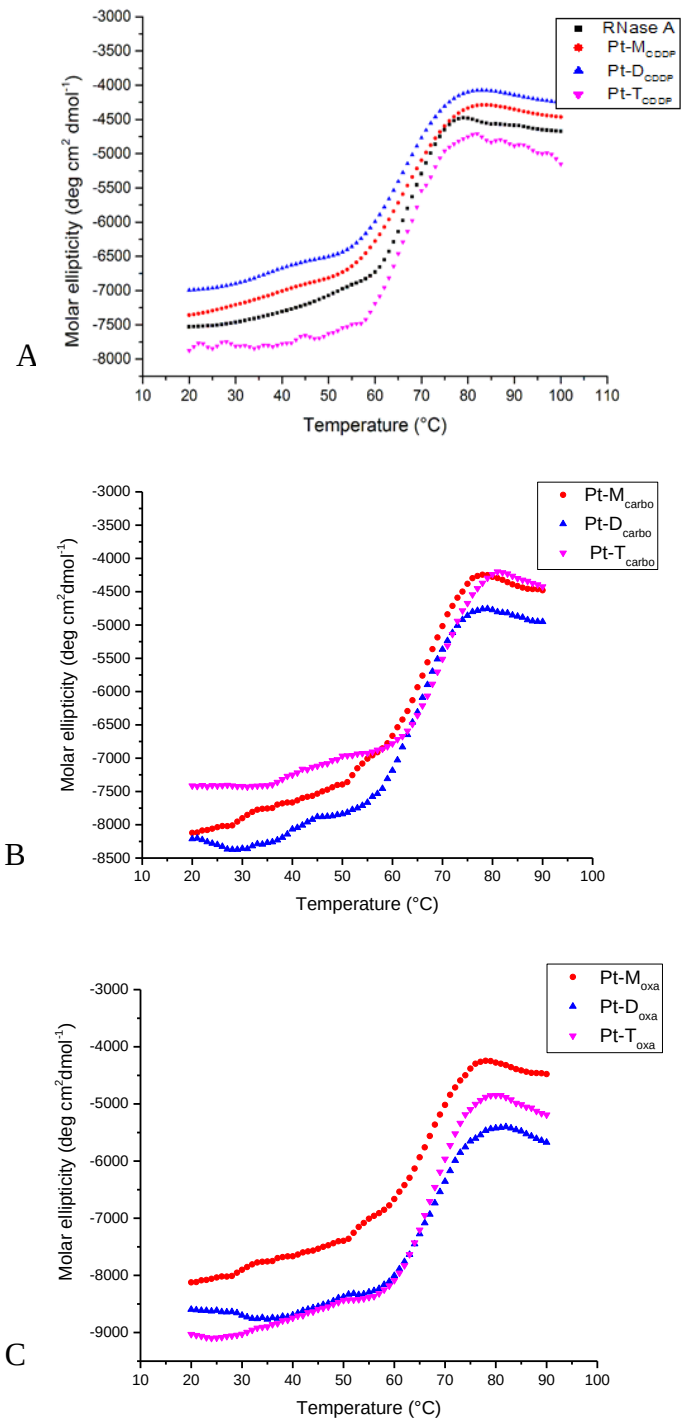

Fig 8 Thermal denaturation analysis on platinated species. Thermal unfolding curves at 222 nm measured at a protein concentration of 0.1 mg×mL^{-1} in 0.20 M sodium phosphate buffer pH 6.7. A: cisplatin; B: carboplatin; C: oxaliplatin. M: monomer (red) ;D:dimer (blu); T:trimer (magenta). The CD spectra recorded for RNase A (black) is also reported in panel A as reference.

Protein	T_m °C)
RNase A	66 ± 1
Pt-M_{CDDP}	66 ± 1
Pt-D_{CDDP}	66 ± 1
Pt-T_{CDDP}	65 ± 1
Pt-M_{carbo}	63 ± 1
Pt-D_{carbo}	62 ± 1
Pt-T_{carbo}	64 ± 1
Pt-M_{oxa}	67 ± 1
Pt-D_{oxa}	67 ± 1
Pt-T_{oxa}	69 ± 1
C-terminal swapped dimer of RNase A*	66.4
N-terminal swapped dimer of RNase A**	50.0 66.4

Tab. 1 Thermal unfolding parameters. Comparison between the denaturation temperatures of platinated oligomers of RNase A obtained upon incubation with cisplatin, carboplatin and oxaliplatin, with those found for RNase A, N-terminal and C-terminal swapped dimers of RNase A.

*Parameters of the temperature-induced denaturation of N-terminal and C-terminal swapped dimer of RNase A have been obtained in 0.1 M phosphate buffer at pH 6.6, through DSC measurement [35].

**N-terminal swapped dimer of RNase A unfolds according to a three-state denaturation mechanism, which includes the formation of an intermediate; for this reason, in this case, two $T_{1/2}$ temperatures are reported [35].

1.3.5 Functional characterization: enzymatic activity

In order to estimate if platination could affect the protein functionality, the enzymatic activity for all platinated species was assayed. As described in "Materials and Methods" section, the ribonucleolytic action of platinated forms was measured by monitoring hydrolysis of yeast RNA at pH 5.0 using the Kunitz method [32]. The absorbance variations at 300 nm (ΔA_{300nm}) as a function of time, upon addition of the same amount of RNase A or platinated species dissolved at a concentration of 0.5 $\mu g \times ml^{-1}$ to 1 ml of a 0.5 $mg \times ml^{-1}$ yeast RNA solution were monitored by UV-spectroscopy. Fig. 9 reports the enzymatic activity profiles recorded for each species, i.e. cisplatin (Panel A), carboplatin (Panel B) and oxaliplatin (Panel C). The platinated species show different enzymatic activity. Indeed, CDDP-species retain a significant, although reduced, enzymatic activity (Fig.9- panel A). CarboPt species show catalytic properties comparable to native RNase (Fig.9-panel B). Finally, oxaliPt adducts show a behaviour similar to the one observed for CDDP-forms (Fig.9-panel C). The enzymatic activity analysed for each form can be summarized according to the scheme: carboplatin $_{activity}$ > oxaliplatin $_{activity}$ > cisplatin $_{activity}$. In Fig. 10 an overview of the behaviours observed for Pt-dimers (Panel A) and Pt-trimers (Panel B) is reported. As clearly indicated in Fig.10, all the carboplatinated purified species (lane magenta) preserve an enzymatic action significantly higher than the other forms obtained from the incubation with cisplatin or oxaliplatin. Interestingly, the aggregation due to the exposure to carboplatin does not affect the hydrolytic properties, differently from what observed in the two other cases, where the functionality significantly decrease in proportion to the molecular weight.

A

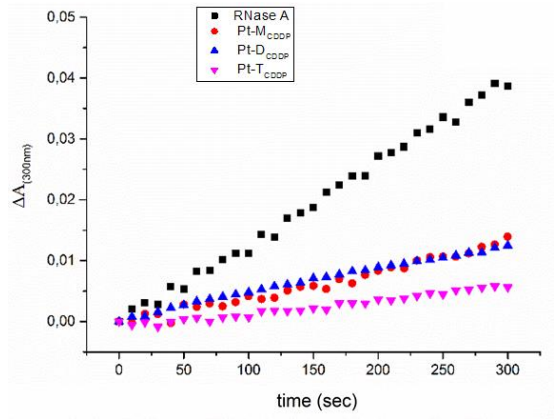

B

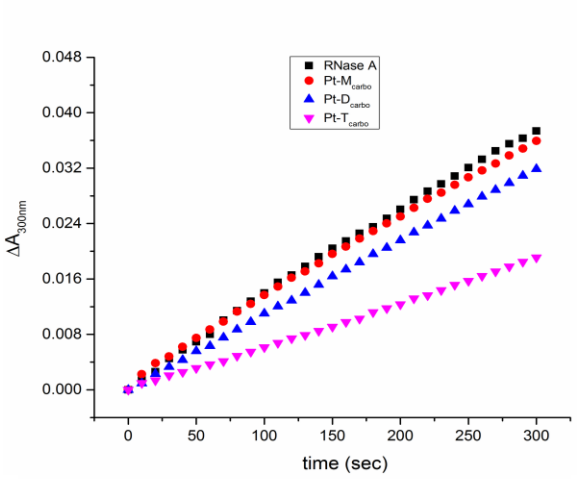

C

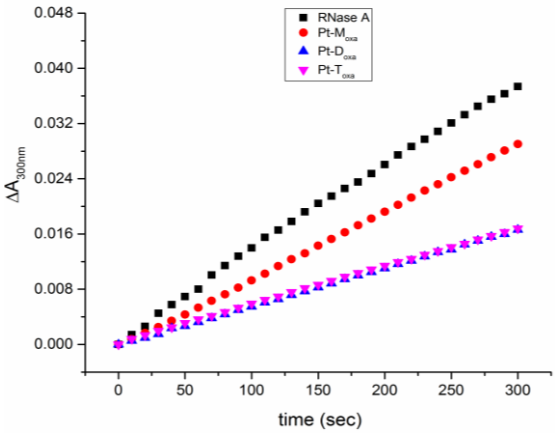

Fig. 9 Enzymatic activity monitored by the Kunitz assay . Cisplatin (A), Carboplatin (B) oxaliplatin (C). RNA hydrolysis was monitored at 300 at 25 °C in 0.050 M sodium acetate buffer pH 5 at a protein concentration of 0.5 $\mu g \times ml^{-1}$. A: cisplatin; B: carboplatin; C: oxaliplatin. M: monomer (red) ;D:dimer (blu); T:trimer (magenta). The ribonucleolytic activity recorded for RNase A (black) is also reported as reference.

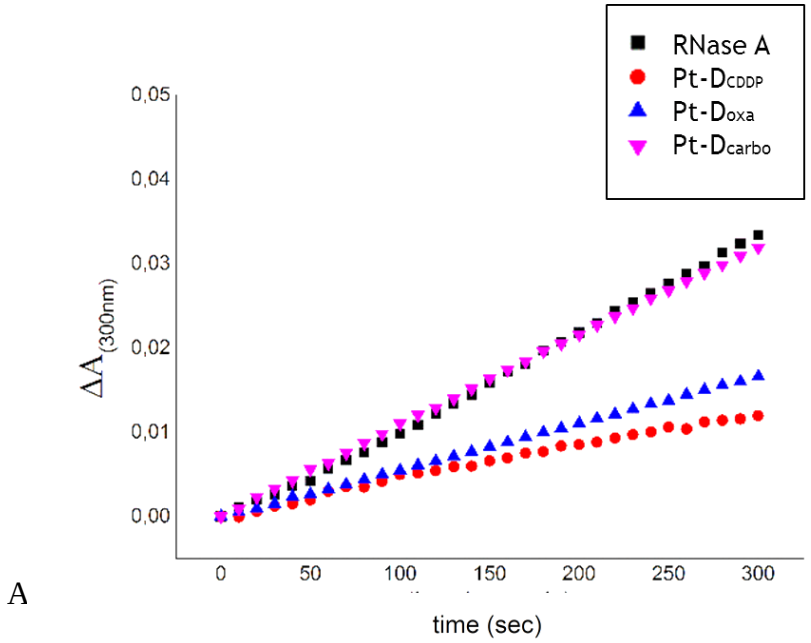

A

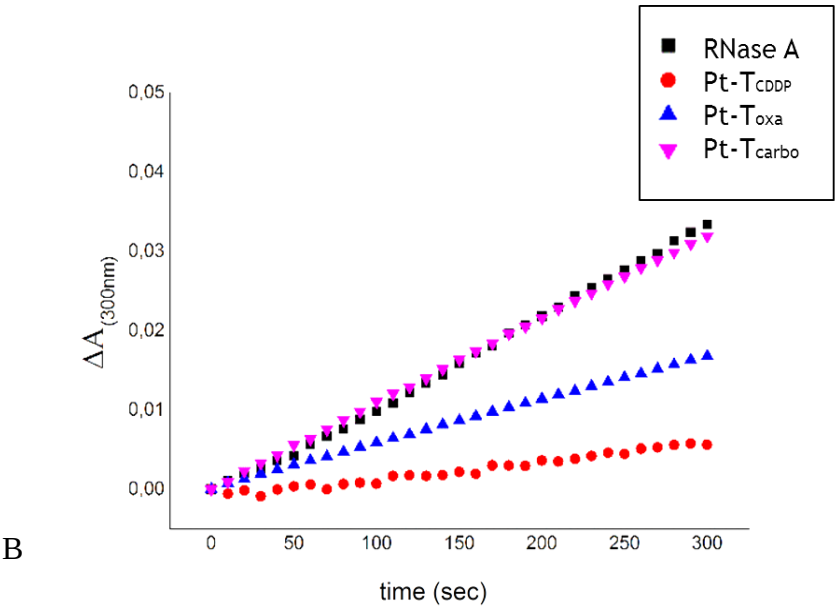

B

Fig. 10 Enzymatic activity monitored by the Kunitz assay. Pt-Dimers (A); Pt-Trimers (C). RNA hydrolysis at 600 at 25 °C in 0.050 M sodium acetate buffer pH 5 at a protein concentration of 0.5 μg×ml^{-1}. CDDP: red; oxaliplatin: blu; carboplatin: magenta. The ribonucleolytic activity recorded for the native monomeric RNase A (black) is also reported as reference

1.3.6 Functional characterization: cytotoxic action

Given the variety of effects observed on the enzymatic activity upon reaction with the different Pt complexes, the cytotoxic action has been also assayed in a panel of cancer cell lines from a series of solid tumors, as A549 (from lung carcinoma), Panc1 (from pancreatic adenocarcinoma) and SKBR3 (from breast cancer). The present study has been performed by the group of Proffs. G. Gotte and M. Donadelli of the University of Verona. Although the cell lines used are well known to be responsive to Pt-based drugs (cisplatin, carboplatin and oxaliplatin), cell proliferation was not affected by any of the platinated RNase A species. In particular, monomer, dimer, trimer and oligomers of RNase A did not significantly affect proliferation of A549, Panc1, and SKBR3 cells also when conjugated with cisplatin drug (Fig. 11, panel A). An equivalent result has been obtained with monomer, dimer, and oligomers of RNase A conjugated with carboplatin or oxaliplatin in A549 cells (Fig. 11, panel B). Altogether, these data indicate that RNase A species conjugated with Pt-based drugs did not acquire any cytotoxic property in cancer cells as compared to RNase A species alone but, instead, metalation significantly reduces the cytotoxicity of the drugs against the analyzed cell lines.

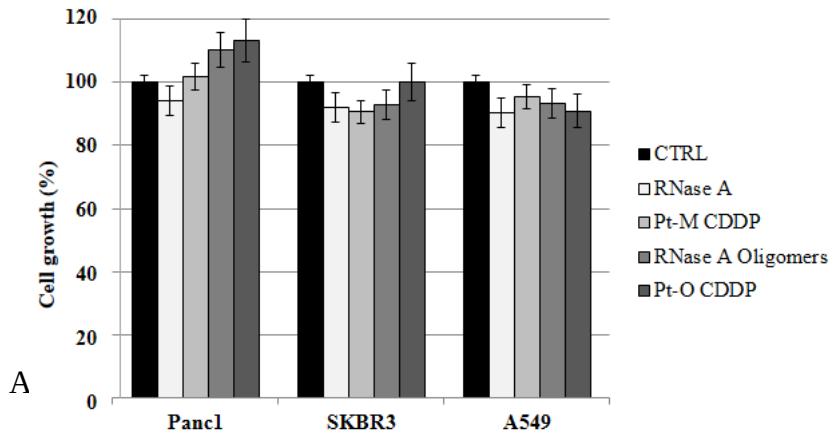

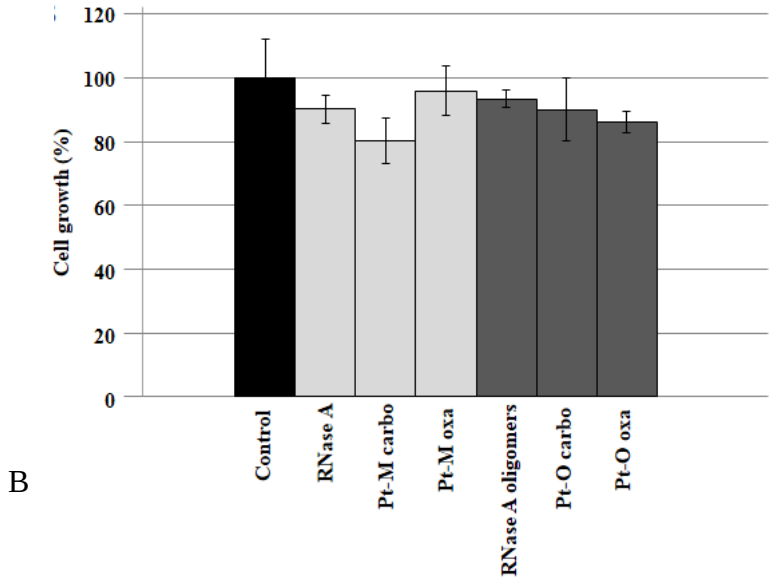

Fig. 11 Effect of platinated RNase A species on the proliferation of cancer cell lines. (A) Panc1, SKBR3 and A549 cells were seeded in 96-well plates, incubated overnight, and treated for 96 hours with 100 µg mL^{-1} of RNase A monomer or oligomers (a pool of dimers, trimers and larger oligomers) before or after incubation with CDDP. (B) A549 cells were seeded in 96-well plates, incubated overnight, and treated for 96 hours with 100 µg/ml of RNase A monomer or oligomers (a pool of dimers, trimers and larger oligomers) before or after incubation with carboplatin or oxaliplatin. Cell proliferation was determined using the Crystal Violet colorimetric assay. Values are means (±SD) of three independent experiments, each performed in triplicate

1.3.7 Structural characterization: crystallographic structures of cisPt-monomer and carbo-Pt monomer

In order to clarify the effect of platinum-based drug on stability and oligomerization, a fine structural analysis has been performed by Prof. Merlino and coworkers. All the purified Pt-species were accurately treated to obtain X-ray diffracting crystals as described in "Materials and Methods" section. Only cisplatined monomer and carboplatin monomer crystalized. Interesting structural hints come from the crystal analysis. The X-ray structures of the adducts formed by soaking native RNase A crystals with a stabilizing solution containing an excess of oxaliplatin were already reported [20]. Oxaliplatin adducts with RNase A crystals, showed that the platinum centre binds the side chain of Asp14 and Asp101, beyond the side chain of His119. The Pt-binding sites for Pt-M $_{CDDP}$ and Pt-M $_{carbo}$ are highlighted in Fig. 12.

Crystals of purified Pt-M $_{CDDP}$, deposited under the PDB code 4 RTE, diffracted X-ray at 1.95 Å resolution. Inspection of the electron density maps revealed that, although with partial occupancy, three distinct binding sites of cisplatin fragment can be identified on the RNase A surface. The r.m.s.d. value of 0.30 Å for Cα atoms between the model of Pt-M and that of the native enzyme derived from isomorphous crystals indicates that negligible perturbations occur in the structure upon cisplatin binding. The main binding site of the drug is located in proximity of Met29 side chain, with the Pt center (occupancy factor= 0.60) bound to the side-chain SD atom retaining, as expected, two ammonia molecules and a chloride ion as ligands. Since in this region residual electron density map is observed, a second Pt atom has been added to the model (occupancy factor = 0.40), which is indicative of an alternative conformation of the cisplatin fragment. The other two (minor) drug-binding sites (Pt occupancy factor between 0.2 and 0.4) are located close to His105 and His119 side chains. In both the cases, the Pt center is bound to an N atom of the imidazole ring

of His after releasing a chloride ion. Since His119 is involved in the catalytic site of RNases, these data can partly explain the results of the decreased enzymatic activity. Crystals of purified carbo-Pt monomer diffract X-ray at 2.07 Å resolution. The X-ray structure is registered under the PDB code 5NA9. The crystallographic structure is very similar to that of the ligand-free protein, and to those of Pt-M $_{CDDP}$ and RNase A-carboplatin adduct obtained by soaking procedure, deposited in the PDB under the accession code 4S0Q: Cα root mean square deviations from the corresponding atoms of the two chains of the RNase A-carboplatin structure obtained by soaking procedure are both equal to 0.49 Å. As observed in RNase A-carboplatin, carboPt-monomer showed a single Pt binding site, close to Met29 side chain.

The low content of Pt bound to the protein and the finding that carboplatin fragments does not bind protein active site residues, contrarily to what was observed for cisplatin and oxaliplatin , can well explain both the the higher catalytic activity exhibited by Pt-M_{carbo} when compared with its analogues. Furthermore, the finding that Pt-M_{carbo} has just one Pt binding site allows to conclude that Met29 is very likely involved in the process that leads to the formation of platinated RNase A dimers and higher oligomers.

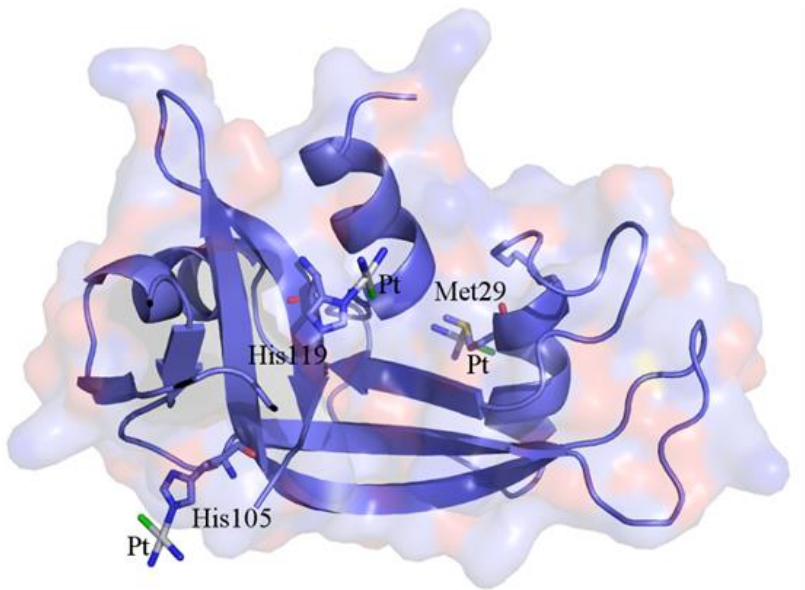

Fig. 12 Pt-binding sites on platinated monomer. Cartoon representation.

1.4 Conclusions and ongoing works

The formation of protein aggregates is a topic of great interest in molecular evolution, medicine and biotechnology. The oligomerization state of a protein can be deeply influenced by several environmental conditions. Metalation is one of the factors that can affect protein stability and aggregation propensity. Recently high attention is focused on the effects of metal-based drugs on protein-protein interaction. In fact, even if the pharmacological effects are mainly related to nucleobases-metals interactions, the direct effects of metalation on cellular uptake, biodistribution and pharmacological clearance of these drugs are not completely clear. In this scenario, this work investigates the relationship between Pt-metalation and protein aggregation. Platinum-based drugs are the most effective chemotherapycs and show different pharmacological response on the basis of their chemical composition. RNase A turned out as a helpful model to study the protein oligomerization propensity induced by the exposure to three common Pt-based drugs: cisplatin, carboplatin and oxaliplatin. This study reveals that all the metallodrugs significantly influence the RNase A aggregation propensity. In more details, the reaction with cisplatin gives rise to a wide range of Pt-aggregates triggering the formation of one dimer, one trimer, one tetramer and higher oligomers. Carboplatin and oxaliplatin are also able of forming RNase A platinated oligomers even if the final amount of dimers and higher oligomers is lower in comparison with the pattern obtained with cisplatin. All the oligomers were purified and deeply characterized. These adducts share similar folding and thermostability, and display SDS resistance and quite prolonged survival in solution. Among the three drugs, CDDP, the most potent oligomerization agent, is also the most effective in inhibiting the ribonucleolytic activity of the protein. Oxaliplatin forms the lower amount of oligomeric adducts and shows functional properties similar to the CDDP-adducts. On the other hand oligomers obtained in the presence of carboplatin are the most active as enzymes. X-

ray structures of the monomeric adducts allowed to identify different binding features of the three Pt compounds that account for their different influence on the catalytic activity and on the aggregation features of the protein complexes. In particular, the different influence of the Pt-based drugs on the catalytic activity can be explained by looking at active site accessibility upon metal binding: carboplatin adducts retain the full catalytic activity because their active site residues are not involved in metal binding and thus the substrate binding is not affected, at variance with what is observed in the adducts of the two other metallodrugs. The aggregation propensity can be explained by looking at the number of metal binding sites on the protein surface and at the chemical features of the Pt coordination sphere. Pt-Mcarbo leads to the formation of a lower amount of oligomers when compared to CDDP, since it possesses a single Pt binding site, whereas Pt-M_{CDDP} can bind three CDDP fragments, two of them involving residues located on the protein surface. The lowest aggregation propensity of the oxaliplatin adduct can be explained considering that the 1,2-diaminocyclohexane (DACH) ligand is not easily released from the Pt centre, even upon the binding to the protein, hampering the assembly of two RNase A chains. The evaluation of the effects of the presence of these adducts in cancer cell proliferation sensitive to the treatment with pancreatic-like RNases [36,37] reveals that the platinated RNase A oligomers are not cytotoxic. Thus, although protein oligomerization generally increases RNase A cytotoxicity [38], platinated oligomers of RNase A do not display any additional feature that could improve a possible cytotoxic activity associated with the formation of oligomers, but on the contrary they deprive the cytotoxic properties of cisplatin, carboplatin, and oxaliplatin. Altogether, these data indicate that possible aggregation processes of proteins by anticancer Pt-based drugs could represent a collateral drawback, which on one hand can affect the functional state of several protein targets triggering their aggregation, whereas on the other hand the efficacy of Pt-based drug treatment can be drastically reduced.

1.5 References

[1] Comess KM and Lippard SJ. (1993) Molecular Aspects of Platinum-DNA Interactions, Molecular Aspects of Anticancer Drug-DNA Interactions. Macmillan, London

[2] Rixe O, Ortuzar W, Alvarez M, Parker R, Reed E, Paull K and Fojo T. (1996) Oxaliplatin, tetraplatin, cisplatin, and carboplatin: Spectrum of activity in drug-resistant cell lines and in the cell lines of the National Cancer Institute's Anticancer Drug Screen panel, *Biochemical pharmacology.* 52, 1855-1865.

[3] Takahara PM, Rosenzweig AC, Frederick C A and Lippard SJ. (1995) Crystal structure of double-stranded DNA containing the major adduct of the anticancer drug cisplatin, *Nature.* 377, 649-52.

[4] Jamieson ER, Jacobson MP, Barnes C M, Chow CS and Lippard SJ. (1999) Structural and kinetic studies of a cisplatin-modified DNA icosamer binding to HMG1 domain B. *J Biol Chem.* 274, 12346-54

[5] Jamieson ER and Lippard SJ. (1999) Structure, recognition, and processing of cisplatin–DNA adducts. *Chem Rev.* 99, 2467–2498.

[6] Arnesano F, Banci L, Bertini I, Felli IC, Losacco M and Natile G. (2011) Probing the interaction of cisplatin with the human copper chaperone Atox1 by solution and in-cell NMR spectroscopy. *Journal of the American Chemical Society.* 133, 18361-9

[7] Messori L. and Merlino A. (2014) Cisplatin binding to proteins: molecular structure of the ribonuclease A adduct. *Inorganic chemistry.* 53, 3929-31

[8] Casini A, Mastrobuoni G, Temperini C, Gabbiani C, Francese S, Moneti G, Supuran C. T, Scozzafava A and Messori L. (2007) ESI mass spectrometry and X-ray diffraction studies of adducts between anticancer platinum drugs and hen egg white lysozyme, *Chemical communications*, 156-158

[9] Tanley SW, Schreurs AM, Kroon-Batenburg LM, Meredith J, Prendergast R, Walsh D, Bryant P, Levy C and Helliwell J.R. (2012) Structural studies of the effect that dimethyl sulfoxide (DMSO) has on cisplatin and carboplatin binding to histidine in a protein, *Acta crystallographica Section D, Biological crystallography.* 68, 601-12

[10] Mizumura Y, Matsumura Y, Hamaguchi T, Nishiyama N, Kataoka K, Kawaguchi T, Hrushesky WJ, Moriyasu F and Kakizoe T. (2001) Cisplatin-incorporated polymeric micelles eliminate nephrotoxicity, while maintaining antitumor activity *Jpn J Cancer Res.* 92, 328-36

[12] Messori, L. & Merlino, A. (2014) Cisplatin binding to proteins: molecular structure of the ribonuclease A adduct, *Inorganic chemistry.* **53**, 3929-31

[13] A. Casini, G. Mastrobuoni, C. Temperini, C. Gabbiani, S. Francese, G. Moneti, C.T. Supuran, A. Scozzafava, L. Messori, Chem. Commun. (2007) 156–158.

[14] Tanley SW, Schreurs AM, Kroon-Batenburg LM, Meredith J, Prendergast R, Walsh D, Bryant P, Levy C and Helliwell JR (2012) *Acta Crystallogr.* D68 601–612.

[15] Kartalou M and Essigmann JM. (2001) Recognition of cisplatin adducts by cellular proteins, *Mutat Res.* 478, 1-21

[16] Messori L and Merlino A. (2016) Cisplatin binding to proteins: A structural perspective, *Coordin Chem Rev.* 315, 67-89.

[17] Pinato O, Musetti C and Sissi C. (2014) Pt-based drugs: the spotlight will be on proteins, *Metallomics : integrated biometal science.* 6, 380-395.

[18] Li HL, Wells S A, Jimenez-Roldan J E, Romer R A, Zhao Y, Sadler PJ and O'Connor PB. (2012) Protein flexibility is key to cisplatin crosslinking in calmodulin, *Protein Sci.* 21, 1269-1279

[19] Picone D, Donnarumma F, Ferraro G, Russo Krauss I, Fagagnini A, Gotte G and Merlino A. (2015) Platinated oligomers of bovine pancreatic ribonuclease: Structure and stability, *Journal of inorganic biochemistry.* 146, 37-43

[20] Messori L, Marzo T and Merlino A. (2015) Interactions of Carboplatin and Oxaliplatin with Proteins: Insights from X-ray structures and mass spectrometry studies of their Ribonuclease A adducts, *Journal of inorganic biochemistry.* 153, 136-142.

[21] Gotte G, Laurents DV, Merlino A, Picone D, Spadaccini R. FEBS Lett2013)15;587(22):3601-8

[22] Liu YS, Hart PJ, Schlunegger M P and Eisenberg D. (1998) The crystal structure of a 3D domain-swapped dimer of RNase A at a 2.1-angstrom resolution, *P Natl Acad Sci USA.* 95, 3437-3442.

[23] Liu YS, Gotte G, Libonati M and Eisenberg D. (2001) A domain-swapped RNase A dimer with implications for amyloid formation, *Nat Struct Biol.* 8, 211-214.

[24] Liu YS, Gotte G, Libonati M and Eisenberg D. (2002) Structures of the two 3D domain-swapped RNase A trimers, *Protein Sci.* 11, 371-380.

[25] Gotte G and Libonati M. (1998) Two different forms of aggregated dimers of ribonuclease A, *Bba-Protein Struct M.* 1386, 106-112.

[26] Gotte G and Libonati M. (2008) Oligomerization of ribonuclease A under reducing conditions, *Bba-Proteins Proteom.* 1784, 638-650.

[27] Gotte G and Libonati M. (2004) Oligomerization of ribonuclease A - Two novel three-dimensional domain-swapped tetramers, *J Biol Chem.* 279, 36670-36679.

[28] Matousek J, Gotte G, Pouckova P, Soucek J, Slavik T, Vottariello F and Libonati M. (2003) Antitumor activity and other biological actions of oligomers of ribonuclease A, *J Biol Chem.* 278, 23817-22.

[29] Fagagnini A, Montioli R, Caloiu A, Ribó M, Laurents DV and Gotte G. (2017) Extensive deamidation of RNase A inhibits its oligomerization through 3D domain swapping. *Biochim Biophys Acta*. 1865(1):76-87

[30] Laemmli UK. (1970). Cleavage of structural proteins during the assembly of the head of bacteriophage T4. *Nature* 227(5259), 680–685

[31] Sica F, Pica A, Merlino A, Russo Krauss I, Ercole C and Picone D. (2013) The multiple forms of bovine seminal ribonuclease: Structure and stability of a C-terminal swapped dimer. *Febs Lett*. 587, 3755-3762.

[32] Kunitz, M. (1946) A spectrophotometric method for the measurement of ribonuclease activity, *J Biol Chem.* 164, 563-8

[33] Crestfield AM, Stein WH and Moore S. (1962) On the aggregation of bovine pancreatic ribonuclease, *Archives of biochemistry and biophysics.* Suppl 1, 217-22.

[34] Greenfield NJ. (2006) Using circular dichroism spectra to estimate protein secondary structure, *Nature protocols.* 1, 2876-90.

[35] Bucci E, Vitagliano L, Barone R, Sorrentino S, D'Alessio G. and Graziano G. (2005) On the thermal stability of the two dimeric forms of ribonuclease A, *Biophys Chem.* 116, 89-95.

[36] Fiorini C, Gotte G, Donnarumma F, Picone D and Donadelli M. (2014) Bovine seminal ribonuclease triggers Beclin1-mediated autophagic cell death in pancreatic cancer cells, *Bba-Mol Cell Res.* 1843, 976-984.

[37] Fiorini C, Cordani M, Gotte G, Picone D and Donadelli M. (2015) Onconase induces autophagy sensitizing pancreatic cancer cells to gemcitabine and activates Akt/mTOR pathway in a ROS-dependent manner, *Bba-Mol Cell Res.* 1853, 549-560.

[38] Gotte G, Helmy AM., Ercole C, Spadaccini R, Laurents DV, Donadelli M and Picone D. (2012) Double Domain Swapping in Bovine Seminal RNase: Formation of Distinct N- and C-swapped Tetramers and Multimers with Increasing Biological Activities, *PloS one.* 7.

CHAPTER

2

Engineered C-terminal domain exploited to study the pleiotropic effects of hinge loop

Abstract

RNase A is a very well characterized protein endowed with the capability to form aggregates under well described conditions. Through 3D-DS, RNase A can exchange both N-domain and C-domain. This propensity could be strictly related to a high flexibility at hinge loops connecting each terminal domain to the protein body. Rnasrpirnase (Onconase), an omologue of RNase A whose structural features are comparable to those of RNase A, is a highly stable protein with short hinge loops. New modifications into the RNase A primary structure were introduced at the C-terminal hinge loop in order to get insights on the pleiotropic properties of this responsive region. The corresponding C-terminal loop of Onconase was used as template to design a new mutant, whose stability and swapping tendency were compared to those of the native RNase A. Differently from the wild-type RNase A, the mutant RNase A- Onc is able to form dimers spontaneously. This work allowed to investigate the relationship between genetic modifications at C-hinge loop and protein folding and misfolding.

2.1 Introduction

Pronounced modifications and alterations of the protein sequence may modulate both the local and global flexibility. Among the possible consequences, the protein stability may be affected and the oligomerization may start triggering a "gain of structure" or a "loss of structure". Many proteins are able to self-assembly by exchanging domains or secondary structure elements by the so-called 3D domain swapping (3D-DS) [1,2]. The structural determinants predictive of a swapping attitude are difficult to identify, as they are diverse and subtle. Experimental biophysical data coming from X-ray crystallography and NMR, and theoretical studies demonstrated the relevant role played in this process by the hinge loop [3,4], and by residues constituting the new interface created in the dimerization event, the so-called "open interface" [2]. Mutational studies on a relevant number of proteins have shown that the shortening or lengthening of the hinge loop can greatly alter their propensity to form domain swapped oligomers [4-8]. RNase A still represents a useful model to understand the peculiar role of hinge loops in oligomerization by 3D-DS. Wild-type RNase A, when lyophilized from 40% acetic acid, can swap and form either an N-terminal or C-terminal swapped dimer. In the N dimer, the first helix swap, whereas in the C dimer, a β-strand is exchanged. The N-terminal hinge loop (16-22), which prompts the swapping of the N-terminal helix, consists of 7 residues, while the C-terminal hinge loop (112-115) is shorter and anchors the C-terminal β-strand to the rest of the protein [6-8] In the C-swapped dimer the hinge region from each monomer extends to form interactions between β-strands and form β-stacking interactions reminiscent of the polar zipper characteristic of amyloid fibirils [3]. Eisenberg and coworkers inserted a poly-Q sequence into the hinge region resulting in an RNase A that swapped and formed amyloid fibrils. Therefore, the role that this region plays for the C-terminal dimerization of RNase A and for amyloid formation in the recombinant construct is decisive. This work focused

attention on the hinge loop at the C-terminus. This region has been engineered by substituting the residues (112-115) of RNase A with the Onconase hinge loop. Onconase is an homologous of RNase A, a ribonuclease endowed with interesting biological and pharmacological properties, such as cytotoxicity and cytostaticity against tumoral cells [9]. Onconase is characterized by a high thermal stability. Recently, Vitagliano and coworkers investigated the influence of supersecondary associations on the thermal stability in natural proteins [10]. Bioinformatics showed that β-hairpins of proteins from thermophilic organisms are characterised by short connecting loops [10]. The loop size can be highly correlated with chirality/orientation preferences of secondary structure elements. This correlation seems to be quite conserved from an evolutionary point of view in thermophilic proteins. Moreover, it seems to be particularly relevant for β-*loop*-β. Both onconase and RNase A possess this motif β-*loop*-β at the C-terminus. In Onconase the C-terminal hinge loop is shorter than the corresponding region of RNase A. This could explain the different stability between the two proteins. Indeed, RNase A has a Tm of 62° C against the 90° C measured for Onconase. In collaboration with Drs L.Vitagliano and L. Esposito (Institute of Biostructures and Bioimages, CNR, Naples) a new RNase A derivative has been designed by genetic modifications at the C-terminal hinge loop of RNase A by using Onconase C-term loop as template. The resulting recombinant protein RNaseA-Onc has been produced and characterised. The aggregation propensity of RNaseA-Onc has been also evaluated in comparison with that of the wild type RNase A.

2.2 Materials and Methods

2.2.1 Production of RNase A mutants: design, cloning, expression and purification

The mutants were designed comparing the sequence of RNase A and ONC. The computational analysis and the resulting design were performed by Vitagliano and coworkers as previously reported [10]. The synthetic gene encoding RNase A-Onc was purchased from GENEWIZ and cloned from the commercial vector pUC57 into the expression vector pET22b^{+} (Novagen). To express the protein, BL21(DE3) cells were transformed with the said plasmid. Expression and purification procedures are reported in more detail in Section C-1. Recombinant RNase A-Onc was obtained in pure monomeric form with a yield of about 12 mg per liter of LB culture medium. Protein identity, purity and homogeneity were confirmed by mass spectrometry and gel electrophoresis.

2.2.2 Circular dichroism spectroscopy

For the CD spectra, solutions of 0.15 mg×ml^{-1} of protein in 0.10 M phosphate buffer pH 6.8 were used. The measurements were performed on a JASCO J-810 spectrometer using a cell with a 0.1 cm path length. The spectra were recorded in the range 195-250 nm, with a time constant of 4s, a 2 nm bandwidth, and a scan rate of 20 nm × min^{-1}. Spectra were signal-averaged over 3 scans and they were baseline corrected by subtracting the buffer spectra recorded under the same conditions. Thermal unfolding was studied by monitoring the CD signal at 222 nm in the temperature range from 25 °C to 85 °C. The scan rate was 0.5 °C × min^{-1}.

2.2.3 Size exclusion chromatography

Liophylized pure monomeric RNase A-Onc was dissolved in water at a final concentration of 10 mg×ml^{-1}. This stock solution was used to prepare three incubation mixtures at a final concentration of 5 mg×ml^{-1} in three different solvents: ultrapure water, sodium phosphate buffer 0.40 M pH 6.7 and acetic acid solution 40% v/v. RNase A-Onc was incubated for 2 hours at 25 °C according to the procedure described by x and y [11]. After this time, each mixture was loaded on a Superdex 75 HR 10/30 column attached to an AKTA FPLC system (GE-Healthcare), at room temperature, previously equilibrated with 0.40 M sodium phosphate pH 6.7. Elution was performed with the same buffer at a flow rate of 0.6 mL ×min^{-1}.

2.2.4 Crystallization and data collection

The crystallographic study was performed by Dr. L. Esposito. The purified protein was concentrated to 15 mg× ml $^{-1}$ in 0.01 M phosphate buffer at pH 6.8. Crystals were grown by hanging-drop vapor diffusion at 296 K. The protein solution was equilibrated with 0.1 M Bis-Tris pH 6.5, and 28% w/v Polyethylene glycol monomethyl ether 2000. A single crystal was transferred to a stabilizing solution containing 15% glycerol as cryoprotectant. X-ray data were then collected at 100 K using in-house X-ray source. A complete data set (93.6% completeness) was collected at 2.31 Å resolution. Data were processed and scaled using the DENZO/SCALEPACK package.

2.3 Results and Discussion

2.3.1 C-terminus engineered RNase A mutant: background and design

The C-terminal hinge loop of Onconase was used as template to design a new mutant, RNase A-Onc. As highlighted in Fig.1, the residues GNPYV in RNase A have been substituted with the residues NQA, reminiscent of the β-loop-β motif of Onconase.

Fig. 1 Design of RNase A-Onc. Genetic modification at C-Terminus hinge loops. Wild type RNase A and RNaseA.Onc sequences are also reported.

2.3.2 C-terminus engineered RNase A mutant: production of RNase A-Onc

Recombinant RNase A-Onc was produced in E.*coli* BL21 (DE3) transformed with a pET22b^{+} expression vector containing the corresponding cDNA. The transformed cells were grown in LB medium at 37° C until reaching the final $OD_{600\ nm}$ of 0.6 when the protein expression was induced adding 0.4 mM IPTG. After 3 hours from the induction, the cells were harvested and subsequently were sonicated to extract the protein. The engineered RNase A was accumulated into the inclusion bodies so, after lysis by sonication, the cytosolic fraction and the insoluble fraction were separated by centrifugation and the following purification procedures were operated on the insoluble fraction. After many cycles of sonication and washing with detergents (Triton X) and denaturants (Urea), the protein was purified from all the endogenous proteins. Subsequently, detergents and denaturants were removed to allow the second purification level concerning the refolding under controlled conditions. The incubation of the protein using the red/ox couple Glutathion reduced and oxyded, was followed to obtain a correctly folded recombinant ribonuclease. After 20 hours, the reaction was stopped and the protein solution was loaded on a Sephadex G-75 (1.5×72 cm) column equilibrated in 0.1 ammonium acetate buffer pH 5.1 in order to purify RNaseA-Onc. The protein was eluted as monomer and its molecular weight was assessed on the basis of the elution volume on a G-75 calibrated column (Fig.2-A). The homogeneity of the sample was also assessed by SDS-PAGE and cathodic PAGE. In particular, as reported in Fig.2-B, the protein migrates as a single pure band on the native polyacrilammide gel. Interestingly, it migrates more than the wild type RNase A, accordingly to its smaller and more compact shape.

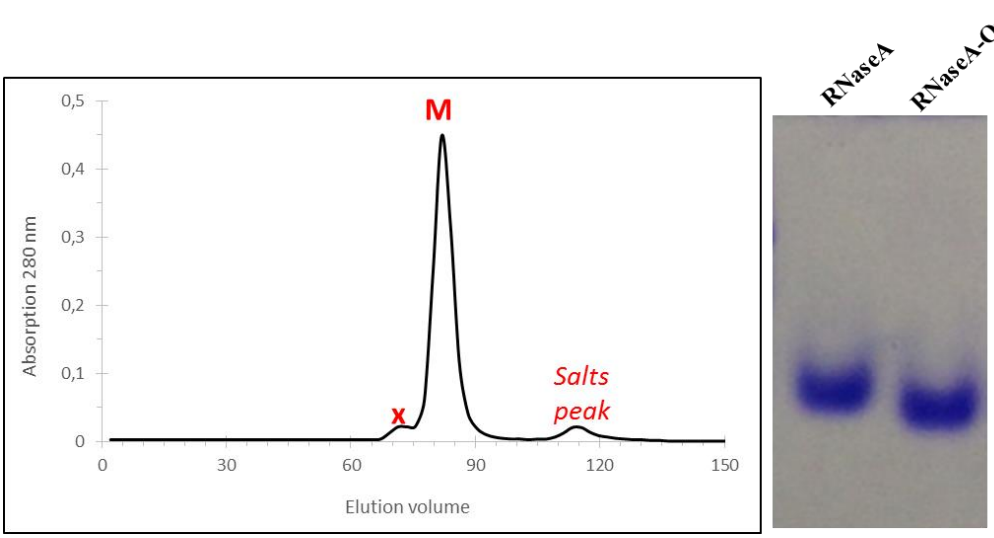

A B

Fig. 2 Purification of RNase A-Onc. (A) Size exclusion chromatography on a Sephadex G-75 (1.5×72 cm) column equilibrated in 0.1 ammonium acetate buffer pH 5.1. M: monomer. (B) Cathodic gel electrophoresis under non-denaturing conditions. Wild type RNase A is also loaded as reference.

2.3.3 Motif β-loop-β in RNase A-Onc: effects on protein stability

The biophysical characterization of RNaseA-Onc was performed using the wild-type RNase A as reference. The proper folding of the monomeric form of RNaseA-Onc was assessed by circular dichroism spectroscopy. As reported in Fig. 3, at 25 °C the CD spectra recorded for the mutant (in red) and the wild type (in black) are superimposable, revealing that the recombinant protein is well folded. CD spectra recorded at high temperature indicate that RNaseA-Onc (in green) undergoes unfolding while retaining a fraction of secondary structure, in line with the observed behavior of RNase A (in blu). This behavior was also confirmed by the sigmoidal thermal unfolding profiles shown in Fig.4. CD data indicate that the thermal stability

of RNaseA-Onc is comparable to the wild-type RNase despite the replacement of the key residues Pro114. Indeed, the T_m are 59 °C and 61 °C for RNaseA-Onc and RNase A, respectively.

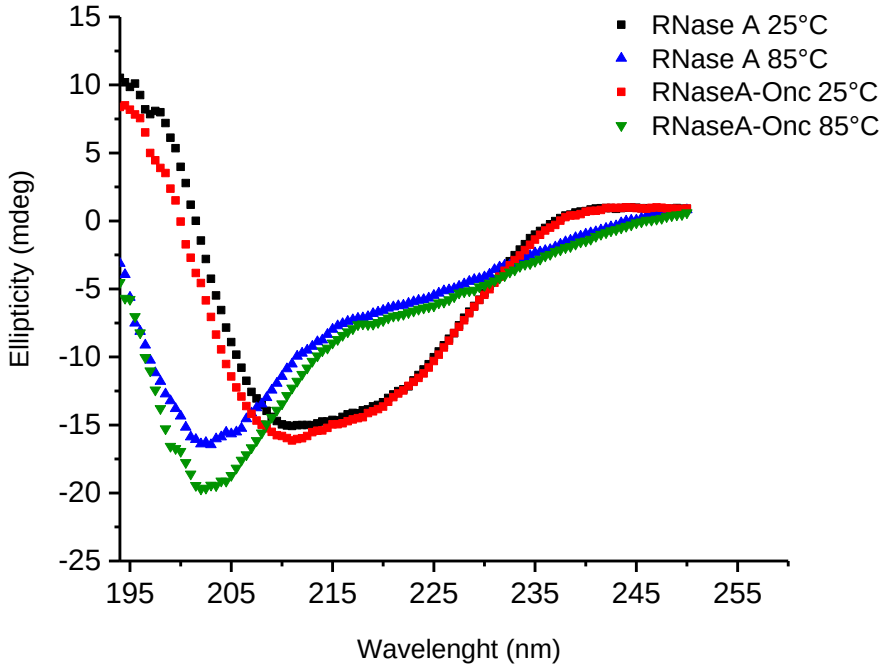

Fig. 3. Spectroscopic analysis on RNase A-Onc and RNase A wild type. CD spectra in 0.10 M sodium phosphate buffer pH 6.8 at a protein concentration of 0.15 mg×ml^{-1}. The temperature of the measurements is also reported with the following color code: 25 °C (RNase A, black), 85 °C (RNase A,blu), 25 °C (RNaseA-Onc, red), 85 °C (RNase A-Onc, green).

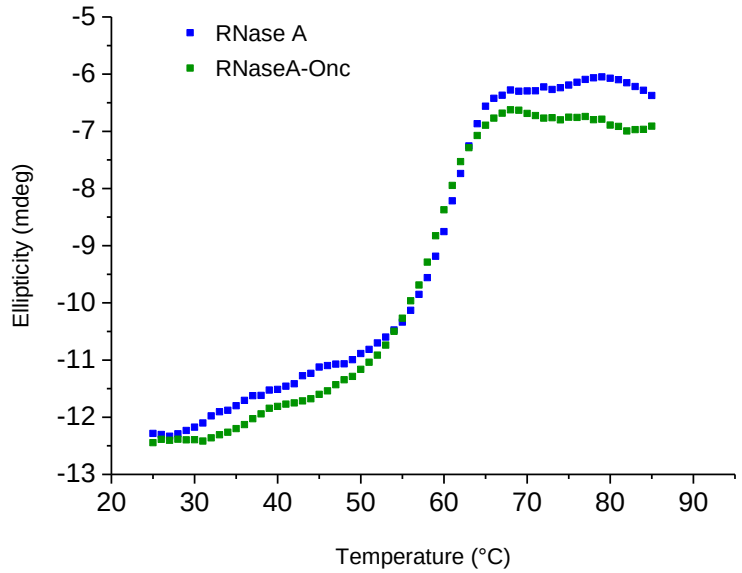

Fig. 4 Spectroscopic analysis on RNase A-Onc and RNase A wild type. Thermal unfolding profiles at 222 nm in 0.10 M sodium phosphate buffer pH 6.8 at a protein concentration of 0.15 mg×ml^{-1}. RNase A-Onc and RNase A are shown in green and in blu, respectively

2.3.4 Crystal structure of RNaseA-Onc monomer

The structure of the variant RNaseA-Onc has been solved at 2.3 Å resolution by Drs. L. Vitagliano and L. Esposito. RNaseA-Onc crystals contain three molecules in the asymmetric unit that are overall very similar. Indeed, the pairwise superposition of C^{α} atoms of two molecules (in the range of residues 3-121) yields RMSDs which are on average 0.42 Å (chain A-B RMSD=0.35 Å; chain A-C RMSD=0.45 Å; chain B-C RMSD=0.46 Å). The chain A is the best defined in the electron density out of the three, therefore it will serve as the reference model in the following discussion. To evaluate the impact of the inserted modification on the RNase A structure, the C^{α} trace of RNaseA-Onc was superimposed with that of RNase A, excluding the segment containing the mutated loop (residues 110-115 in RNaseA-Onc numbering). The RMS deviation is 0.37 Å, thus indicating that the fold is essentially unaffected

by the shortening and replacement of the loop. The main differences are concentrated in the loop region as also highlighted in Fig 5.

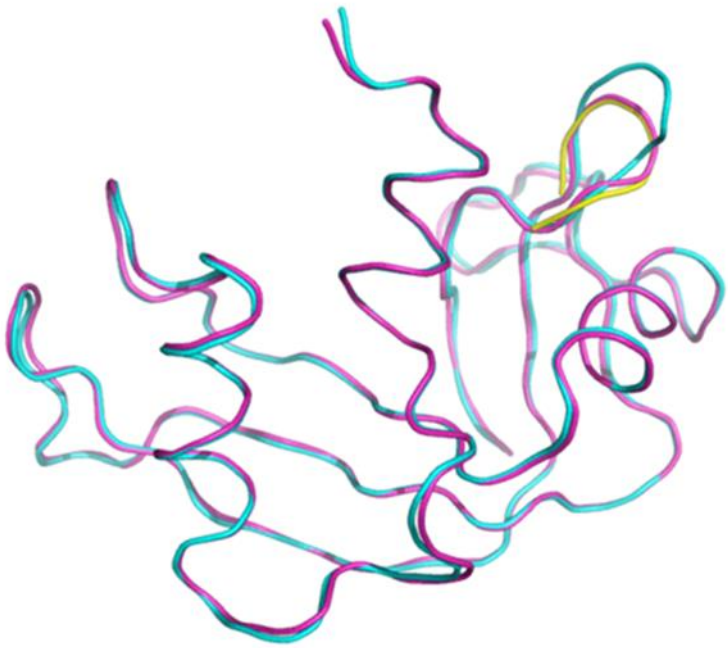

Fig. 5. Ribbon representation of the backbone trace of superimposed RNase A (cyan) and RNaseA-Onc (magenta). In yellow is shown the segment ^{90}CENQAP^{95} of Onconase which corresponds to segment 110-115 of RNaseA-Onc.

In RNaseA-Onc the modified loop adopts the same conformation of the loop in Onconase ; indeed the Cα RMSD for the segment 110-115 is as low as 0.22 Å. Specifically, the tetrapeptide E111-A114 forms a β-turn (type I') in which the two central residues (N112 and Q113) adopt unusual conformations located in the α_L region of the Ramachandran plot. As for Onconase, the local structure of RNaseA-Onc is stabilized by the hydrogen bonds E111 O…N A114 and E111 N…O A114.

Moreover, the side chains of the replaced ^{112}NQA^{114} residues do not display intramolecular interactions, being at the surface of the molecule. Therefore, the stabilization of RNaseA-Onc, in line with the design is due to a better adherence to the topology rules on the preferred combinations of secondary structure elements.

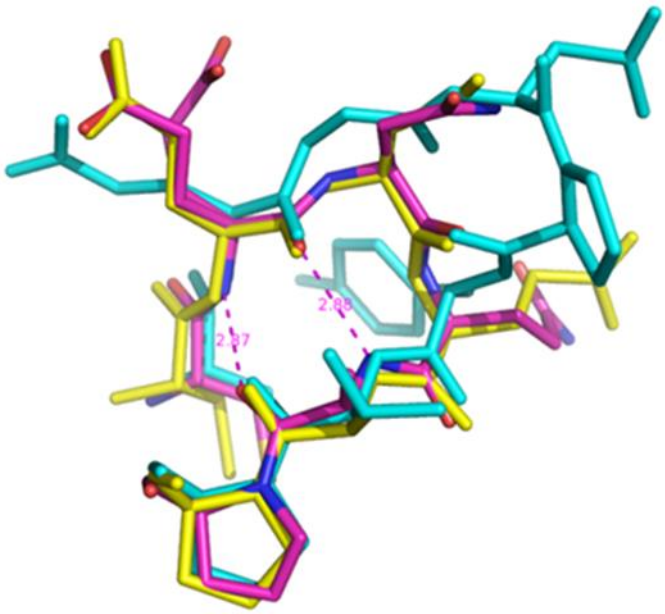

Fig. 6 The modified loop is shown in stick representation. Superimposed structures of 110-117 RNase A (cyan), 110-115 RNaseA-Onc (coloured by element: C magenta, O red, N blue, S yellow), and 90-95 Onconase (yellow). The two backbone H-bonds between E109 and A114 in RNaseA-Onc are also shown as dashed line

Furthermore, the electron density of the loop E111-A114 clearly shows that all peptide bonds adopt a trans state (Fig. 6). It is important to remember that the correspondent N113-P114 in RNase A is in *cis* state.

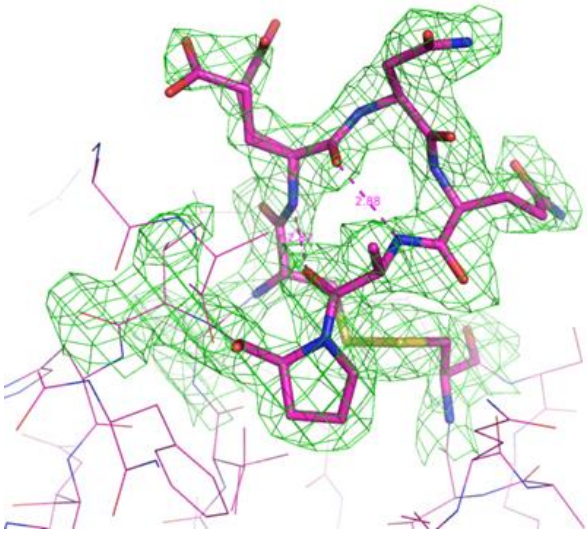

Fig. 6. The omit electron density of the mutated region in RNaseA-Onc is contoured in green. The loop 110-115 loop as well as the Cys 58 of the disulfide bridge Cys58-Cys110 are shown in stick representations, whereas the rest of the neighboring residues are depicted as lines.

2.3.5 Aggregation propensity

The aggregation propensity of the recombinant RNase A-Onc has been evaluated. A little amount of protein was incubated in 40% acetic acid solution at a concentration of 5 mg×ml^{-1} for 2 hours at 37 °C and then lyophilized. The powder obtained was dissolved in sodium phosphate buffer 0.40 M pH 6.7. As control, a similar amount

of protein was dissolved in ultrapure water at a final protein concentration of 5 $mg \times ml^{-1}$ and incubated at 37 °C for 2 hours. Furthermore, an aliquot of native RNase A was also incubated in acid acid solution 40% v/v and in water for comparison. After 2 hours, each protein sample was loaded on a Superdex 75 HR 10/30 column attached to an AKTA FPLC system previously equilibrated in sodium phosphate buffer 0.40 M pH 6.7. The chromatographic profiles reported in Fig.9, show that RNaseA-Onc oligomerizes both under denaturing conditions, i.e upon acetic acid liophylization, and under native conditions, i.e. in water. The 20% of the protein was eluted as dimer, independently on the incubation condition. On the other hand, as expected RNase A does not give rise to oligomers in ultrapure water but only under denaturing conditions, i.e. dissolution in 40% acetic acid solution (Fig.10). Thus, the chromatographic profiles obtained showed that the mutant RNase A-Onc is endowed with a spontaneous aggregation propensity, differently from the parental protein.

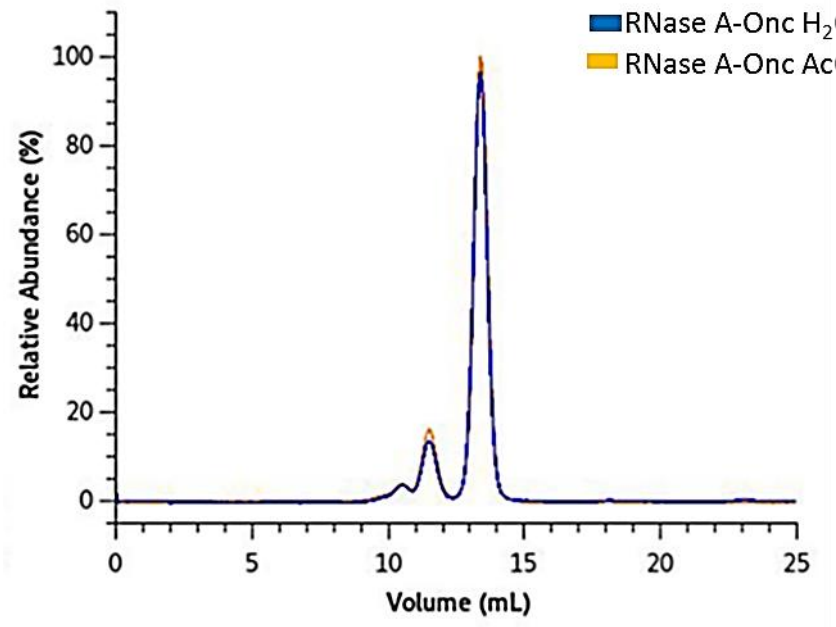

Fig. 9 Gel filtration profiles. RNase A-Onc incubation under native (blue) and denaturing (orange) conditions.

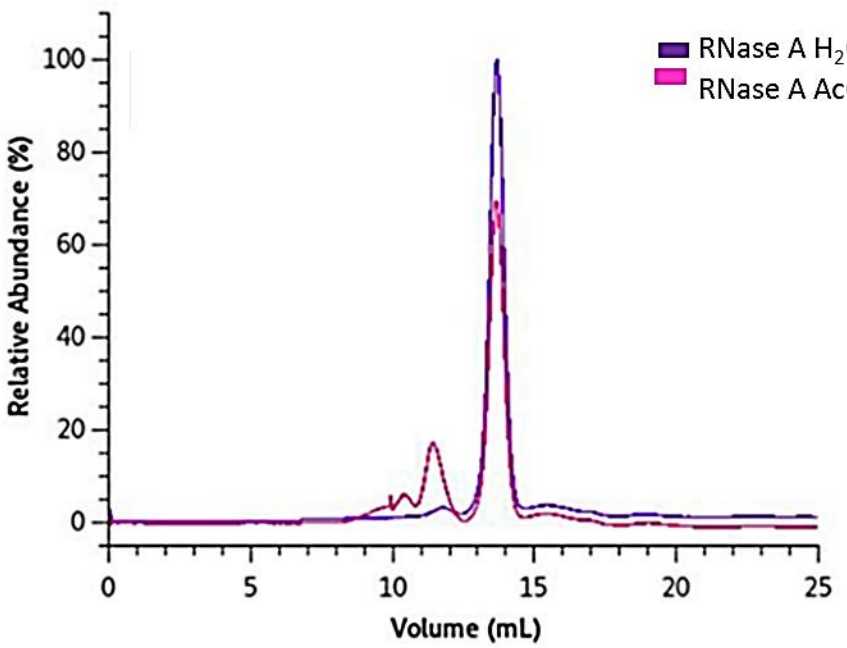

Fig. 10 Gel filtration profiles. RNase incubation under native (blue) and denaturing (magenta) conditions

2.4 Conclusions and ongoing works

Ribonucleases represent wide-spread models to study protein stability and aggregation propensity in vitro. In particular, RNase A is a very well characterised protein whose aggregation path is due to the well-known 3D-DS. According to this molecular mechanism proposed by Eisenberg, proteins can oligomerize through the reciprocal exchange of small or large regions (peptide(s) or entire domain(s)) of the monomeric subunits. Monomers exploit short flexible hinge-loops present in their sequence to address a definite domain (or more than one) into the corresponding partner subunit that will reciprocally swap an identical domain with the former subunit. Several studies indicate that hinge loops can be putative regions to trigger RNAse A oligomerization via 3D-DS involving both the hinge loops at N-terminus and that one at C-terminus. In this work, the role of C-terminal hinge loop sequence has been investigated. The short Onconase C-terminal β-hairpin element has been used as template to design a new RNase A mutant: RNase A-Onc. The effect of the mutations introduced in this sensitive region has been investigated with the aim to shed light on the pleiotropic role played by the C-hinge loop in folding/misfolding and stability. Biophysical data reveal that the shortness of the loop does not compromise the folding and the thermal stability. Moreover, the local structural arrangement was not disturbed resulting in a tertiary structure comparable to the native RNase A in the region modified. Interestingly, despite the absence of proline in this loop, RNase A-Onc shows a spontaneous aggregation propensity. Indeed, it forms dimers also under native conditions, i.e. when dissolved in water differently from the parental RNase A. According to Laurents and coworkers [12], RNase A is chiefly unfolded in 40% acetic acid; indeed even if it partially retains the native helices, the β-sheet is fully denatured and all X-Pro peptide bonds are in the *trans* conformation. Refolding occurs via an intermediate, I_N, with non-native X-Pro peptide bonds. The intermediate is an “activated form” triggering the system to swap

domains and oligomerize. In the mutant RNase A-Onc all the peptide bonds in the modified hinge loop (i.e. E111-A114) are in *trans* conformation. This evidence could explain why RNaseA-Onc aggregates spontaneously without requiring a denaturation step, as revealed by gel-filtration experiments. The structural characterization of these aggregates has not yet been performed, but it is reasonably assume that all of them are stabilized through 3D-DS. At any rate, further studies on the purified protein forms will provide a deeper characterization of the relationships between loop length and flexibility on protein aggregation, folding and stability.

2.5 References

[1] Bennett MJ, Schlunegger MP, Eisenberg D. (1995) 3D domain swapping: a mechanism for oligomer assembly. *Protein Sci.* 4(12):2455-68

[2] Liu Y, Eisenberg D. (2002) 3D domain swapping: as domains continue to swap *Protein Sci.* 11(6):1285-99

[3] Teng PK,AndersonNJ,GoldschmidtL, Eisenberg D.(2012) Ribonuclease A suggests how proteins self-chaperone against amyloid fiber formation. *Protein Sci.* 21(1):26-37

[4] Ercole C, Laurents DV. (2011) 3D domain swapping provides a minor alternative refolding pathway for ribonuclease A. *Protein Pept Lett* 18(5):467-70.

[5] Miller K.H,Karr J.R., and Marqusee S. (2010) A hinge region cis-proline in ribonuclease A acts as a conformational gatekeeper for C-terminal domain swapping. *J. Mol. Biol.* 400, 567–578

[6] Merlino A, Picone D, Ercole C, Balsamo A and Sica F. (2012) Chain termini cross-talk in the swapping process of bovine pancreatic ribonuclease. *Biochimie* 94 1108-1118

[7] Gotte G, Laurents DV and Libonati M. (2006) Three-dimensional domain-swapped oligomers of ribonuclease A: identification of a fifth tetramer, pentamers and hexamers, and detection of trace heptameric, octameric and nonameric species.*Biochim. Biophys. Acta* 1764. 44-54.

[8] Sambashivan S, Liu Y, Sawaya MR, Gingery M and Eisenberg D. (2005) Amyloid-like fibrils of ribonuclease A with three-dimensional domain-swapped and native-like structure. *Nature*.437 266-269.

[9] Notomista E, Catanzano F, Graziano G, Dal Piaz F, Barone G, D'Alessio G and Di Donato A. (2000) Onconase: an unusually stable protein. *Biochemistry.* 39(30):8711-8.

[10] Balasco N, Esposito L, De Simone A, Vitagliano L. (2013) Role of loops connecting secondary structure elements in the stabilization of proteins isolated from thermophilic organisms.*Protein Sci.* 22(7):1016-23.

[11] Crestfield AM, Stein WH and Moore S. (1962) On the aggregation of bovine pancreatic ribonuclease, *Archives of biochemistry and biophysics.* Suppl 1, 217-22.

[12] Lòpez-Alonso J, Bruix M, Font J, Ribo M ,Vilanova M, Jiménez MA, Santoro J, Gonzalez C, Laurents DV. (2010) NMR spectroscopy reveals that RNase A is chiefly denatured in 40% acetic acid: implications for oligomer formation by 3D domain swapping. *J.Am.Chem.Soc.* 132(5): 1621-3

Part B

Artificial models

MNEI

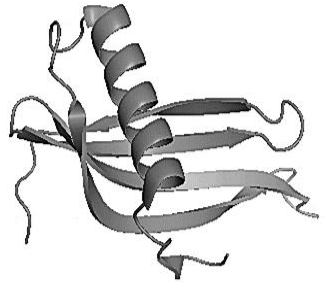

State of art

Amyloid-type protein aggregation is an important subject worth of investigation in biochemical and biophysical field [1-3].The growth of this research area has been improved by the pathological significance of the aggregation events [4-7]. From a biophysical point of view, amyloid has attracted attention because of its regular fibrous architecture and its correlation to the protein-misfolding problem [8]. Amyloidgenesis is the nucleation-dependent aggregation process mostly initiated in partially denatured states of amyloidgenic proteins [9-11]. It was also demonstrated that the amyloid-like fibrous aggregation with a β-sheet rich structure is a universal phenomenon which is not restricted to a special category of proteins [12,13]. Many unsolved problems still remain that may be coupled with diversity in the amyloid formation mechanisms.

In this Thesis, the sweet-tasting protein MNEI has been proposed to investigate fibrous aggregation.

MNEI is a single-chain derivative of the sweet protein monellin that, in recent years, has become an accepted model for studying protein dynamic properties, folding and aggregation [14-17]. Monellin is one of the best-known sweet-tasting proteins; it has been first isolated from the fruit of the tropical berry *Dioscoreophyllum cumminsii* by Morris and Cagan at the Monell Institute of California [18]. Monellin is a heterodimeric protein composed of two subunits, made of 45 (A chain) and 50 residues (B chain), respectively [19]. The protein is very stable against acidification of the solution, but undergoes heat and chemical denaturation rather easily at neutral or alkaline pH [20]. These denaturation processes are often irreversible [20] thus hampering industrial applications in food preparations of monellin as edulcorant. In order to increase the physicochemical stability and to retain the perceived sweetness, two classes of single-chain monellin derivatives have been designed, where the two chains are covalently linked [21,22]. The first single-chain monellin designed, named SCM, is a protein of 94 residues; it was obtained by directly joining the C-

terminal residue of B chain (B50E) to the N-terminal residue on the A chain (A1R) [21]. The second single-chain monellin, known as MNEI, is a protein of 96 residues obtained by linking the A and B chains through the G51-F52 dipeptide [22]. In Fig. 1 the aminoacidic sequence corresponding to monellin, SCM and MNEI is reported. The mutant SCM was the first to be characterized both in the solid state [23] and in solution [24]. Structural information about MNEI has been derived from NMR [25] and X-ray methods [26]. The topology of MNEI, like that of the parental monellin and of SCM, consists of a α-helix cradled into the concave side of a strand of five anti-parallel β-sheets [25,26]. The total folding pattern is analogous to a pathologically important amyloidgenic protein, cystatin C [27,28]. In Fig. 2, the NMR structure of MNEI is reported (PDB code: 1FA3). Even if MNEI was engineered to be more stable than the natural monellin against physicochemical changes, it shows a prominent aggregation propensity like the parental precursor and its homologous SCM [14,15]. ThT fluorescence and TEM show that MNEI gives rise to amyloid aggregation upon incubation at high temperature in presence of 0.150 M NaCl [15]. For this environment-driven aggregation-prone behaviour, MNEI represents a widespread model to study the influence of pH, temperature, ionic strength on amyloid-like protein aggregation.

Monellin

Chain A: **REIKGYEYQLYVYASDKLFRADISEDYKTRGRKLLRFNGPVPP**

Chain B:

GEWEIIDIGPFTQNLGKFAVDEENKIGQYGRLTFNKVIRPCMKKTIYEEN

SCM

GEWEIIDIGPFTQNLGKFAVDEENKIGQYGRLTFNKVIRPCMKKTIYEENREIK

GYEYQLYVYASDKLFRADISEDYKTRGRKLLRFNGPVPP

MNEI

GEWEIIDIGPFTQNLGKFAVDEENKIGQYGRLTFNKVIRPCMKKTIYENE(GF)

REIKGYEYQLYVYASDKLFRADISEDYKTRGRKLLRFNGPVPP

Fig. 1 Primary structure of Monellin, SCM and MNEI

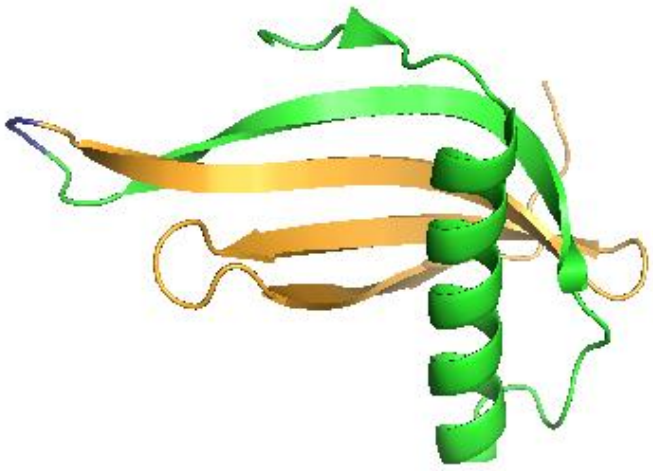

Fig. 2 3D structure of MNEI solved by NMR. PDB code 1FA3.
Green: A chain ; Orange B chain ; Blue: dipeptide linker GF

References

[1] Fink AL. (1998) Protein aggregation: Folding aggregates,inclusion bodies and amyloid. *Fold. Des.* 3: R9–23.

[2] Kelly JW. (1998) The alternative conformations of amyloidogenic proteins and their multi-step assembly pathways. *Cur. Opin. Struct. Biol.* 8: 101–106.

[3] Dobson CM. and Karplus M. (1999) The fundamentals of protein folding: Bringing together theory and experiment. *Curr. Opin. Struct. Biol.* 9: 92–101.

[4] Sipe JD. (1992) Amyloidosis. *Annu. Rev. Biochem.* 61: 947–975.

[5] Tan SY. and Pepys MB. (1994)Amyloidosis. *Histopathology* 25: 403–414.

[6] Prusiner SB,Scott MR, De Armond SJ and Cohen F.E. (1998) Prion protein biology. *Cell* 93: 337–348

[7] Koo EH, Lansbury PT Jr and Kelly JW. (1999) Amyloid diseases: Abnormal protein aggregation in neurodegeneration. *Proc. Natl. Acad. Sci.* 96:9989–9990.

[8] Dobson CM and Ellis RJ. (1998) Protein folding and misfolding inside and outside the cell. *EMBO J.* 17: 5251–5254.

[9] Jarrett JT and Lansbury PT Jr. (1993) Seeding “one-dimensional crystallization” of amyloid: A pathogenic mechanism in Alzheimer’s disease and scrapie? *Cell* 73: 1055–1058

[10] Kelly JW. (1998) The alternative conformations of amyloidogenic proteins and their multi-step assembly pathways. *Cur. Opin. Struct. Biol.* 8: 101–106.

[11] Rochet JC and Lansbury PT Jr. (2000) Amyloid fibrillogenesis: Themes and variations. *Curr. Opin. Struct. Biol.* 10: 60–68.

[12] Guijarro JI,Sunde M, Jones JA, Campbell I and Dobson CM. (1998) Amyloid fibril formation by an SH3 domain. *Proc. Natl. Acad. Sci.* 95: 4224–4228.

[13] Chiti F, Webster P, Taddei N, Clark A, Stefani M, Ramponi, G and Dobson CM. (1999) Designing conditions for in vitro formation of amyloid protofilaments and fibrils. *Proc. Natl. Acad. Sci.* 96: 3590–3594

[14] Rega MF, Di Monaco R, Leone S, Donnarumma F, Spadaccini R, Cavella S and Picone D (2015) Design of sweet protein based sweeteners: Hints from structure–function relationships. *Food Chem* 173, 1179–1186.

[15] Esposito V, Guglielmi F, Martin SR, Pauwels K,Pastore A, Piccoli R and Temussi PA (2010) Aggregation mechanisms of cystatins: a comparative study of monellin and oryzacystatin. *Biochemistry* 49, 2805–2810.

[16] Spadaccini R, Leone S, Rega MF, Richter C, Picone D. (2016) Influence of pH on the structure and stability of the sweet protein MNEI. *FEBS Letters* 590: 3681–3689I.

[17] Konno T, (2001) Multistep nucleus formation and a separate subunit contribution of the amyloidgenesis of heat-denatured monellin *Protein Sci*.(10):2093-101

[18] Morris JA and Cagan RH (1972) Purification of monellin, the sweet principle of Dioscoreophyllum cumminsii. *Biochim Biophys Acta (BBA) – General Subjects* 261, 114–122

[19] Morris JA. and Cagan RH. (1980) Formation of oligomeric monellin in protein denaturants. *Proc. Soc. Exp. Biol. Med.* 164: 351–354.

[20] Konno T, Murata K and Nagayama K (1999) Amyloid-like aggregates of a plant protein: a case of a sweet-tasting protein, monellin. *FEBS Lett* 454, 122–126.

[21] Kim SH, Kang CH, Kim R, Cho JM, Lee Y-B and Lee TK (1989) Redesigning a sweet protein: increased stability and renaturability. *Protein Eng* 2, 571–575.

[22] Tancredi T, Iijima H, Saviano G, Amodeo P and Temussi PA (1992) Structural determination of the active site of a sweet protein A 1H NMR investigation of pMNEI. *FEBS Lett* 310, 27–30.

[23] Somoza JR, Jiang F, Tong L, Kang CH, Cho JM and Kim SH. (1993) Two crystal structures of a potently sweet protein. Natural monellin at 2.75 A resolution and single-chain monellin at 1.7 A resolution. *J. Mol. Biol.* 234: 390–404.

[24] Lee SY, Lee JH, Chang HJ, Cho JM, Jung JW and Lee W. (1999) Solution structure of a sweet protein single-chain monellin determined by nuclear magnetic resonance and dynamical simulated annealing calculations. *Biochemistry*, 38, 2340-2346

[25] Spadaccini R, Crescenzi O, Tancredi T, De Casamassimi N, Saviano G, Scognamiglio R, Di Donato A and Temussi PA (2001) Solution structure of a sweet protein: NMR study of MNEI, a single chain monellin. J Mol Biol 305, 505–514.

[26] Hobbs JR, Munger SD, Conn GL. (2007) Monellin (MNEI) at 1.15 A resolution. *Acta Crystallogr Sect F Struct Biol Cryst Commun.* 1;63(Pt 3):162-7.

[27] Ghiso J, Jensson O and Frangione B (1986) Amyloid fibrils in hereditary cerebral hemorrhage with amyloidosis of Icelandic type is a variant of gamma-trace basic protein (cystatin C). *Proc. Natl. Acad. Sci.* 83: 2974–2978.

[28] Murzin AG. (1993) Sweet-tasting protein monellin is related to the cystatin family of thiol proteinase inhibitors. *J. Mol. Biol.* 230: 689–694.

CHAPTER

3

From monomers to fibres: temperature, pH and ionic strength influence MNEI stability

Abstract

Several physicochemical factors can influence the solubility of the sweet protein MNEI and its aggregation propensity. This study aimed to increase the knowledge about the factors that could affect the solubility of MNEI and direct towards different kinds of aggregates, corroborating the validity of MNEI as a model to study protein aggregation in vitro. An explorative investigation on the influence of the environmental changes, i.e. pH, temperature and ionic strength, on the protein stability has been performed. These parameters can affect the solubility and improve the tendency to form SDS-resistant aggregates. A detailed FT-IR spectroscopy analysis allowed monitoring the behaviour of MNEI both in solution and in solid state. FT-IR spectroscopy has revealed that MNEI can form aggregates rich in β-structures. A morphological characterization by AFM has allowed discriminating between ordered and amorphous species. New conditions of pH, temperature and ionic strength where MNEI gives rise to fibrillar aggregates were found.

3.1 Introduction

Protein aggregation is a general, widely observed phenomenon in proteins, but most of the times it only leads to the formation of amorphous masses of denatured proteins [1]. For biophysicists who study conformational changes of proteins, aggregation has often been an artefact disturbing their analyses. However, this situation has largely changed recently, since it has become evident that deposits of aggregates of proteins or peptides in biological tissues are often correlated with the pathogenesis of important human diseases. The conversion of globular native proteins into amyloid fibrils represents the crucial pathogenic event of systemic amyloidoses and its molecular mechanism has been extensively studied *in vitro* [2]. For prototypic globular amyloidogenic proteins, such as lysozyme [3], transthyretin [4] and wild-type β2-microgobulin (WT β2m) [5], the fibrillogenesis *in vitro* is primed by non-physiological conditions including high temperature, prolonged incubation at acidic pH, or addition of organic solvent. Structures of the fibrillar aggregates of several amyloidoogenic proteins and the mechanisms of their formation are now one of the most attractive subjects of biochemical and biophysical research. In this Thesis, the small globular protein MNEI has been proposed as a model to study the physicochemical factors that can trigger the system towards different aggregation patterns. MNEI is a very well characterized protein and it represents a prototype system for many structure-function relationship studies [6],as well as for folding, stability and self-assembly investigations [6-8]. Previous experiments carried out on this system have shown that MNEI can form amyloid fibrils when heated above its T_m at low pH in presence of NaCl [9]. The molecular mechanism leading to the fibrous aggregation is still unclear. It has been hypothesized [9], that under these conditions MNEI can open by a translocation of the α-helix; the β- elements become more exposed thus favouring the stacking between subunits and the formation of higher ordered aggregates.

Fig. 1 Schematic model for MNEI aggregation. Image adapted from Esposito et. al (2010) [9]

In this work, an extensive study on the conditions that affect protein stability has been pursued. Biochemical and spectroscopic analysis allow monitoring the conditions triggering the fibrillar aggregation. In collaboration with Prof. S.M. Doglia and Dr. A. Natalello of the University of Milan "Bicocca" a detailed FT-IR spectroscopy study has been pursued to screen new conditions where MNEI may form fibres. Additionally, in collaboration with Proffs. C. De Rosa and F. Auriemma and Dr. R. Di Girolamo, a morphological analysis of the insoluble aggregates by AFM has been performed .

3.2 Materials and methods

3.2.1 Production of recombinant MNEI

To express the recombinant protein, cells of *Escherichia coli* BL21(DE3) were transformed with the expression plasmid pET22b^{+} containing the cDNA encoding for MNEI. Protein expression and purification were performed following the procedures reported in Section C "Recombinant Proteins- Procedures", part 2. Protein identity, purity and homogeneity were assessed by mass spectrometry and electrophoresis.

3.2.2 Sample preparation

In order to ensure experimental reproducibility, before each experiment MNEI was dissolved at a protein concentration of at 10 mg×mL^{-1} in 1 mM HCl (pH 3.0) and incubated at 60 °C for 20 hours. This approach is necessary to increase solubility at high protein concentration and to to have an optimal starting point for subsequent experiments.

3.2.4 Circular dichroism (CD) spectroscopy

Circular dichroism measurements have been performed on a Jasco J815 spectropolarimeter (Jasco, Essex, UK), equipped with a Peltier temperature control system, using a 0.1 cm quartz cell. Thermal denaturation experiments were recorded following the signal at 215 nm while varying the temperature from 30 to 95 °C at a rate of 1 °C×min^{-1}. For each condition, three independent measures were performed. Experimental points were fitted to a Boltzmann curve, and fraction of unfolded protein (f_u) was calculated according to the formula (1):

$$f_u = \frac{\theta_f - \theta}{\theta_f - \theta_u} \qquad (1)$$

where θ_f and θ_u are the CD signal of the folded and unfolded state from the fitted curve, respectively, and θ is the CD signal at each temperature. In all experiments, the concentration of MNE was 0.2 mg mL^{-1} as measured by UV absorbance at 280 nm using an ε (0.1%) of 1.41. The thermal denaturation curves have been obtained at different pHs, namely: 2.5, 3.5, 5.1, 6.8 and 8.4 in 0.020 M sodium phosphate buffer. In selected pH conditions, i.e. pH 2.5 and 6.8, the thermal denaturation curves were measured for two conditions of ionic strength: 0 and 0.150 M NaCl.

3.2.3 Electrophoresis

MNEI was incubated at a concentration of 5 mg ×mL^{-1} in 0.020 M sodium phosphate buffer at different pHs (2.5, 3.5, 5.1, 6.8, 8.4) with or without 0.150 M NaCl at different temperatures (4-37-60 °C) for 2 or 24 hours. At the appropriate time points, aliquots of 20 µl were withdrawn from the experimental mixture. The remaining sample was centrifuged at 13.000 rpm for 3 min, to separate the soluble and unsoluble fractions. The latter one was resuspended in 100 µl of loading buffer. Identical volumes (20 µl) of supernatant and precipitated fractions, together with 20 µl of the total mixture, were then loaded on the same gel, to evaluate protein solubility and tendency to form SDS- resistant aggregates. SDS polyacrylamide gel electrophoresis (PAGE) was performed according to the Laemmli protocol [10] using 15% polyacrylamide gels. The oligomerization patterns were also analysed by cathodic electrophoresis under non denaturing conditions using 12% acidic polyacrylamide gels [11]. Gels were stained with Coomassie Brilliant Blue R-250.

3.2.5 Fourier Transform Infrared Spectroscopy (FT-IR)

Aliquots of MNEI at 5 mg × mL^{-1} were incubated from 2 to 24 hours in 0.020 M sodium phosphate buffer at different pHs (2.5, 3.5, 5.1, 6.8, 8.4) at different temperatures (4-60-75-85 °C) with or without 0.150 M NaCl. The protein conformational changes occurring in the time course of MNEI aggregation were monitored by FTIR measurements in Attenuated Total Reflection (ATR). For these analyses, 2 µl of the protein samples were deposed on the single reflection diamond crystal of the ATR device (ATR; Quest, Specac, USA) and dried at room temperature in order to obtain a protein hydrated film [12-13] .FT-IR spectra of the hydrated films were acquired were collected by the Varian 670-IR spectrometer (Varian Australia Pty Ltd, Mulgrave VIC, Australia) under the following parameters: 2 cm^{-1} resolution, scan speed of 25 kHz, 1000 scan coadditions, triangular apodization, and a nitrogen-

cooled Mercury Cadmium Telluride detector. Spectra were smoothed using the Savitsky-Golay method before the second derivative analysis, both performed with the Resolutions-Pro software (Varian Australia Pty Ltd., Mulgrave VIC, Australia).

3.2.6 Thioflavin T (ThT) binding assay

MNEI was incubated at a concentration of 3 mg × mL^{-1} in 0.020 M sodium phosphate buffer pH 2.5 and pH 6.8 at 75 °C with or without 0.150 M NaCl for one week. At each aggregation kinetic time point, a sample aliquot was withdrawn and diluted to 10 µM in 0.020 M sodium phosphate buffer pH 2.5 and pH 6.8 containing 30 µM of ThT just before the measurement. Fluorescence emission spectra were acquired on a HORIBA Fluoromax spectrofluorimeter in the range 460–600 nm with scan speed of 100 nm×min^{-1}, upon excitation at 440 nm. Excitation and emission slits were both set at 5 nm. Fluorescence intensity values at 485 nm were normalized with respect to the values obtained for a 30 µM ThT sample recorded in the same day, and plotted as a function of time. The reported values represent the means from three independent experiments.

3.2.7 Atomic Force Microscopy (AFM)

MNEI was incubated at 3 mg ×mL^{-1} 0.020 M phosphate buffer at pH 2.5 and 6.8 with or without 0.150 M NaCl at 75 °C. After one week of incubation, a sample aliquot was withdrawn and diluted 100-fold (0.03 mg×mL^{-1}) in ultrapure water, deposited on a clean mica sheet and air dried. The mica was then washed with ultrapure water to remove any deposited salt and gently dried again. AFM measurements were carried on a Bruker Multimode 8. Images were taken in air under ambient conditions at a scan frequency of 1 Hz. Scan size was varied from 2 x 2 µm to 0.5 x 0.5 µm, depending on sample homogeneity.

3.3 Results and Discussion

3.3.1 Thermal stability

In order to evaluate the structural stability of MNEI in a wide range of physicochemical conditions, the thermal denaturation profiles were compared by CD spectroscopy at five different pH values, 2.5, 3.5, 5.1, 6.8 and 8.4. Full heat denaturation curves were acquired by monitoring the CD signal intensity at 215 nm over the range 30–90 °C, as described in the experimental section. All the curves recorded are consistent with a simple two state equilibrium between folded and unfolded forms (Fig. 2). In table 1 are reported the T_m estimated for each condition of pH.

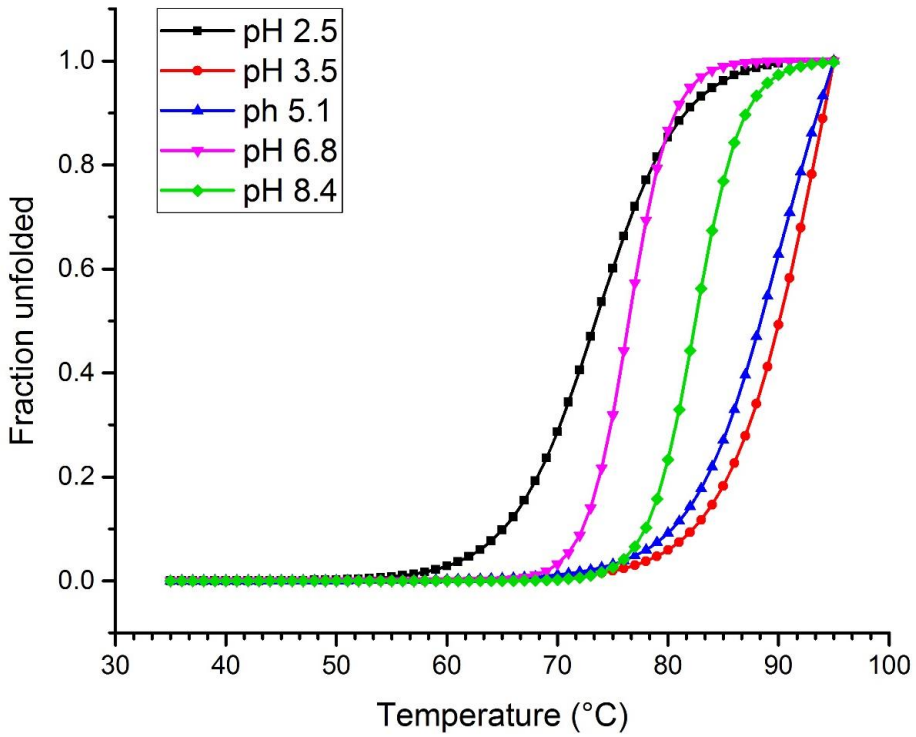

Fig. 1 Spectroscopic analysis at different pHs. Thermal unfolding profiles at 222 nm in 0.020 M sodium phosphate buffer pH 2.5 (black), 3.5 (red), 5.1 (blue), 6.8 (magenta), 8.4 (green).

pH	T_m (°C)
2.5	73 ±1
3.5	88 ±1
5.1	86 ±1
6.8	76 ±1
8.4	79 ±1

Tab. 1 Thermal unfolding parameters. Comparison between the denaturation temperatures of MNEI at pH 2.5, 3.5, 5.1, 6.8 and 8.4

CD data show that pH affects thermal stability at different levels. At pH 2.5 MNEI is less stable as indicated by its lower T_m; maximum stability is observed at intermediate acidic pHs (3.5 and 5.1). At neutral (pH 6.8) and alkaline (8.4) pHs, stability reverts to values close to those observed at pH 2.5.

3.3.2 Aggregation propensity under non-denaturing conditions

Several conditions were firstly explored by SDS-PAGE 15% to assess the aggregation propensity of MNEI. As reported in the experimental section, MNEI was incubated at a final protein concentration of 5 mg×ml^{-1} for 2 hours in 0.020 M sodium phosphate buffer at different pH (2.5, 5.1, 6.8, 8.4) and at 4, 37 and 60 °C, i.e. at temperatures under its T_m. After 2 hours of incubation, aliquot of 20 µl were withdrawn for the control, while the remaining parts were centrifuged at 13000 rpm for 5 minutes to separate the soluble fraction from the insoluble one. Identical volumes of 20 µl of supernatant and precipitate were then loaded on the same gel.

As reported in Fig. 2 (panels A-D) a prominent aggregation is revealed in all the explored conditions. The oligomers formed in every experimental condition, would appear to be SDS resistant.

The observations deriving from these experiments can be summarized in more details as follows:

- at acidic pH (2.5, panel A) MNEI can form dimers and minor amounts of higher oligomers . Higher temperature (60 °C) favours solubility, because the amount of insoluble species decreases if compared to the patterns obtained at 4 or 37 °C;
- at weakly acidic pH (5.1, panel B), high temperature compromises solubility, as indicated by the presence of aggregates into the precipitated fraction. The amount of soluble dimer slightly decreases;
- at neutral pH (6.8, panel C) and alkaline pH (8.4, panel D), higher size insoluble oligomers are predominantly formed. Differently from the acidic condition, a temperature increase has a deleterious effect on the protein solubility, leading to massive precipitation. Additionally, at pH 8.4, significant amount of oligomers of high molecular weight are detected also into the upper side of the stacking gel.

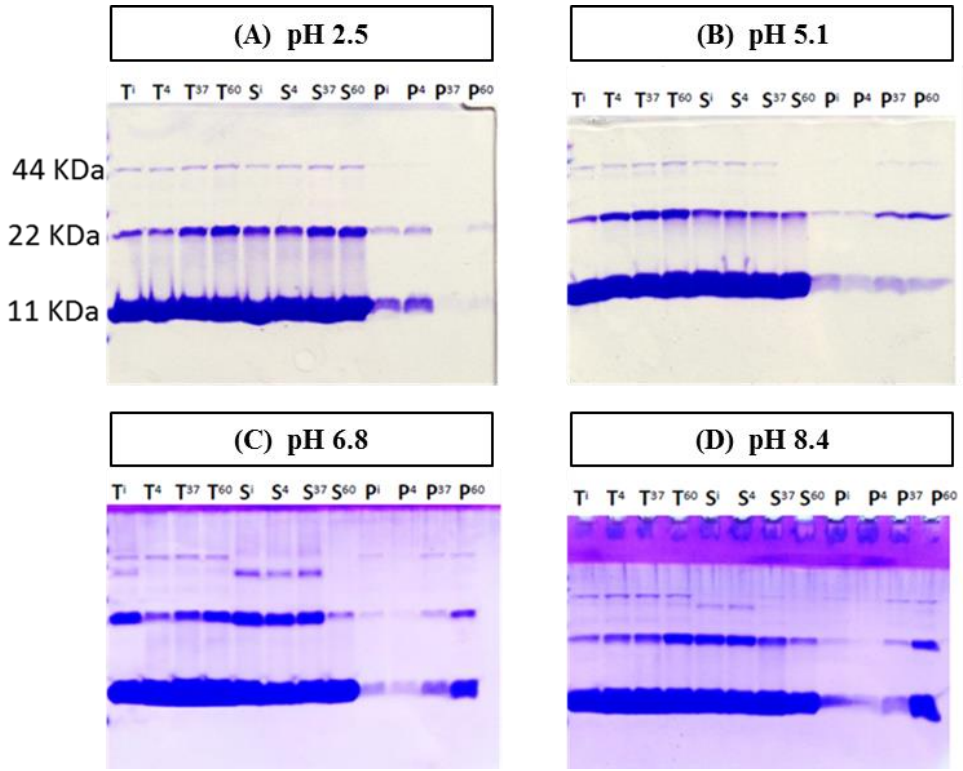

Fig. 2 MNEI aggregation profiles. Gel-electrophoresis under denaturing conditions (SDS-PAGE 15%) after 2 h of incubation of MNEI (5 mg×ml^{-1}) at 4,37 and 60 °C in sodium phosphate buffer pH 2.5 (A), pH 5.1 (B), pH 6.8 (C), pH 8.4 (D). T: total; S: supernatant; P: precipitated. Temperatures are indicated as superscript. A starting point is also reported and indicated with I: initial point.

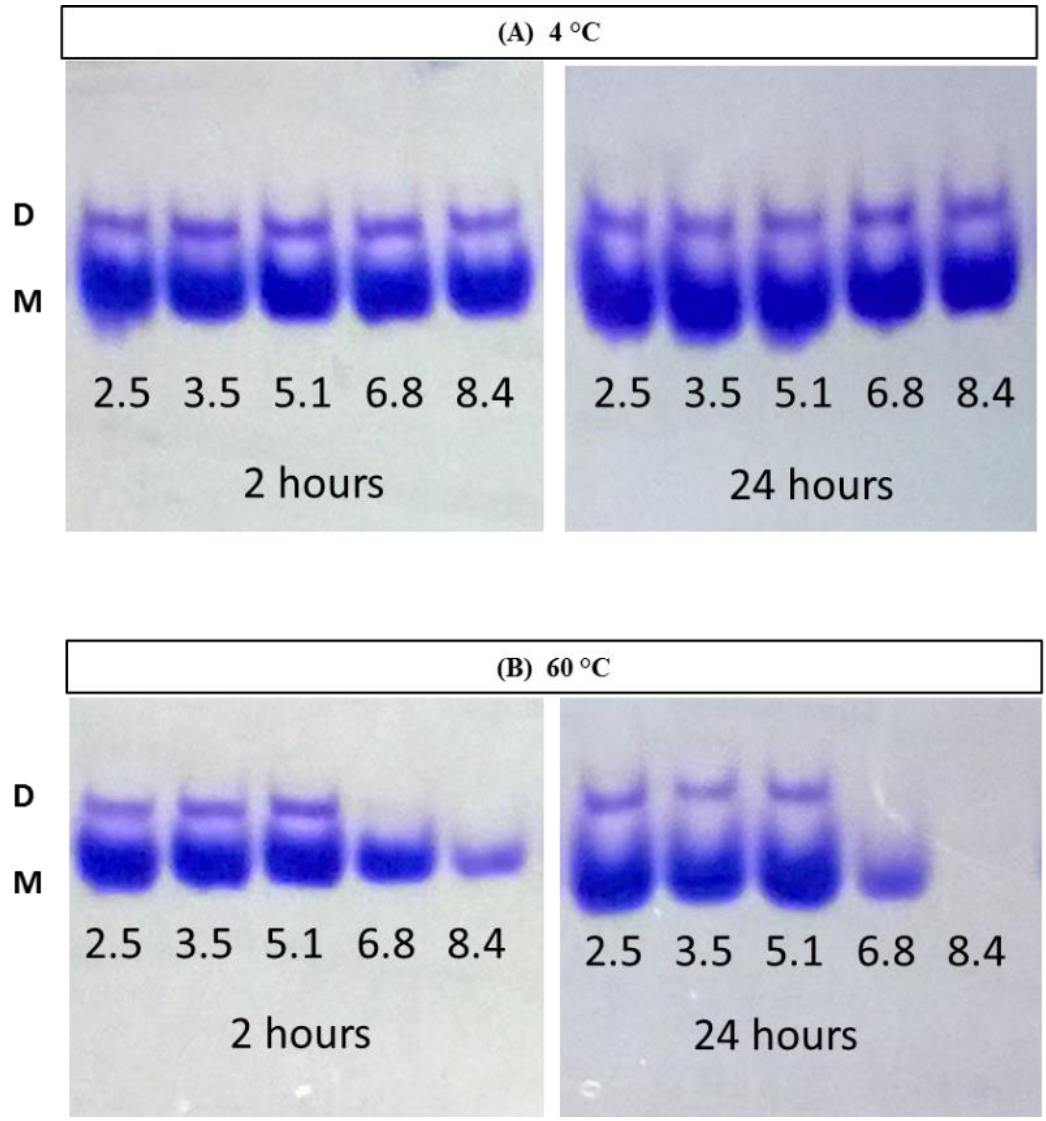

Fig. 3 MNEI aggregation profiles. Cathodic gel-electrophoresis under non-denaturing conditions (native-PAGE 12%) after 2 and 24 h of incubation of MNEI (5 mg×ml^{-1}) at 4 °C (A) and 60 °C (B) in 0.020 M sodium phosphate buffer pH 2.5, 5.1, 6.8 and 8.4. M: monomer; D: dimer.

Furthermore, in order to minimize effects related to the SDS treatment that could partially dissolve the higher oligomers formed, the behaviour of MNEI was also investigated by cathodic PAGE (Fig. 3). MNEI was incubated at a final concentration of 5 mg×ml^{-1} in 0.020 M sodium phosphate buffers at pH 2.5-3.5-5.1-6.8 and 8.4 for

2 or 24 hours at 4 °C (panel A) and 60 °C (panel B). As reported in Fig.4-A, lower temperature does not affect protein solubility in any of the pH conditions. Indeed significant amounts of about 20% of dimer still remain in solution and are detectable on gels. Major differences in the aggregation patterns are more remarked at 60 °C (Fig.3-B). In particular:

- at acidic pHs (2.5-3.5 and 5.1), both the monomer and the dimer remain in solution after 24 hours;
- at neutral (6.8) and alkaline (8.4) pHs, the solubility prominently decreases in a time dependent way. In fact, after 24 hours, only a little amount of monomer is revealed in solution at neutral pH. At alkaline pH, the solubility is instantly decreased and after 24h no precipitation is quantitative.

Comparison of the aggregation patterns obtained by denaturing and non-denaturing PAGE reveals that higher oligomers may be detectable only by SDS-denaturing electrophoresis upon partial dissolution of these forms that migrate as dimers and small size aggregates. On the other hand, besides the monomeric protein, only dimeric forms are detectable on the native PAGE because of the low solubility of the higher oligomers.

3.3.3 FT-IR spectroscopy: a new tool to study soluble and insoluble species

In order to improve the investigation on the effects of pH and temperature on MNEI aggregation, kinetics measurements performed by FT-IR spectroscopy were collected. Whit this aim, MNEI was incubated at 5 mg × ml^{-1} in 0.020 M sodium phosphate buffers at pH 2.5- 3.5- 5.1- 6.8- 8.4 at 4 and 60 °C. As described in the experimental section, aliquots of 2 µl of samples were deposed on the ATR diamond and FT-IR spectra were collected before and after 2-6 and 24 hours of incubation. After 24 hours, the mixtures were centrifuged at 13000 rpm for 5 minutes to

additionally analyse the precipitated fraction eventually formed during prolonged incubation. FT-IR approach allowed monitoring the behaviour of MNEI with an eye both on the soluble and insoluble species at the same time thus extending the information deriving from the electrophoretic analyses and overcoming the side effects of SDS treatment. FT-IR spectroscopy very precisely discriminates between closely related protein secondary structures by analysing the Amide I band mainly associated with C=O stretching vibrations of the peptide bonds in the 1700-1600 cm^{-1} spectral regions [15-17]. Tab. 2 reports the peak positions related to secondary structures elements, which were considered during FT-IR analyses to monitor the conformational changes.

Fig. 4 (panels A-D) reports the second derivative spectra acquired at 4 °C. In all the conditions of pH explored, MNEI preserves all its secondary structure elements. Indeed, the signal around 1660 cm^{-1} is not affected revealing that the α-helix was not perturbed. At the same time, the signal at 1635 cm^{-1} referred to intramolecular β-sheets is also preserved even if its intensity slowly increases in a time dependent way suggesting that the intramolecular interactions, mainly H-bounds, became weaker [16,18]. On the other hand, a shoulder around 1620 cm^{-1} start appearing: it is diagnostic for intermolecular β-sheets and hints aggregation. This negative peak is more clearly appreciable into the precipitated fraction isolated by centrifugation after 24 hours (red lines). This behaviour suggests that a low temperature only a weak aggregation occurs even if no significant differences among the pH are significant.

Peak position form second derivatives (cm-1)	Assignment to the protein secondary structures
≈1679	Turn
≈1660	α-helix/random coil
≈1635	Intramolecular β-sheets
≈1614.5	Intermolecular β-sheets

Tab. 2 FT-IR spectroscopy. Spectral regions and secondary structure elements.

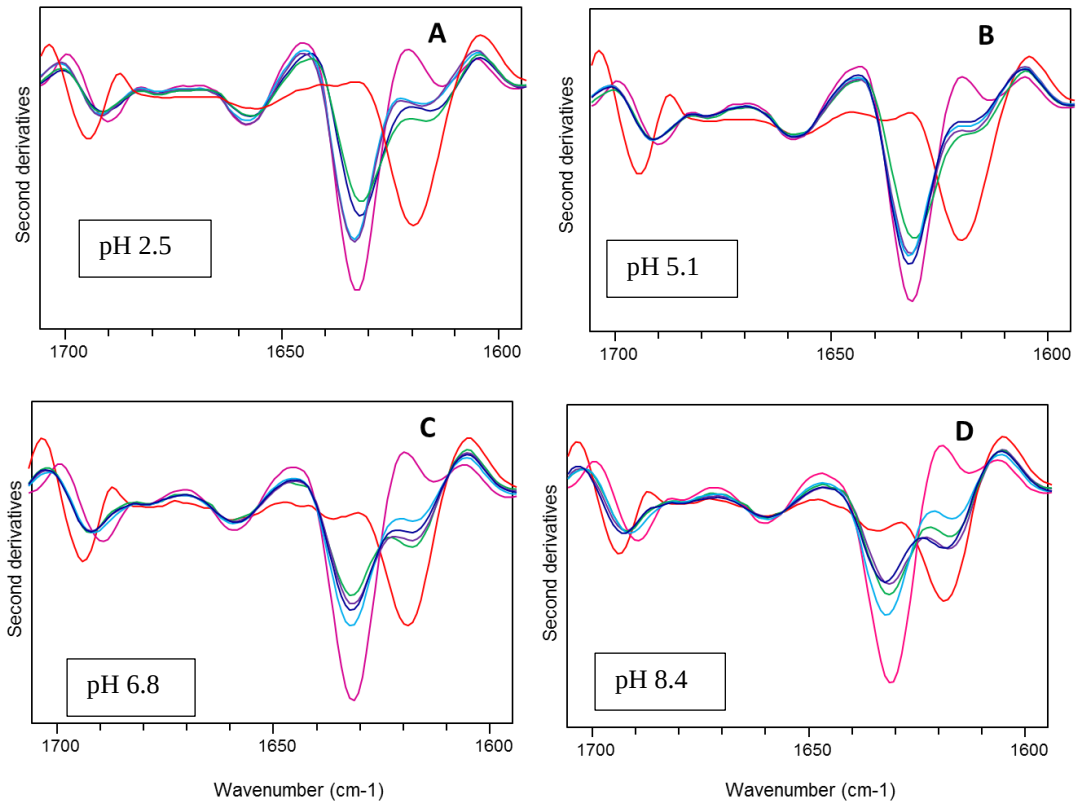

Fig. 4 MNEI aggregation profile at 4 °C monitored by FT-IR spectroscopy in ATR mode. Second derivative spectra recorded after 2-6 and 24 h. MNEI incubation in 0.020 M phosphate buffers at different pH: 2.5(A); 5.1 (B); 6.8 (C); 8.4 (D). Each line corresponds to different time of incubation: starting point (blue); 2 h (cyan); 6 h (violet); 24 h (green). After 24 h, the supernatant (magenta line) and precipitate (red line) are also analysed.

At 60 °C, major differences between acidic, neutral and alkaline pH were observed (Fig. 5, panels A-D). As reported in panels A-B, MNEI has a similar behaviour when incubated at low and weakly acidic pH, because the comparison of panels A and B shows that all the secondary structure elements are conserved and the negative peak around 1620 cm^{-1} is only found after prolonged incubation in the precipitated fraction (red lines), suggesting that aggregation occurs slowly.

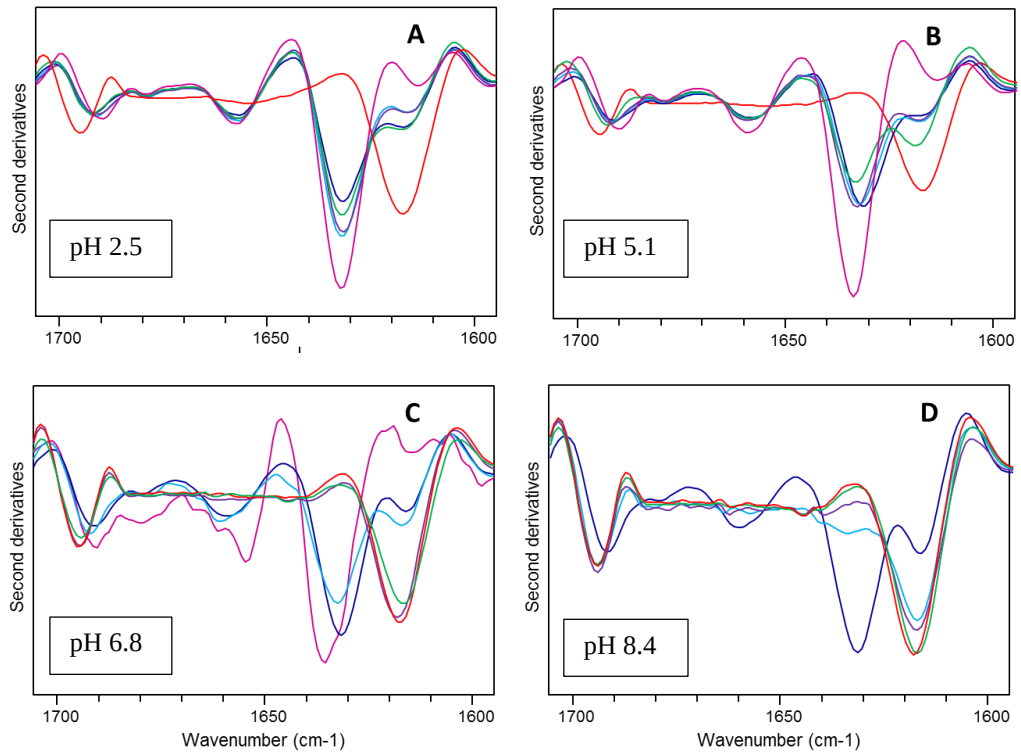

Fig. 5 MNEI aggregation profile at 60 °C monitored by FT-IR spectroscopy in ATR mode. Second derivative spectra recorded after 2-6 and 24 h. MNEI incubation in 0.020 M phosphate buffers at different pH: 2.5(A); 5.1 (B); 6.8 (C); 8.4 (D). Each line corresponds to different time of incubation: starting point (blue); 2 h (cyan); 6 h (violet); 24 h (green). After 24 h, the supernatant (magenta line) and precipitate (red line) are also analysed.

Conversely, at neutral and alkaline pH (panels C-D), the aggregation kinetics are faster. In more details: at pH 6.8, the negative peak at 1620 cm^{-1} is detected after only 6 hours (panel C, violet line), while at pH 8.4 this diagnostic peak is revealed already after 2 hours (panel D, cyan line). Interestingly, at these pHs the looseness of α-helix signal and the peak shift from 1635 to 1620 cm^{-1} were detected already in the protein mixture, i.e. without centrifuge the samples. This result suggests that aggregation occurs rapidly depriving the solution of the native folded monomeric species solution, as revealed by the noisy spectra on the supernatant fraction (magenta line). Interestingly, at 60 °C it was also observed that the intensity of the

negative peak at 1620 cm $^{-1}$ significantly decreases when pH changes suggesting that the aggregates are characterised by stronger interactions (H-bounds) between the β-elements [16,18].

FT-IR spectroscopy clearly reveals the formation of insoluble aggregates confirming the behaviours observed by electrophoresis, i.e. that neutral and alkaline pHs deeply influence solubility and aggregation. The temperature only affect the rate of the process.

3.3.4 The influence of NaCl on the formation of high molecular aggregates

We have so far ascertained that pH deeply influences the solubility and the size of aggregates and that, at neutral or alkaline pH, temperature accelerates the aggregation. In the following experiments, the influence of ionic strength on the aggregation propensity was also investigated. The analyses were restricted to two conditions of pH reproducing the acidic and the neutral environment, i.e. pH 2.5 and pH 6.8. Thermal stability was assessed by CD spectroscopy, collecting the thermal denaturation profiles with or without 0.150 M (Fig.6) at pH 2.5 (panel A) and pH 6.8 (panel B). NaCl does not affect the thermal stability of MNEI. In fact, as shown in Fig.6 and also summarized in Tab.2, at pH 2.5 (panel A) MNEI increases its T_m of 3 °C while at pH 6.8 (panel B) no further gain in stability is promoted by the addition of salt.

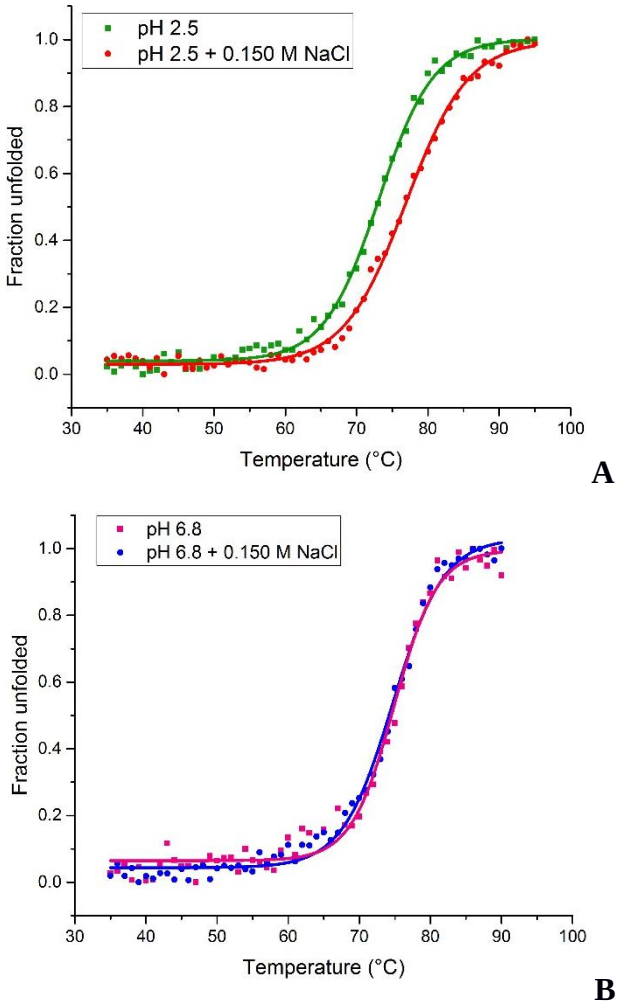

Fig. 6 Effects of NaCl on thermal stability.. Thermal unfolding profiles at 222 nm in 0.020 M sodium phosphate buffer pH 2.5 (A) and pH 6.8 (B) with or without 0.150 M NaCl.

pH	NaCl	T_m (°C)
2.5	NO	73 ±1
2.5	0.150 M	76 ±1
6.8	NO	76 ±1
6.8	0.150 M	76 ±1

Tab.2 Thermal unfolding parameters. Comparison between the denaturation temperatures of MNEI at pH 2.5 and 6.8 with or without 0.150 M NaCl

In order to evaluate the influence of NaCl on oligomerization, MNEI was incubated in these two conditions of pH, i.e. 2.5 and 6.8 sodium phosphate buffers, with 0.150 M NaCl at 60 °C, under T_m. The oligomerization has been monitored by cathodic electrophoresis under non-denaturing conditions. As reported in Fig.7-A, NaCl affects the solubility of MNEI in all the conditions of pH explored.

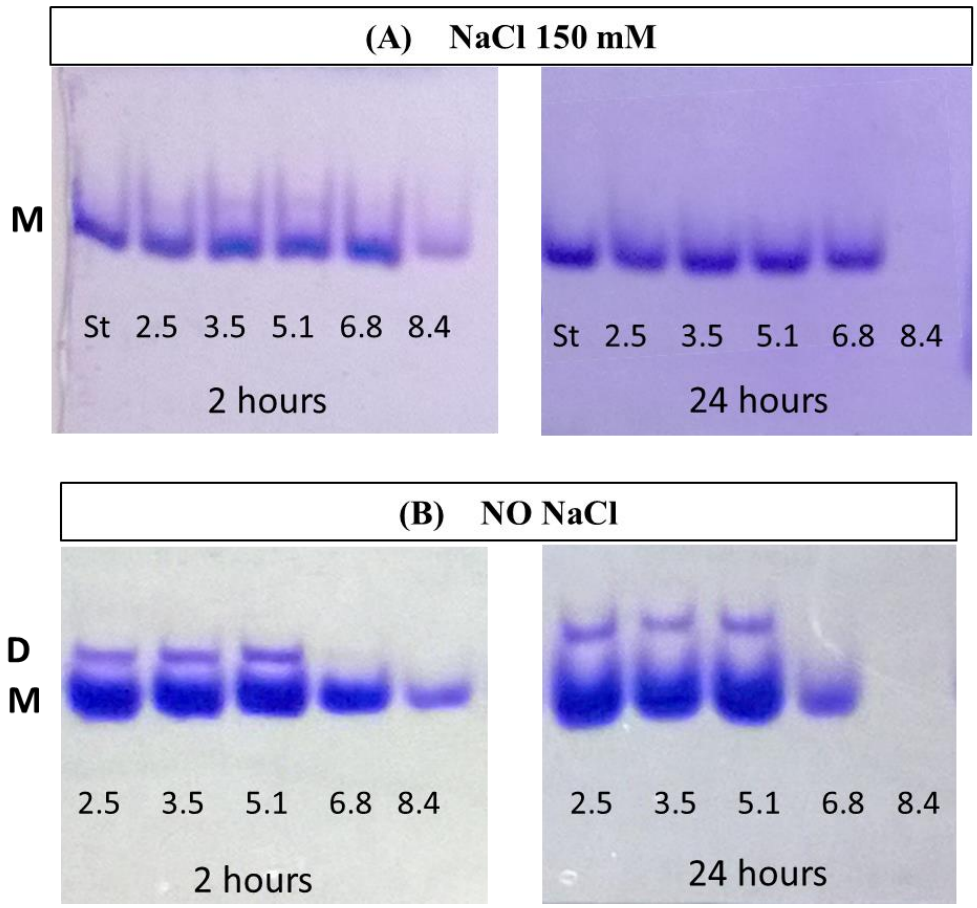

Fig. 7 MNEI aggregation profiles. Cathodic gel-electrophoresis under non-denaturing conditions (native-PAGE 12%) after 2 and 24 h of incubation of MNEI (5 mg×ml^{-1}) at 60 °C in 0.020 M sodium phosphate buffer pH 2.5,3.5, 5.1, 6.8 and 8.4 with (A) or without (B) 0.150 M NaCl. M: monomer; D: dimer. St: MNEI monomeric form used as reference.

Differently from what observed without NaCl (panel B), no dimers are detectable on the gels and the amount of monomers also significantly decreases prolonging the

time of incubation, especially at neutral and alkaline pH. This result suggests that NaCl triggers the formation of insoluble species.

3.3.5 MNEI fibrillization: new conditions

It has been reported that MNEI forms fibrillar aggregates at low pH, high temperature and by adding 0.150 M NaCl [9]. As described in the previous sections, both at acidic and neutral pH, MNEI gives rise to insoluble aggregates characterised by intermolecular β-sheets. In this section, new FT-IR spectroscopic analyses were aimed to understand if any of the conditions so far explored could lead to the formation of ordered fibrils instead of amorphous aggregates. FT-IR spectra were collected upon incubation of MNEI at pH 2.5 and 6.8 with or without 0.150 M NaCl at 75 °C and 85 °C, i.e. around and above the T_m. Two regions on the IR spectra were monitored: 1620 cm^{-1} (focusing on the diagnostic peak shift from 1635 cm^{-1}) and 1660 cm^{-1} (focusing on the looseness of the α-helix signal). The second derivatives of the IR absorption spectra at pH 2.5 with or without 0.150 M NaCl at 75 and 85 °C are reported in Fig.8 (panels A-D). It is worth to recall that condition D (pH 2.5-0.150 M NaCl- 85 °C) corresponds to the one investigated by Esposito et al., [9] who detected the presence of fibrils by TEM. At 75 °C without NaCl (panel A), a negative peak around 1620 cm^{-1} appears in the sample analysed after 2 hours and progressively increases after 4 hours. The signal around 1660 cm^{-1} was not affected. Conversely, whit NaCl (panel B), the negative peak at 1620 cm^{-1} rapidly appears and the signal at 1660 cm^{-1} disappears already after 2 hours. Specular behaviours were observed at 85 °C (panels C-D). The high similarity of the FT-IR patterns recorded at 75°C in presence of NaCl with the experimental conditions where MNEI forms fibres, suggests that fibres could form also around the T_m. Without NaCl, MNEI also shows a pattern diagnostic for fibrillization, even if the overall aggregation rate is lower suggesting that NaCl deeply influences the kinetics of the process.

At neutral pH different behaviours were observed (Fig. 9, panels A-D): by comparing the two conditions of ionic strength at 75 ° C (panels A-B), similar aggregation patterns are revealed with or without NaCl showing that the formation of intermolecular β-sheets and the looseness of α-helix occur very quickly already after 2 hours. Similarly, MNEI also promptly aggregates at 85 °C whit or without NaCl (Panels C-D). All the patterns obtained at neutral pH are also comparable to those collected at low pH with NaCl, suggesting that at pH 6.8 the role of NaCl is not so decisive.

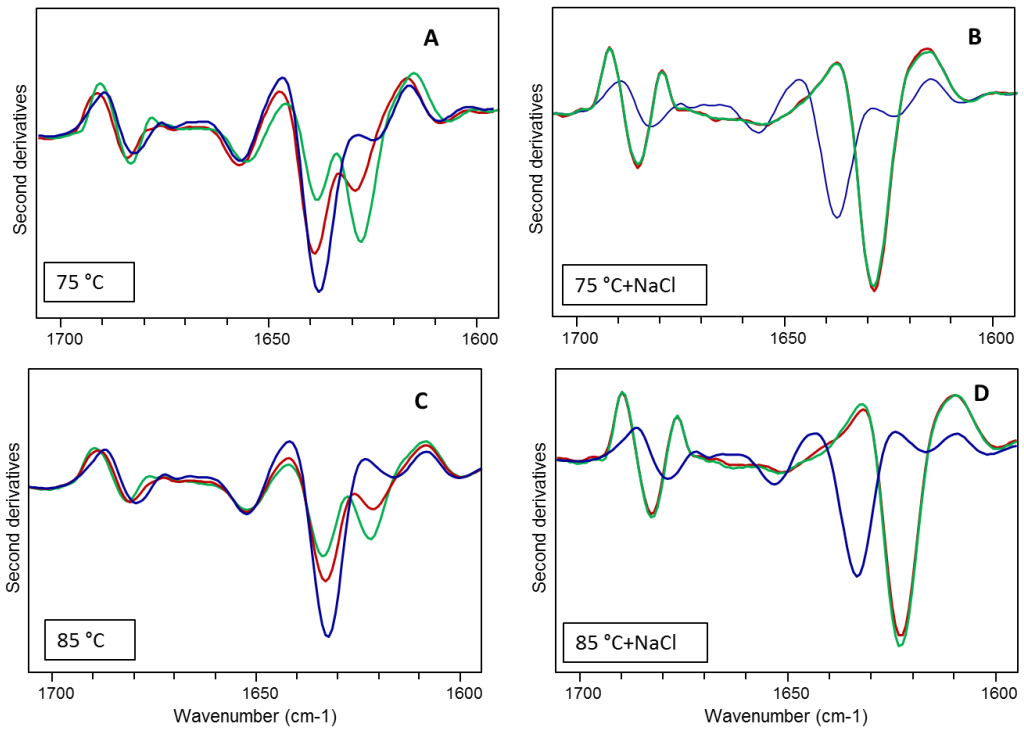

Fig. 8 MNEI aggregation profiles at pH 2.5 at high temperature with or without NaCl monitored by FT-IR spectroscopy. Second derivative spectra recorded for 4 hours. MNEI incubation in 0.020 M sodium phosphate buffers at: 75 °C without NaCl (A); 75 °C with 0.150 M NaCl (B); 85 °C without NaCl (C); 85 °C with 0.150 M NaCl (D). Each line corresponds to different time of incubation: starting point (blue); 2 h (purple); 4 h (green).

These FT-IR profiles reported that decreasing even at lower temperature, i.e. around its T_m , MNEI shows patterns compatible to one obtained in fibrilization condition reported in literature.

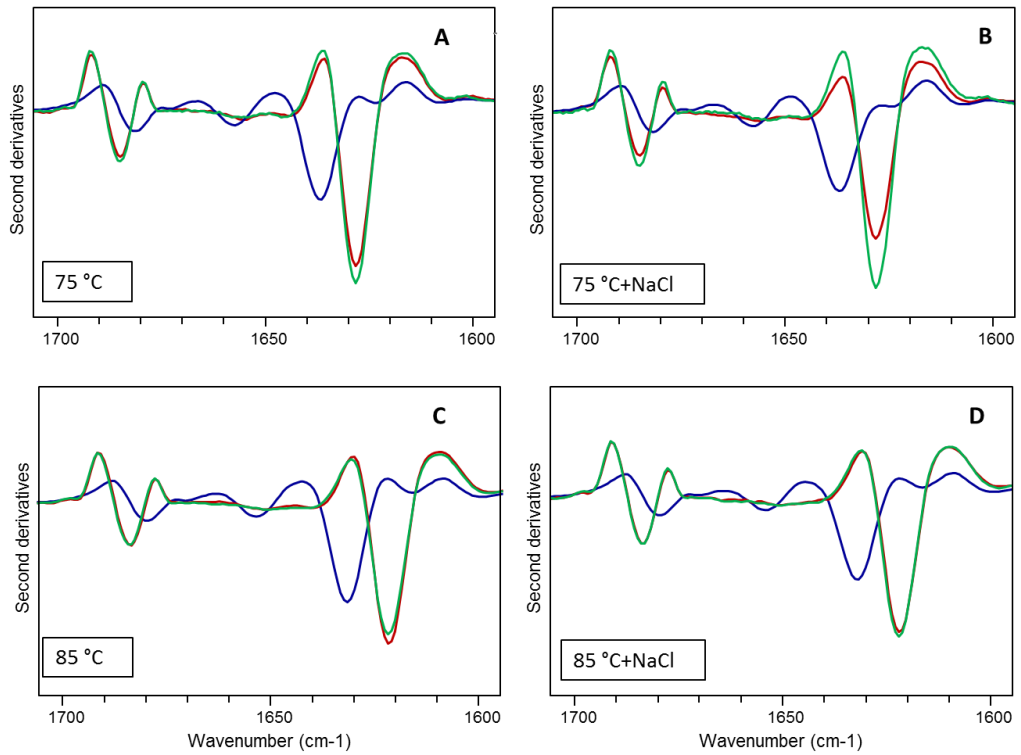

Fig. 9 MNEI aggregation profiles at pH 6.8 at high temperature with or without NaCl monitored by FT-IR spectroscopy. Second derivative spectra recorded for 4 hours. MNEI incubation in 0.020 M sodium phosphate buffers at: 75 °C without NaCl (A); 75 °C with 0.150 M NaCl (B); 85 °C without NaCl (C); 85 °C with 0.150 M NaCl (D). Each line corresponds to different time of incubation: starting point (blue); 2 h (purple); 4 h (green).

3.3.5 ThT binding

Electrophoretic data provide a rational basis to select new conditions of pH, temperature and ionic strength leading to insoluble species. FT-IR restrict the investigation on the conditions triggering fibrilization. Indeed, it suggests that both at acidic and neutral pH at 75 °C, intermolecular β-sheet can form with or without NaCl and α-helix signal also progressively disappears. These behaviours may hints the formation of fibrillar structures. A common hallmark of fibrillar aggregates rich in β-elements is the capability to bind Thioflavin T (ThT). Thus, preliminary checks were pursued by evaluating the ThT binding on β structures thorough a fluorescence assay. MNEI has been dissolved at 3 $mg \times ml^{-1}$ in 0.020 M sodium phosphate at pH 2.5 and pH 6.8, with and without 0.150 M NaCl and incubated at 75 °C until one week (168 hours) . At this time, a clear ThT fluorescence intensity plateau was detected. ThT fluorescence intensities in function of time are reported in Fig.10, panels A-B. In all the conditions explored, a positive ThT fluorescence signals were detected but some differences in the kinetics of ThT binding are revealed.

a) ThT fluorescence emission was pH dependent. In fact, at acidic pH (panel A) the kinetics is lower than what observed at neutral pH (panel B), where the fluorescence reaches plateau very fast, already after 24 hours of incubation while at pH 2.5 the plateau is detectable after one week.
b) The ionic strength deeply influence the formation of ThT^{+} aggregates at acidic pH (panel A). In fact with NaCl at pH 2.5 the ThT fluorescence intensities progressively for one week. Without NaCl the kinetics of ThT binding is slower. At neutral pH (panel B) no significant differences among the two conditions of ionic strength are appreciable at the end point.

In both the conditions of pH considered, no lag phases were detected suggesting that the aggregation is very fast. These results are in accordance with the biochemical

and spectroscopic studies previously described. Furthermore, this behavior could hint the formation of amyloid-like aggregates also close to T_m .

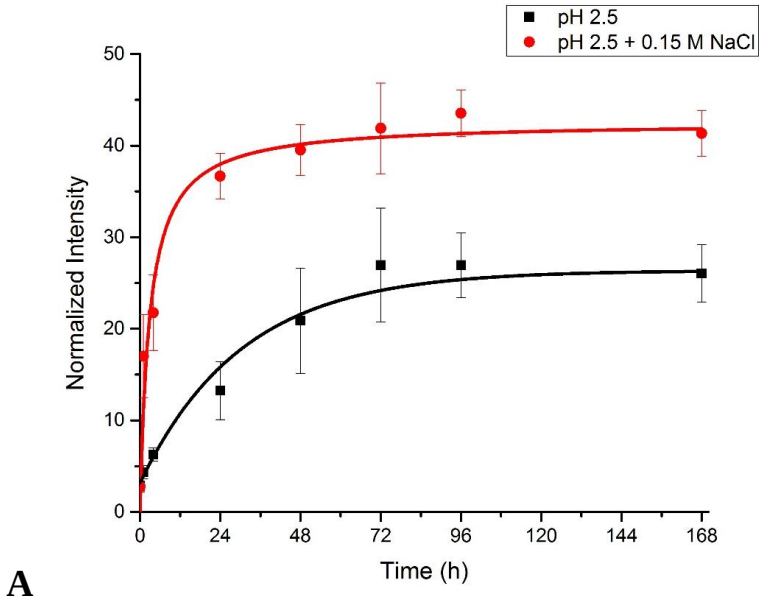

A

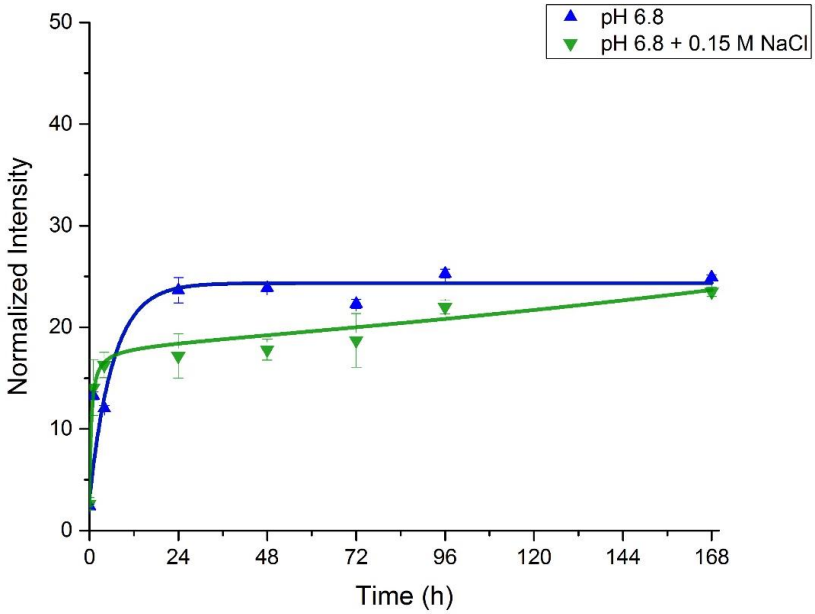

B

Thioflavin T binding assay. Fluorescence intensity at 485 nm upon incubation of MNEI (3 mg×mL^{-1}) at 75 °C in 0.020 sodium phosphate buffer pH 2.5 (A) and pH 6.8 (B) with or without 0.150 M NaCl for one week.

3.3.6 Fibres and amorphous species

In order to reveal the nature of the insoluble aggregates formed close to the T_m ,a morphological investigation has been performed by AFM, choosing to use 75 °C as incubation temperature at pH 2.5 and pH 6.8 with or without 0.150 M NaCl for one week. The AFM images were acquired by Dr. R. Di Girolamo. As reported in Fig.10 (panels A-B) at 75° C, fibres were detected at pH 2.5 with or without NaCl corroborating the data deriving from FT-IR analyses and the aggregation kinetics followed by ThT mesaurements. On the other hand, as reported in Fig.11 (panel A-B) only disordered aggregates were detected at neutral pH with or without salt. This behaviour is in accordance with the biochemical and spectroscopic data that revealed a too fast aggregation, also confirmed by the early plateau detected by ThT measurements. At neutral pH the system evolves towards disordered species that rapidly collapse into an amorphous precipitated form.

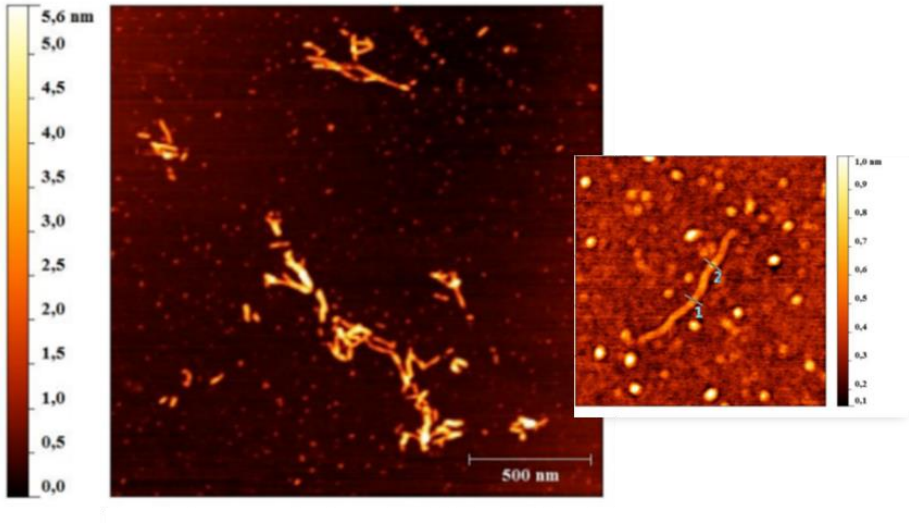

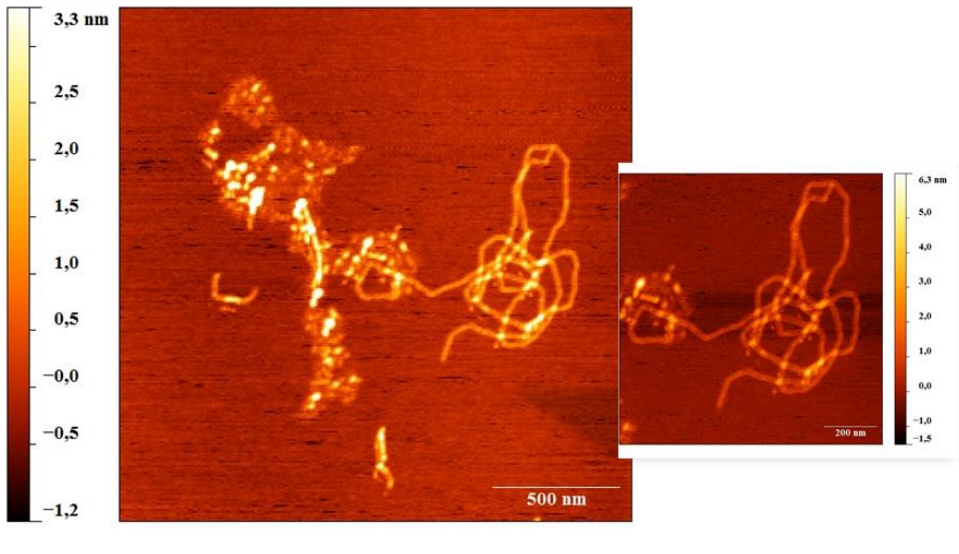

Fig. 10 Morphology characterization by AFM at pH 2.5. MNEI fibres upon incubation in 0.020 M sodium phosphate buffer pH 2.5 at 75 °C with 0.150 M NaCl (A) or without NaCl (B). A zoom section of the fibres is also reported.

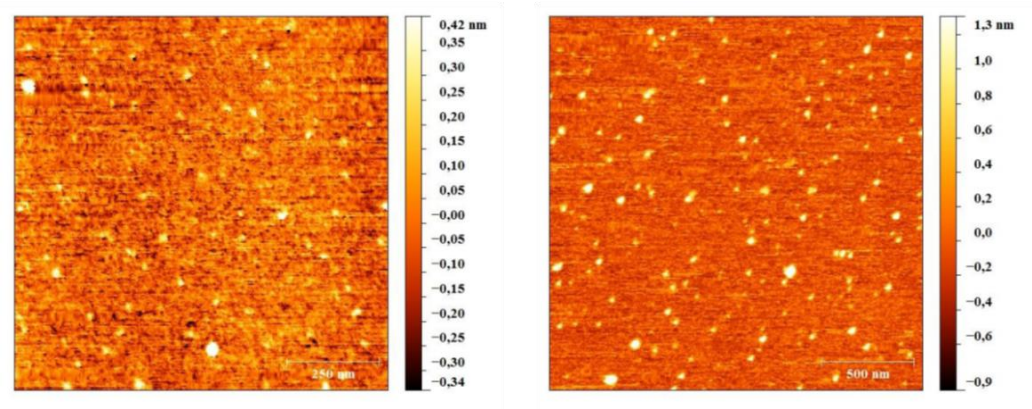

A **B**

Fig. 11 Morphology characterization by AFM at pH 6.8. MNEI amorphous aggregates upon incubation in 0.020 M sodium phosphate buffer pH 6.8 at 75 °C with 0.150 M NaCl (A) or without NaCl (B).

3.4 Conclusions and ongoing works

In this study, a very careful exploration of MNEI aggregation has been performed. Several physicochemical factors have been investigated, including pH, temperature and ionic strength. Biochemical and FT-IR spectroscopic data reveal that MNEI shows a remarkable aggregation propensity, that can be powerfully influenced by different factors. At low temperature, MNEI is stable in solution in all the pHs examined and only a little amount of dimer is detectable in solution. When the temperature is increased, MNEI rapidly oligomerizes giving rise to high size species that are endowed with a surprising SDS resistance. Around its T_m , MNEI forms insoluble aggregates which show a typical FT-IR profile found in fibrillar structures, i.e. the peak shift from 1635 cm^{-1} to 1620 cm^{-1} and the looseness of the signal around 1660 cm^{-1} , which ar diagnostic of the formation of intermolecular β-sheets and the disappearing of the native α-helix. FT-IR spectroscopy allows to define new

conditions triggering fibrilization. Indeed, fibrillar-like profiles were detected at 75 °C at pH 2.5 whit 0.150 M NaCl; the profiles collected without NaCl hints that fibrilization could occur also without NaCl even if the lag phase was slower. These suggestions were confirmed by ThT binding assays where high fluorescence intensities were detected after one week. A similar fibrillar-like behaviour was also observed at neutral pH even if the aggregation occurs very quickly whit or whitout NaCl, as revealed by FT-IR spectroscopy and ThT assay. In order to resolve the morphology of these insoluble aggregates, an AFM analysis was performed. It has been found that at low pH MNEI forms ordered aggregates with or without NaCl, thus supporting the biochemical and spectroscopic data. Indeed, they are SDS resistant. Additionally they show a negative peak of very low intensity on FT-IR curves around 1620 cm^{-1}, suggesting that several weak interactions (H-bonds) strongly connect the β-elements in an ordered structure. On the other hand, at neutral pH the system evolves towards disordered species with or without NaCl. In this condition, the aggregation occurs too fast and the system collapses into an amorphous precipitated form. The influence of pH, temperature and ionic strength is worth of further investigation. The understanding of the behaviour of MNEI under new environmental conditions triggering fibrilization could allow understanding the underlying molecular mechanism. A better knowledge could also support a rational design of new mutants endowed with controlled aggregation propensity, as well as support new biotechnological applications in the field of biopolymers.

3.5 References

[1] Pastore A, Temussi PA. (2012) Protein aggregation and misfolding: good or evil? *J. Phys.: Condens. Matter* 24 244101-244110

[2] Bellotti, V., and Chiti, F. (2008) Amyloidogenesis in its biological environment: challenging a fundamental issue in protein misfolding diseases. *Curr. Opin. Struct. Biol.* 18, 771-779

[3] Booth, D. R., Sunde, M., Bellotti, V., Robinson, C. V., Hutchinson, W. L., Fraser, P. E., Hawkins, P. N., Dobson, C. M., Radford, S. E., Blake, C. C., and Pepys, M. B. (1997) Instability, unfolding and aggregation of human lysozyme variants underlying amyloid fibrillogenesis. *Nature* 385, 787-793

[4] Colon, W., and Kelly, J. W. (1992) Partial denaturation of transthyretin is sufficient for amyloid fibril formation in vitro. *Biochemistry* 31, 8654-8660

[5] Naiki, H., Hashimoto, N., Suzuki, S., Kimura, H., Nakakuki, K., and Gejyo, F. (1997) Establishment of a kinetic model of dialysis-related amyloid fibril extension in vitro. *Amyloid* 4, 223-232

[6] Rega MF, Di Monaco R, Leone S, Donnarumma F, Spadaccini R, Cavella S and Picone D (2015) Design of sweet protein based sweeteners: Hints from structure–function relationships. *Food Chem* 173, 1179–1186.

[7] Aghera N and Udgaonkar JB (2012) Kinetic studies of the folding of heterodimeric monellin: evidence for switching between alternative parallel pathways. *Mol Biol* 420, 235–250.

[8] Konno T (2001) Multistep nucleus formation and a separate subunit contribution of the amyloidgenesis of heat-denatured monellin. Protein Sci 10, 2093 2101.

[9] Esposito V, Guglielmi F, Martin SR, Pauwels K, Pastore A, Piccoli R, Temussi PA., (2010) Aggregation mechanisms of cystatins: a comparative study of monellin and oryzacystatin. *Biochemistry.* 6;49(13

[11] Goormaghtigh, E., Raussens, V., and Ruysschaert, J. M. (1999) Attenuated total reflection infrared spectroscopy of proteins and lipids in biological membranes. *Biochim. Biophys. Acta* 1422, 105-185

[14] Natalello, A., Frana, A. M., Relini, A., Apicella, A., Invernizzi, G., Casari, C., Gliozzi, A., Doglia, S. M., Tortora, P., and Regonesi, M. E. (2011) A major role for side-chain polyglutamine hydrogen bonding in irreversible ataxin-3 aggregation. *PLoS One* 6, e18789

[15] Seshadri, S., Khurana, R., and Fink, A. L. (1999) Fourier transform infrared spectroscopy in analysis of protein deposits. *Methods Enzymol.* 309, 559-576

[16] Barth, A. (2007) Infrared spectroscopy of proteins. *Biochim. Biophys. Acta* 1767, 1073-1101

[17] Natalello, A., and Doglia, S. M. (2015) *Insoluble Proteins*, Springer New York, New York

[18] Zandomeneghi G, Mark RH, Krebs M. and Fändrich M. (2004) FTIR reveals structural differences between native β-sheet proteins and amyloid fibrils. *Protein Science.* 13:3314–3321

CHAPTER

4

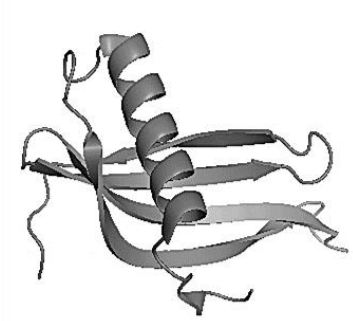

MNEI early steps of unfolding: new NMR insight

Abstract

MNEI aggregation propensity can be evaluated at different level, since the protein is able to form a wide range of aggregates making it a suitable model to study the oligomerization process *in vitro*. Even if more stable than the parental protein monellin, MNEI is an aggregation prone protein which, like its natural precursor, is able to form fibrillar aggregates. In Chapter 3, a deep explorative study allowed to find new conditions favouring fibrilization under prolonged incubation at acidic pH around its Tm, with or without NaCl. In order to depict the correlation between folding intermediates and the beginning of aggregation process, NMR studies have been pursued. The analysis aimed to identify the early steps of unfolding process at atomic detail to explain the fibrilization propensity under different experimental conditions, i.e. evaluating the influence of temperature and ionic strength at acidic pH, where MNEI is able to form ordered aggregates.

4.1 Introduction

MNEI and its derivatives have been proposed as potential low-caloric sugar replacers for food and beverages, but their usage in this framework has been slowed down by their intrinsic structural fragility. Although displaying higher thermal stability than the heterodimeric natural precursor monellin [1], MNEI is still sensitive to pH and temperature changes, that can trigger its unfolding, aggregation and precipitation, thus reducing its usage for food preparation [2,3,4]. In recent years, MNEI has also become a well-accepted model to study folding and aggregation properties of β-sheet-rich proteins. In particular, the dynamics of the folding and unfolding processes have been studied in great detail instance by the Udgaonkar group [5,6,7]. It had been previously found that the stability of MNEI at neutral pH is determined by the protonation state of residue Glu23, located in a hydrophobic pocket and possessing a pKa around 7.5 [8]. The anomalous value of this pKa is explained by the general observation that side chains of acidic residues embedded in hydrophobic environments titrate with high pKa, whereas the opposite behaviour is observed for basic residues. Furthermore, it is generally reported that residues located within hydrophobic pockets control the pH-dependent stability in proteins [9,10]. Very recently Molecular Dynamic simulation studies at high temperature showed, that deprotonation of Glu23 increases flexibility in loop Lα2, which connects the helix to the β-strand 2, and leads to the disruption of a stabilising hydrogen bond zipper between side chains and, in turn, lowers the thermal stability of the protein [12]. This study had been confirmed experimentally by NMR; furthermore it has been found that the proton chemical shift of the side-chain of Gln28 follows exactly the titration of Glu23 [13] resulting in a rigid structure at acidic pH and more flexible one at alkaline pH.

As discussed in Chapter 3, MNEI is highly sensitive to changes in pH and temperature that can result in aggregation and/or precipitation. Biochemical and biophysical studies previously described in Chapter 3, revealed that MNEI at low pH

can form a little amount of soluble dimer. Increasing temperature MNEI can form unsoluble fibrillar aggregates. At high temperature and low pH, the presence of NaCl accelerates the fibrilization. On the other hand, at neutral pH the amount of monomer in solution rapidly decreases and the system evolves towards unsoluble and amorphous species. In this study, the behaviour of MNEI at acidic pH has been analysed in more detail. High resolution NMR studies have been performed to investigate the role of temperature and ionic strength on the early unfolding events of MNEI. NMR analysis have been performed in collaboration with Dr. D.V. Laurents of the CSIC-IQFR (Consejo Superior de Investigation Cientificas - Istituto de Quimica-Fisica “Rocasolano”) in Madrid.

4.2 Materials and Methods

4.2.1 Protein expression and purification

The protein, MNEI, was expressed in *Escherichia coli* BL21 (DE3) cells harbouring the pET-22b+ plasmid and purified as described in Section C "Recombinant Proteins- Procedures", part 2. The ^{15}N ^{13}C labelled protein was expressed in M9 medium containing 0.5 g×l^{-1} of $^{15}NH_4Cl$ and 20 g×l^{-1} of ^{13}C-glucose as sources of labelled nitrogen and carbon, respectively. Sample purity and folding were confirmed by SDS/PAGE, gel-filtration, circular dichroism and mass spectrometry analysis. Protein secondary structure elements are described according to the following nomenclature: Nt (1–3), β1 (4–6), Lα1 (7–9),α1 (10–27), Lα2 (28–34), β2 (35–48), L23 (49–54), β3 (55–64), L34 (65–68), β4 (69-78), L45 (79–83), β5 (84–90), Ct (91–96).

4.2.2 NMR spectroscopy

^{15}N ^{13}C-MNEI was dissolved in 0.020 M sodium phosphate buffer pH 2.9, 10% D_2O at 5 mg×ml^{-1} for reference spectrum. 0.1 mM DSS salt was added for internal referencing Standard experiments commonly used for protein assignment were performed at 35 °C, including ^{15}N HSQC, CACB(CO)N(H), HNCO, HNCA, HNN and HNH spectra. The assignment process was carried out manually using Sparky software (T. D. Goddard and D. G. Kneller, SPARKY 3,University of California, San Francisco). To follow chemical shift variations as function of temperature or ionic strength, series of ^{15}N-HSQC spectra were acquired by dissolving MNEI in and the same buffer used for the assignment at a concentration of 2.5 mg×mL^{-1}. Spectra were acquired by increasing the temperature from 35-45-55-65 °C, and then going back from 65 to 35 °C with or without 0.150 M NaCl. All the spectra were

acquired using a Bruker Avance II 800 MHz spectrometer equipped with triple axis gradient cryo-probe. Chemical shift variations were calculated as weighted averages of overall backbone amides between 35 °C and 45 °C, 35 °C and 55 °C and between 35 °C and 65 °C using the formula:

$$\Delta(\text{avg}) = \frac{\sqrt{(\Delta\text{HN})^2 + (\Delta\text{N})^2}}{2}$$

4.2.3 Hydrogen/ Deuterium exchange

Hydrogen exchange experiments were performed dissolving the labelled MNEI in 99.9% D_2O at pH 2.9 with or without 0.150 M NaCl. A series of successive ^{15}N-HSQC spectra was recorded at 35 °C for 20 hours using a Bruker Avance 600 MHz spectrometer equipped with cryoprobe.

4.3 Results and Discussion

4.3.1 HSQC spectrum at high magnetic field

MNEI ^{15}N-^{13}C was dissolved at a final concentration of 5 mg×ml^{-1} in sodium phosphate buffer pH 2.5 to acquire a full dataset necessary to complete the assignment at 35 °C, as described in the experimental section. The ^{15}N-HSQC spectrum reported in Fig. 1 indicate that all the residues were identified. The spectrum acquired in this conditions has been used as reference to identify the amide and proton chemical shift variations in different experimental conditions of temperature and ionic strength.

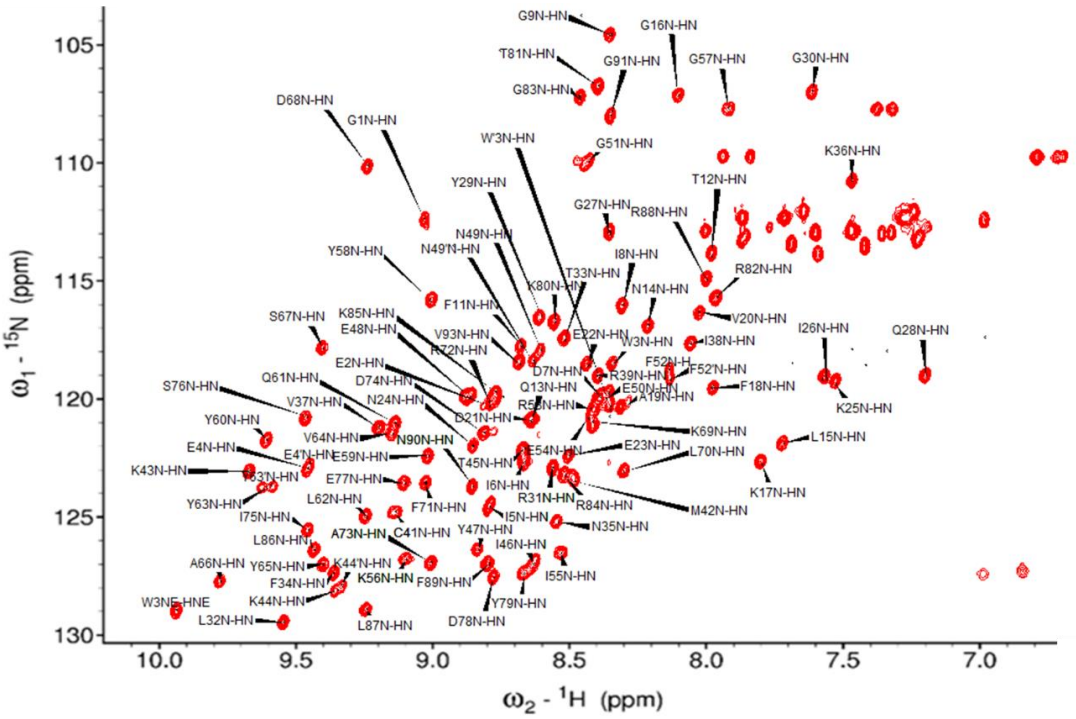

Fig. 1 ^{15}N-HSQC spectrum of MNEI at 35 °C

4.3.2 Temperature effect

With the aim to investigate at atomic detail the variations on tertiary structure occurring when temperature was changing, ^{15}N-HSQC spectra were acquired by increasing progressively the temperature of 10° C, i.e from 35 to 45 °C, from 45 to 55 °C and from 55 to 65 °C. At the end, an additional spectrum was acquired cooling back the sample to the starting point, i.e. decreasing temperature from 65 to 35 °C. In order to find the putative regions involved in local unfolding events, the shift of the resonances of amide and proton chemical shifts for each aminoacidic residue have been calculated for each range of temperature. Fig. 2 summarizes the chemical shift variations upon heating of MNEI when temperature was increased from 35 to 45 °C (blue bars), from 35 to 55 °C (green bars) and from 35 to 65 °C (red bars). The secondary structure elements are also reported on the top of the figure, using the following color-code: loop (magenta), α-helix (grey), β-sheet (yellow).

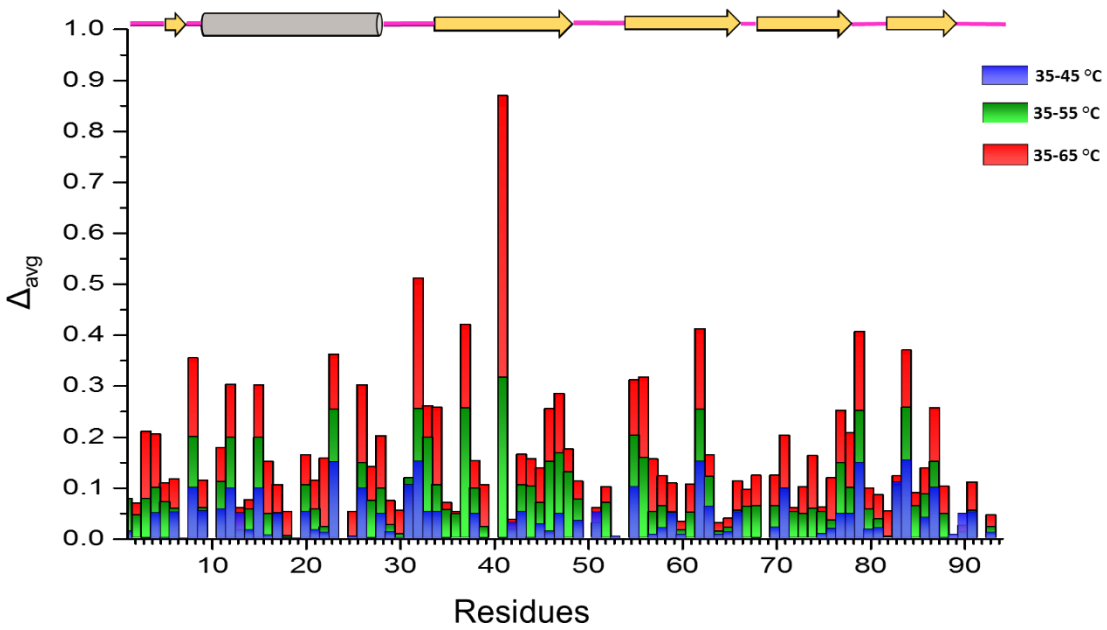

Fig. 2 Chemical shift variations (Δ_{avg}) upon MNEI heating. The temperature was increased of 10 °C (blue), 20 °C (green) and 30 °C (red), progressively. Missing values correspond to peaks not assigned for overlap/broadening.

As indicated by the blue bars, when temperature was increased of 10 °C, only the residues located in loop regions show significant chemical shifts variations. By increasing the temperature of additional 10 °C, until 55 °C (green bars), it can be observed that loop regions are still influenced, together C41. Furthermore, the signals relative to residues D7 (Lα1), A19 (α1), E50-R53-E54 (L23) and F89 (β5) were shifted in very crowded region of the spectrum (8.3-8.0 ppm on ^{1}H axis, 123-118 ppm on ^{15}N axis), making difficult their identification. When temperature was increased until 65 °C (red bars), besides the loop regions and C41 (β2), also the residues located in β4 (I75-S76- E77- D78-Y79) and β5 (R84-L86) significantly change their positions.

Interestingly, MNEI signals were completely recovered when the temperature was decreased from 65 °C to 35 °C (data not shown) suggesting that, the protein completely refolds and its 3D structure is completely restored.

4.3.3 NaCl effect

In order to extend the analysis at acidic pH, the influence of NaCl on MNEI stability has been also investigated. A set of ^{15}N-HSQC spectra were acquired following the peak positions upon increasing temperature from 35 °C to 65 °C as previously described. When 0.150 M NaCl was added, the better quality of the spectra allowed to carefully assign the residues when temperature was increased. The amide and proton chemical shift variations upon MNEI heating were calculated and were reported on histograms (Fig. 3). Blue bars correspond to chemical shift variations calculated when temperature was increased of 10 °C (i.e. from 35 to 45 °C), green bars correspond to chemical shift variations calculated when temperature was increased of 20 °C (i.e. from 35 to 55 °C) while red bars are relative to chemical shift variations observed when temperature was increased of 30 °C (i.e. from 35 to 65 °C).

The secondary structure elements are also reported: loop (magenta), α-helix (grey), β-sheet (yellow).

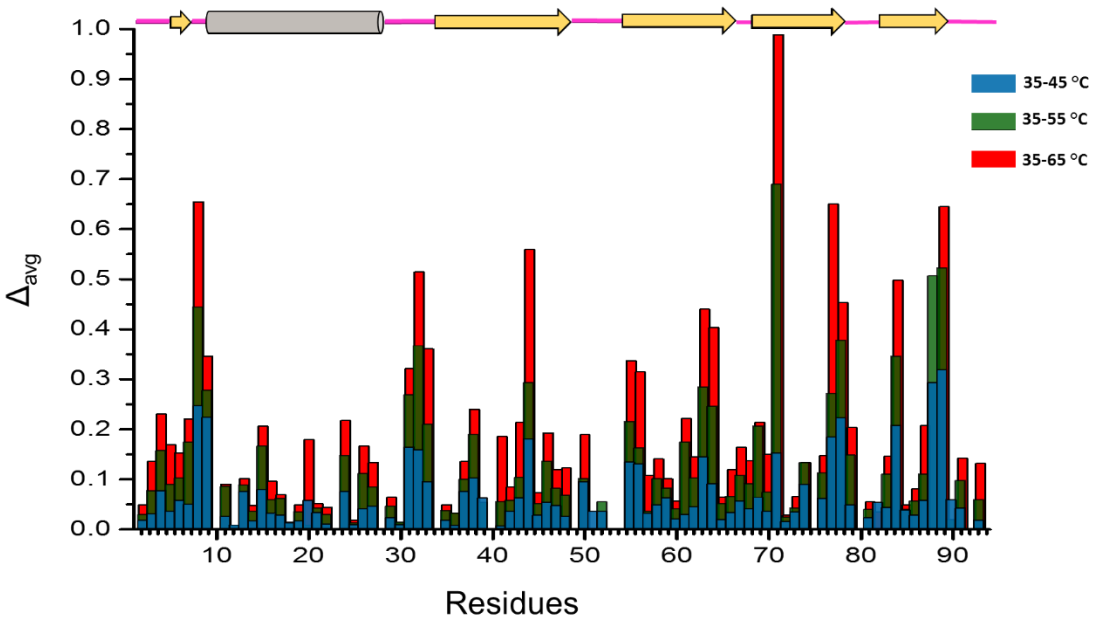

Fig. 3 Chemical shift variations (Δ_{avg}) upon MNEI heating with NaCl 150 mM. The temperature was increased of 10 °C (A), 20 °C (B) and 30 °C (C), progressively. Missing values correspond to peaks difficult to assign.

When temperature was increased of 10 °C (blue bars), only a few residues belonging to the loop regions and the residues R88-F89 located in β5 show significant amide chemical shift variations. By increasing the temperature of further 10 °C reaching 55 °C (in green), loop regions are still deeply influenced as revealed by their high chemical shift variations; additionally, the signal for G51 disappears. Residues R88 and F89 are still characterised by high chemical shift variations together with F71 which is located in β4 strand. Finally, when temperature was increased up to 65 °C (in red) all the loop regions are strongly influenced; in more detail, the signal of residues located in the loop 23, i.e. 49-54, become very broad and are no more detectable in the spectrum. Moreover, high chemical shift variations were detected for K43 in β2 and for many residues located in β4 and β5 strands, suggesting that

also in presence of NaCl, this region has a primary importance in the early unfolding of MNEI.

To make more clearly evident the local effects of the temperature increase, the residues whose resonances are affected by a value higher than 0.2 ppm (selected arbitrarily as threashold, are highlighted in the Fig. 4 (panel A: no NACl added, panel B: 150 mM NaCl)

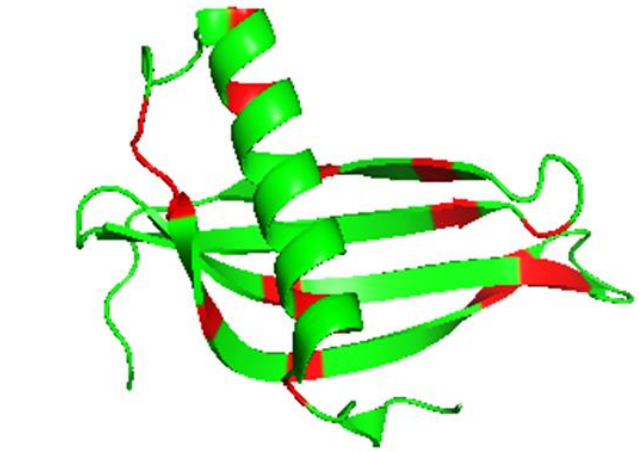

A

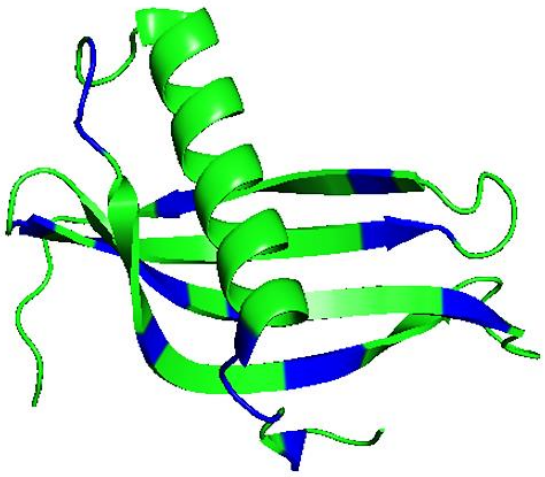

B

Fig.4 Topological maps. Local effects of temperature on MNEI at pH 2.5 without NaCl (A) and with 0.150 M NaCl (B). In green: the most stable residues. In red: the most affected residues without NaCl. In blue: the most affected residues with 0.150 M NaCl.

4.3.4 Stability and compactness: H/D exchange experiments

Detailed information on MNEI solvent accessibility was derived from H/D exchange experiments. ^{15}N MNEI was dissolved in 99% D_2O at pH 2.9 and a series of HSQC data sets was collected at 35 °C every 40 minutes for 20 hours. Based on the intensity of HN signal over time, the amide protons were classified as fast or slow exchanging. In detail, peaks that disappeared soon after the protein dissolution, i.e. were absent already in the first spectrum acquired in D_2O, were classified as fast-exchanging. Peaks that were still present in the last spectrum, i.e. 20 hours after the protein dissolution in D_2O, were classified as slow-exchanging. All other peaks detected were considered as medium-exchanging ones. In Fig. 6 and 7, the topological maps of MNEI comparing the H/D exchange with or without NaCl are reported. The slow exchanging residues are highlighted with the following color-code:

- green: absent at the beginning, i.e. high accessibility;
- red: still present at the beginning, i.e. medium accessibility;
- blue: still present after 20 hours, i.e. low accessibility.

In Tab.1 and Tab.2 a detailed classification of each residue is reported by estimating the H/D exchange at different time in both the condition of ionic strength explored, i.e. 0 mM NaCl in Tab.1 and 150 mM NaCl in Tab.2, respectively. After 20 hours, only few residues were detected including: 4E- I6 (β1), A19-I26 (α1), V37-I38-R39 (β2),E54-E59-Y60-Q61-L62-Y63-V64-Y65-A66 (β3), L70-F71-R72-I75 (β4), L87-V93 (C-t). In the sample containing 0.150 M NaCl, more residues are classified slow exchangers, including Q13-L15-G16-K17-V20-E22-E23 (α1), N35-K36-V37-I38-M42-K43-T45-I46-E48 (β2), E54-K56-Y58-E59-Y60-Q61-L62-V64-Y65 (β3), K69-L70-F71-D74-I75-S76 (β4), L87-N90 (β5) and V93 (Ct) (Fig.7). Overall, the comparison between these experiments suggest that MNEI is more compact and rigid with NaCl.

Aa	t 1 40’	t 2 20h	H/D exchange	Aa	t 1	t 2 20h	H/D exchange	Aa	t 1 40’	t 2 20h	H/D exchange
G1	-	-	F	L32	x	-	I	Y63	x	x	S
E2	-	-	F	T33	-	-	F	V64	x	x	S
W3	-	-	F	F34	-	-	F	Y65	x	x	S
E4	x	x	S	N35	-	-	F	A66	x	x	S
I5	x	-	I	K36	-	-	F	S67	-	-	F
I6	x	x	S	V37	x	x	S	D68	-	-	F
D7	-	-	F	I38	x	x	S	K69	-	-	F
I8	-	-	F	R39	x	x	S	L70	x	x	S
G9	-	-	F	C41	-	-	F	F71	x	x	S
F11	-	-	F	M42	-	-	F	R72	x	x	S
T12	-	-	F	K43	-	-	F	A73	-	-	F
Q13	x	-	I	K44	-	-	F	D74	-	-	F
N14	-	-	F	T45	x	-	I	I75	x	x	S
L15	x	x	S	I46	-	-	F	S76	x	-	I
G16	-	-	F	Y47	-	-	F	E77	-	-	F
K17	-	-	S	E48	-	-	F	D78	-	-	F
F18	x	-	I	N49	-	-	F	Y79	-	-	F
A19	x	x	S	E50	-	-	F	K80	-	-	F
V20	x	x	S	G51	-	-	F	T81	-	-	F
D21	-	-	F	F52	-	-	F	R82	-	-	F
E22	-	-	F	R53	-	-	F	G83	-	-	F
E23	-	-	F	E54	x	x	S	R84	-	-	F
N24	-	-	F	I55	-	-	F	K85	-	-	F
K25	-	-	F	K56	x	-	I	L86	-	-	F
I26	x	x	S	G57	-	-	F	L87	x	-	I
G27	-	-	F	Y58	x	-	I	R88	x	-	I
Q28	-	-	F	E59	x	x	S	F89	-	-	F
Y29	-	-	F	Y60	x	x	S	N90	-	-	F
G30	-	-	F	Q61	x	x	S	G91	-	-	F
R31	-	-	F	L62	x	x	S	V93	x	-	I

Tab. 1 H/D exchange experiments at pH 2.9 (noNaCl added). Classification of residues as Fast (F), Intermediate (I) and Slow (S) exchangers. Time of HSQC spectra acquisition is also reported: t 1 and t 2, corresponding to 40 minutes and 20 hours after dissolution of MNEI in D_2O.
(x): identification; (-): no identification

Aa	t 1 40’	t 2 20h	H/D exchange	Aa	t 1 40’	t 2 20h	H/D exchange	Aa	t 1 40’	t 2 20h	H/D exchange
G1	-	-	F	L32	x	-	I	Y63	-	-	F
E2	x	x	S	T33	x	-	I	V64	x	x	S
W3	-	-	F	F34	-	-	F	Y65	x	x	S
E4	x	x	I	N35	x	x	S	A66	x	x	S
I5	x	-	I	K36	x	x	S	S67	x	-	I
I6	x	x	S	V37	x	x	S	D68	-	-	F
D7	-	-	F	I38	x	x	S	K69	x	x	S
I8	-	-	F	R39	x	-	I	L70	x	x	S
G9	x	-	I	C41	-	-	F	F71	x	x	S
F11	-	-	F	M42	x	x	S	R72	-	-	F
T12	-	-	F	K43	x	x	S	A73	-	-	F
Q13	x	x	S	K44	-	-	F	D74	x	x	S
N14	x	-	I	T45	x	x	S	I75	x	x	S
L15	x	x	S	I46	x	x	S	S76	-	-	F
G16	x	x	S	Y47	-	-	F	E77	x	-	I
K17	x	x	S	E48	x	x	S	D78	-	-	F
F18	x	x	S	N49	-	-	F	Y79	-	-	F
A19	-	x	F	E50	-	-	F	K80	-	-	F
V20	x	x	S	G51	-	-	F	T81	-	-	F
D21	x	-	I	F52	-	-	F	R82	-	-	F
E22	x	x	S	R53	-	-	F	G83	-	-	F
E23	-	-	F	E54	x	x	S	R84	-	-	F
N24	-	-	F	I55	-	-	F	K85	-	-	F
K25	x	-	I	K56	x	x	S	L86	-	-	F
I26	x	-	I	G57	-	-	F	L87	x	x	S
G27	-	-	F	Y58	x	x	S	R88	x	-	I
Q28	-	-	F	E59	x	x	S	F89	-	-	F
Y29	-	-	F	Y60	x	x	S	N90	x	x	S
G30	-	-	F	Q61	x	x	S	G91	-	-	F
R31	-	-	F	L62	x	x	S	V93	x	x	S

Tab. 2 H/D exchange experiments at pH 2.9 containing 150 mM NaCl. Classification of residues as Fast
(F), Intermediate (I) and Slow (S) exchangers. Time of HSQC spectra acquisition is also reported: t 1 and t 2, corresponding to 40 minutes and 20 hours after dissolution of MNEI in D_2O.
(x): identification; (-): no identification.

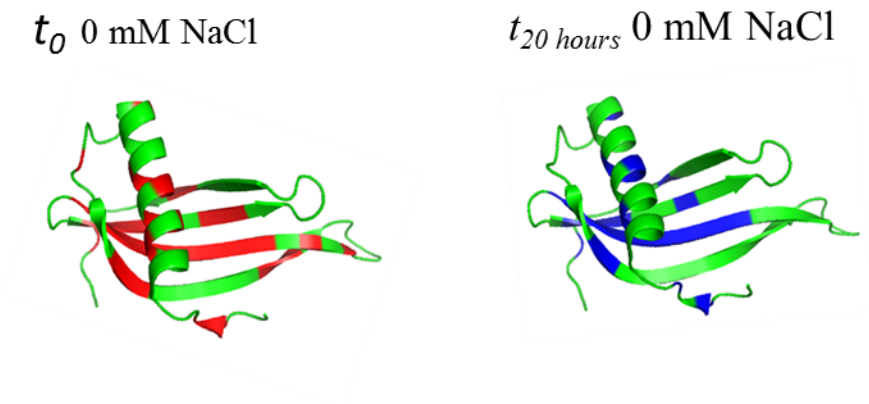

Fig. 6 Topological maps of MNEI. H/D exchange experiments at pH 2.9 without NaCl. Fast exchanger residues (green); intermediate exchanger residues still present at the starting point (red); low exchanger residues still present after 20 hours (blue)

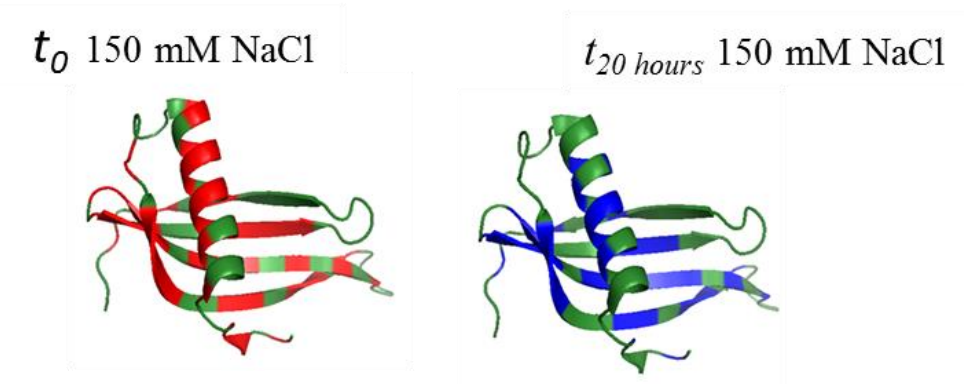

Fig.7 Topological maps of MNEI. H/D exchange experiments at pH 2.9 with 150 mM NaCl. Fast exchanger residues (green); intermediate exchanger residues still present at the starting point (red); low exchanger residues still present after 20 hours (blue)

By comparing the information obtained from temperature titration experiments and from the H/D exchange measurements, putative regions of early unfolding steps were identified. In both the conditions of ionic strength explored, except form the loop regions, which are naturally more influenced by environment, the aminoacid residues located in β4 (I75-S76- E77- D78-Y79) and β5 strands (R84-L86) were strongly

affected by temperature increasing, as revealed by high chemical shift variation values. At the same time, they were also in a fast H/D exchanging regime and more accessible to the solvent. Since these residues are more affected by the physicochemical variations analysed, based on this analysis it is possible to hypothesize that the terminal part of β4 and the initial part of β5 strands could represent a putative site for early unfolding.

4.4 Conclusions and ongoing works

This work investigated, for the first time by NMR, the influence of temperature and ionic strength on MNEI folding/misfolding at low pH. As reported in previous works, at low pH at 86 °C, in the presence of 0.150 M NaCl, MNEI forms fibres [14], reproducing the behaviour of its natural precursor monellin [15-16]. In Chapter 3, it has also been described that at acidic pH, MNEI fibrilization also occurs by decreasing temperature from 86 °C to 75 °C, the last one corresponding to MNEI melting temperature at pH 2.5. Moreover, data discussed in the same Chapter 3, indicated that MNEI forms ordered aggregates with or without NaCl, although a prolonged incubation time is required. In order to investigate the influence of temperature and ionic strength on the unfolding of MNEI, NMR measurements have been performed. NMR analysis reveals that MNEI is more compact and rigid in presence of NaCl than without salt. High-resolution experiments showed that, as expected, the main chemical shift perturbations occur primarily into the loop regions. In more detail, the assignment was cryptic in the loop region L23 (49-54) corresponding to the engineered linker; indeed when temperature was increased the signals fall in a crowded region of the spectra precluding their identification. Focusing the attention on the structured regions of MNEI, the analysis of proton and amide chemical shift variations allowed to individuate the residues located in β4

(I75-S76- E77- D78-Y79) and β5 strands (R84-L86), corresponding to the C-terminal and the N-terminal part of these two β-strands, as the most affected by the experimental conditions examined. H/D exchange experiments also confirmed that this region is more exposed to the solvent being in a fast exchanging regime with D_2O. The results confirm that these regions could be putative sites for early unfolding of MNEI.

Further NMR studies increasing temperature until 75 °C where MNEI forms fibres, as described in Chapter 3, could help to a better understanding of the correlation between unfolding and aggregation. Additionally studies at neutral may allow shedding light on the differences that in such a case lead to the formation of disordered aggregates.

Finally, these data provide structural hints to understand how temperature/pH/ionic strength can modulate the formation of ordered aggregates of MNEI, which could drive the design of new mutants with improved resistance to physicochemical stress or even with potential applications as new protein-based biomaterials.

4.5 References

[1] Morris JA and Cagan RH (1972) Purification of monellin, the sweet principle of Dioscoreophyllum cumminsii. *Biochim Biophys Acta (BBA)* – General Subjects 261, 114–122.

[2] Aghera N, Earanna N and Udgaonkar JB (2011) Equilibrium unfolding studies of Monellin: the doublechain variant appears to be more stable than the singlechain variant. *Biochemistry* 50, 2434–2444.

[3] Aghera N and Udgaonkar JB (2012) Kinetic studies of the folding of heterodimeric monellin: evidence for switching between alternative parallel pathways. *Mol Biol* 420, 235–250.

[4] Aghera N and Udgaonkar JB (2013) The utilization of competing unfolding pathways of monellin is dictated by enthalpic barriers.*Biochemistry* 52, 5770–5779.

[5] Goluguri RR and Udgaonkar JB (2015) Rise of the helix from a collapsed globule during the folding of monellin. *Biochemistry* 54, 5356–5365.

[6] Jha SK, Dhar D, Krishnamoorthy G and Udgaonkar JB (2009) Continuous dissolution of structure during the unfolding of a small protein Proc Natl Acad SciUSA 106, 11113–11118.

[7] Rega MF, Di Monaco R, Leone S, Donnarumma F, Spadaccini R, Cavella S and Picone D (2015) Design of sweet protein based sweeteners: Hints from structure–function relationships. Food Chem 173, 1179–1186.

[8] Spadaccini R, Crescenzi O, Tancredi T, De Casamassimi N, Saviano G, Scognamiglio R, Di Donato A and Temussi PA (2001) Solution structure of a sweet protein: NMR study of MNEI, a single chain monellin. J Mol Biol 305, 505–514.

[9] Garcia-Seisdedos H, Ibarra-Molero B and Sanchez- Ruiz JM (2012) How many ionizable groups can sit on a protein hydrophobic core? *Proteins* 80, 1–7.

[10] Harms MJ, Casta~neda CA, Schlessman JL, Sue GR, Isom DG, Cannon BR and Garcıa-Moreno EB (2009) The pKa values of acidic and basic residues buried at the same internal location in a protein are governed by different factors. *J Mol Biol* 389, 34–47.

[11] Langsetmo K, Fuchs JA and Woodward C (1991) The conserved, buried aspartic acid in oxidized Escherichia coli thioredoxin has a pKa of 7.5. Its titration produces a related shift in global stability. *Biochemistry* 30, 7603–7609.

[12] Leone S and Picone D (2016) Molecular dynamics driven design of pH-stabilized mutants of MNEI, a sweet proteinPLoS One 11, e0158372.

[13] Spadaccini R, Leone S,Rega MF, Richter C and Picone S. (2016) Influence of pH on MNEI structure and stability. *FEBS Letters* 590 3681–3689

[14] Esposito V, Guglielmi F, Martin SR, Pauwels K, Pastore A, Piccoli R, Temussi PA., (2010) Aggregation mechanisms of cystatins: a comparative study of monellin and oryzacystatin. *Biochemistry.* 6;49(13)

[15] Konno T, Murata K and Nagayama K (1999) Amyloid-like aggregates of a plant protein: a case of a sweet-tasting protein, monellin. *FEBS Lett* 454, 122–126.

[16] Konno T (2001) Multistep nucleus formation and a separate subunit contribution of the amyloidgenesis of heat-denatured monellin. Protein Sci 10, 2093 2101.

Part C

Recombinant Proteins

Procedures

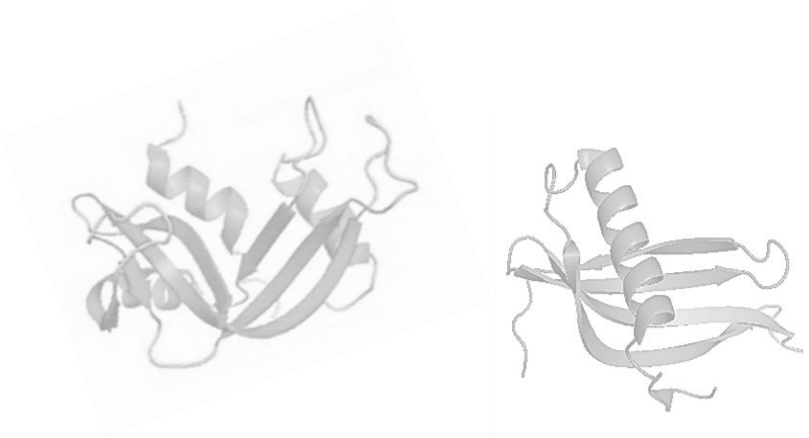

C.1 Expression and purification of recombinant RNase A-Onc

Here is reported the effective expression of recombinant onconase in *Escherichia coli* inclusion bodies, the refolding of the protein, followed by its purification in high yields.

Preparation of the mutant RNase A-Onc: design

RNase A and Onconase share high sequence identity. The C-terminal hinge loop of Onconase was used as template to design the new mutant RNase A-Onc. As highlighted in Fig.1, the residues GNPYV corresponding to the sequence 112-116 of RNase A have been substituted with the residues NQA.

Fig.1 RNase A and RNase A-Onc aminoacidic sequences

The corresponding cDNA sequence was obtained from the aminoacid one

CATATG AAA GAA ACA GCT GCA GCG AAA TTT GAG CGT CAA CAC ATG GAC AGT AGC ACT TCT GCA GCC TCA TCC AGC AAC TAT TGC AAC CAG ATG ATG AAA TCA CGC AAT CTG ACC AAA GAT CGC TGT AAA CCG GTG AAC ACG TTT GTG CAT GAA TCG TTA GCG GAT GTT CAG GCC GTA TGC TCT CAG AAG AAC GTT GCG TGC AAG AAT GGC CAG ACC AAC TGC TAT CAG AGC TAT TCC ACC ATG TCG ATT ACG GAC TGT CGT GAA ACC GGT AGT AGC AAA TAC CCG AAT TGT GCG TAC AAA ACG ACT CAA GCC AAC AAA CAC ATC ATT GTC GCG TGT GAG AAT CAA GCT CCA GTC CAT TTC GAT GCA TCG GTG **TGA GGTACC GGATCC**

At the 5' of the nucleotide sequence was added the CATATG restriction site for Nde I; the enzymatic cutting between A and T produces a fragment with the start-codon ATG in frame for the N-terminal Methyonine synthesis. At the 3' of the cDNA 3 sequences were included: a) the stop-codon TGA; b) the GGTACC restriction site for Kpn I to screen the positive clones after ligase reaction into the expression vector; c) the GGATCC restriction site for BamHI. The two restriction sites GGTACC and GGATCC, were added after the stop-codon TGA.

Preparation of the mutant RNase A-Onc: cloning procedures

The cDNA encoding the mutant designed was purchased from GENEWIZ,Inc cloned into a pUC57-KAN commercial vector between BamHI and NdeI restriction sites (Fig.2). The vector pUC57-KAN was linearized with NdeI and BamHI to isolate the cDNA encoding RNase A-Onc (Fig.3). The expected fragment was isolated after

agarose-gel extraction and inserted with T4 ligase reaction into the expression vector pET22b^{+} between the NdeI/BamHI restriction sites (Fig.4). The resulting vector was used to transform TOP10 E.coli cells to follow the subsequent screening procedures. The transformed cells were growth on LB-agar plates containing 100 µg of AMP; five well-shaped cell colonies were picked and inoculated in LB medium containing 100 µg of AMP. After the overnight growth at 37 °C, the cells were harvested and the plasmidic DNA was extracted by miniprep procedures. The integrity and the purity of the plasmidic DNA was checked by agarose gel electrophoresis. Each DNA sample was digested with KpnI to screen the effective internalization of the sequence encoding the RNase A-Onc mutant (Fig. 5). The KpnI^{+} clone, was selected and used to follow the expression procedures.

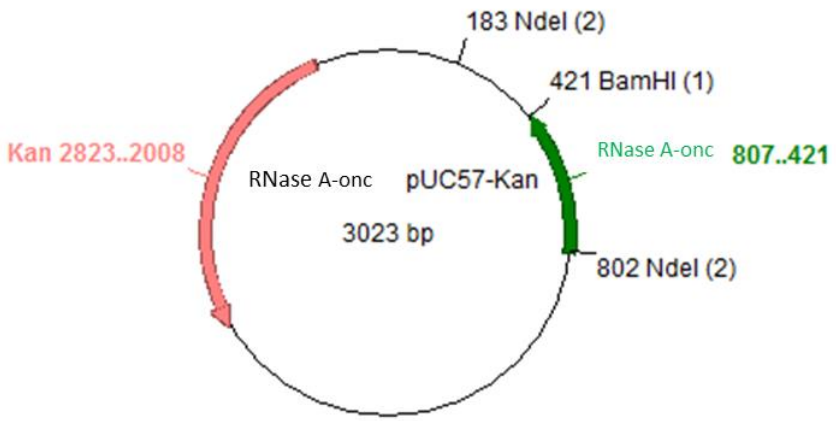

Fig. 2 RNase A-Onc pUC57-Kan vector map

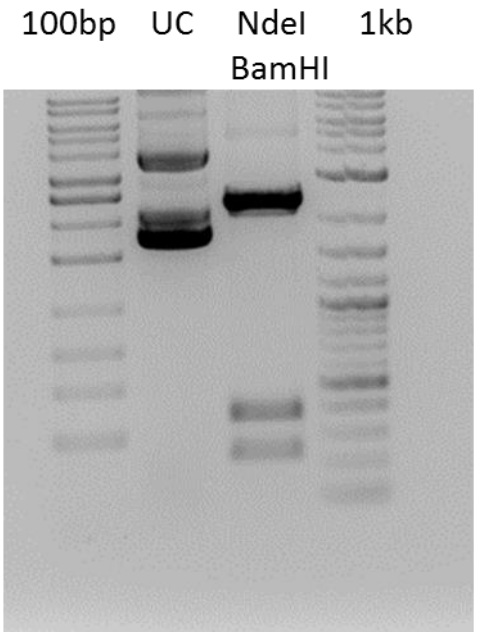

Fig. 3 Agarose gel electrophoresis. UC: uncut plasmid

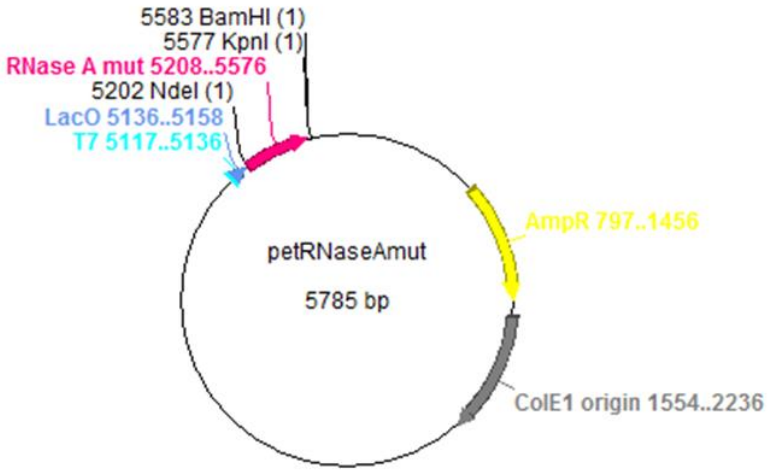

Fig. 4 pET22b+RNaseA-Onc vector map

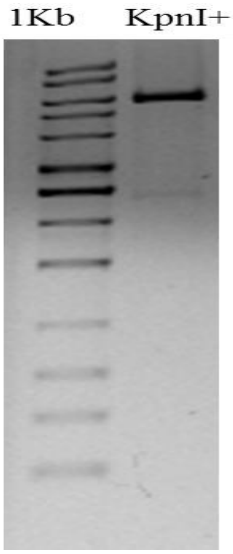

Fig. 5 Agarose gel electrophoresis. KpnI enzymatic restriction screening

Recombinant expression of RNaseA-Onc

The plasmid obtained was transferred in BL21(DE3) cells strain of *E.coli.* The transformed cells were grown in LB medium at 37° C on analytical scale (5 mL) until reaching the final $OD_{600\ nm}$ of 0.6 when the protein expression was induced adding 100 mM IPTG. After 3 hours from the induction, 1 mL of cultured cells was harvested while the remaining culture was keep at 37 °C for a comparative overnight induction. The corresponding pellets were treated with SDS-lysis buffer and boiled to extract the proteins. A little amount of sample corresponding to 5 µg of total proteins was loaded on SDS-poliacrilamide gel to check the RNaseA-Onc expression (Fig.6).

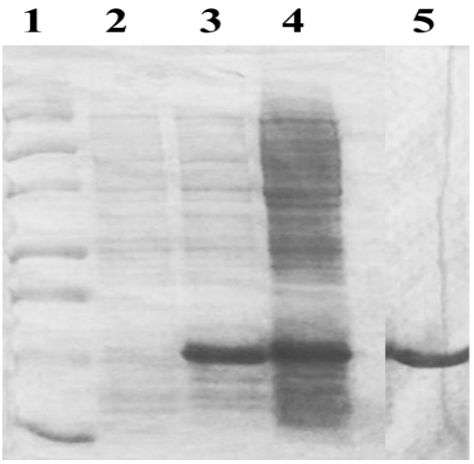

Fig. 6 SDS-PAGE. RNase A-Onc effective expression. 1: Marker; 2: No induction; 3: Induction fro 3 hours; 4: Overnight induction; 5: RNase A wild type

As showed in Fig. 6 (lane 3), an effective protein expression was reached after 3 hours of induction while increasing the incubation time for the night does not significantly increase the RNaseA-Onc expression but only endogenous proteins were over-expressed.

For preparative purposes, the transformed cells were inoculate in 1L fresh LB/AMP medium and grown until reaching the final $OD_{600\ nm}$ of 0.6 when the protein expression was induced adding 0.4 mM IPTG. After 3 hours of induction, the cell were divided into 4 aliquots and harvested for centrifugation at 6000 rpm at 4 °C for 30'.

Isolation and denaturation of inclusion bodies

Each aliquot was suspended in 20 ml of cold 0.10 M Tris-acetate pH 8.4 containing 5 mM EDTA. The cell lysis was performed by sonication at 15 W for 20' (30'' on-30''off cycle) using a Microson Ultrasonic Homogenizer XL2000. The engineered RNase-Onc was accumulated into the inclusion bodies so, after lysis, the cytosolic

fraction and the insoluble fraction were separated by centrifugation at 17500 RCF for 1 hour at 4 °C. The resulting pellets, containing the inclusion bodies, were treated with 15 ml of a detergent and denaturing solution of 0.10 M Tris-acetate, pH 8.4 containing 2% Triton X100, 2M Urea,10 mM EDTA and sonicated for 20'. After that the samples were centrifuged for 30' at 4 °C at 12500 RCF. After another sonication and centrifugation step, the pellet was washed in 15 ml of 0.10 M Tris-acetate pH 8.4 containing 10 mM EDTA to remove Triton and urea. Finally, the pellet corresponding to inclusion bodies mainly containing the recombinant RNaseA-Onc, was washed in 0.10 mM Tris-acetate pH 8.4. All the washing procedures are checked on SDS-PAGE. Inclusion bodies were then dissolved in 15 ml of 0.10 M Tris-acetate pH 8.4 containing 10 mM EDTA, 6 M Gdn-HCl and 25 mM DTT, purged with N_2, and incubated at 37 °C for 3 hours. The protein solution was dialyzed overnight versus 20 mM acetic acid at 4 °C to remove denaturants and reducing agents. Any insoluble material was removed by centrifugation in order to obtain a supernatant fraction containing the RNaseA-Onc in the completely reduced and denatured form.

Renaturation procedures

Renaturation of the derivatized protein was achieved by diluting samples in 100 mM Tris-acetate pH 8.4 at a final protein concentration of 0.1 mg $\times mL^{-1}$ followed by addition of a redox mixture containing 3 mM glutathione-reduced and 0.6 mM glutathione-oxyded purged with N_2. Maximal renaturation was obtained after 20 hours at 25 °C. The renaturation reaction was stopped removing the redox glutathione by ultrafiltration on AMICON YM3 membrane (3000 Da exclusion cut-off). By ultrafiltration, the sample containing RNase A-Onc was also equilibrated in 20 mM acetic acid solution to change the pH from alkaline to acidic to inhibit the reoxidation reaction.

Purification of RNase A-Onc monomeric form

The last step in the RNase A-Onc production, was represented by a gel filtration chromatography. The protein solution obtained from AMICON ultrafiltration, was loaded on a Sephadex G75 (1.5×72 cm) column previously equilibrated in 0.10 M ammonium acetate buffer pH 5.1. The monomeric RNase A-Onc was successfully purified from high molecular weight contaminants, as shown in Fig.7. The purity was also assessed by SDS-PAGE 15% and native PAGE 12% as reported in Fig. 8. The final yeld of pure monomeric RNaseA-Onc obtained by the corresponded to 13 mg per liter of cultured cells in LB medium.

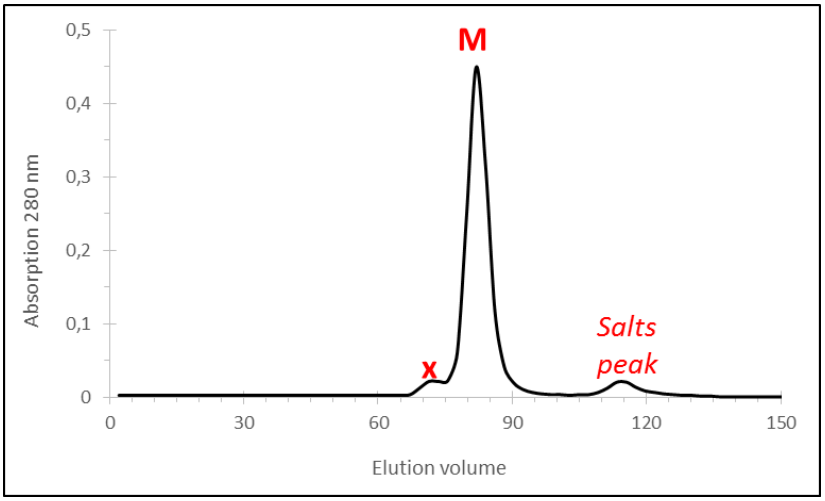

Fig. 3 G75 pattern. RNase A-Onc isolated as monomeric form (M)

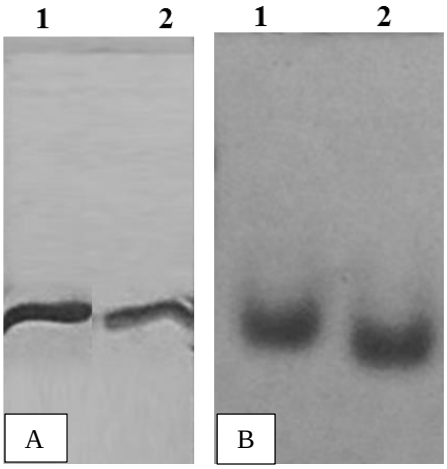

Fig. 4 Gel electrophoresis. A: SDS- PAGE 15%. B: native PAGE 12%. 1: RNase A wild type; 2: RNase A-Onc

C.2 Expression and purification of recombinant MNEI

Expression procedures

The recombinant protein MNEI was expressed using a protocol set up in my laboratory. Cells of *Escherichia coli* BL21 (DE3) were transformed with plasmid pET22b+ carrying the gene encoding for MNEI. Cells were cultured on LB/Agar with ampicillin 100 $mg \times L^{-1}$ and they were grown over night at 37 °C. Subsequently, the cells were grown in LB medium containing the same antibiotic, at 37 °C with stir. Protein expression was induced at 0.8 OD/mL by supplying lactose 5 mM and carried on at 25 °C for 20 hours. The cells were harvested by centrifugation (4 °C,

4000 x *g*, 20 min), washed with cold PBS 1x (NaCl 7.6 g/L, Na_2HPO_4 1.875 g/L, NaH_2PO_4 0.41 g/L) and stored frozen until protein extraction.

Purification procedures

To extract the protein, cells were re-suspended in cold sodium acetate 50 mM at pH 5.5 and lysed by sonication on ice with a Microson Ultrasonic Homogenizer XL2000 for 20' (30'' on-30'' off). The protein-containing supernatant was recovered by centrifugation (4 °C, 7500 x *g*, 25 min). Purification was achieved by a one-step Ion-Exchange Chromatography procedure: the cell lysate was applied to an anionic exchanger DEAE-Sepharose column (20 mL, GE Lifesciences) connected in series to a Macro-Prep High S cationic exchanger column (15 mL, Bio-Rad). The chromatography was monitored by UV absorbance at 280 nm. After loading the supernatant and washing the columns until to absorbance baseline, the recombinant protein was eluted from the Macro-Prep High S with NaCl 100 mM in sodium acetate 50 mM, pH 5.5. The protein containing fractions were pooled, desalted by Size Exclusion Chromatography on a Sephadex G-25 column (GE Lifesciences) and eluted with acetic acid 100 mM. The fractions containing the desalted protein were put togheter and subjected to freeze-drying. Purity was assessed by Coomassie stained SDS-PAG. Protein yield was estimated by UV absorbance at 280 nm using the ε (0.1%) of 1.41 and corresponds to 50 mg per liter of cultured cells in LB medium.

Final remarks

The two proteins selected as natural and artificial models are very useful systems for aggregation studies. Thanks to their wide aggregation propensity, they allowed to investigate the influence of chemical, genetic and physical agents.

RNase A is presented as a model to study the metalation of proteins. The interaction between RNase A and Pt drugs improves protein oligomerization. Pt oligomers are endowed with peculiar characteristics such us SDS resistance and prolonged stability in solution. These results might suggest alternative aggregation mechanisms different from the well-known domain swapping. Pt-drugs selected also affect the biological action of RNase A evaluated both as enzymatic activity in a standard assay and also as cytotoxicity on tumoral cells.This suggest that the Pt-drugs deeply influence the structure and the function pf the protein as explained by solving the crystallographic structure of the cisplatinated monomer and of the carboplatinated monomer adducts. Further investigation on dimers may allow obtain structural information on Pt-dependent dimerization.

RNase A is also presented as a helpful model to design new mutant with different structural features. The structural characterization of the mutant RNase A-Onc showed that shortening of the C-terminal hinge loop does not affect the global folding but can improve the aggregation propensity that, in this protein occurs spontaneously. Very likely, in this case 3D-DS is involved. Biophysical studies on dimers obtained in native conditions allow to characterise them and to compare their structures with the well-known swapped dimers.

In this thesis, the artificial model MNEI was also presented as a suitable system. It represents a very fascinating model to study the influence of several physicochemical factors. It has been proven that pH, temperature and ionic strength deeply influence MNEI solubility and the aggregation towards amyloid-like patterns. The aggregation mechanism is worth of investigation whit the aim to obtain ordered assemblies under controlled conditions or avoid their formation and preserve the native structural and functional elements.

Publications (include submitted and in preparation):

Picone D, Donnarumma F, Ferraro G, Russo Krauss I, Fagagnini A, Gotte G, Merlino A. Platinated oligomers of bovine pancreatic ribonuclease: structure and stability. J Inorg Biochem, 2015 May; 146:37- 43

Rega M.F, Di Monaco R, Leone S, Donnarumma F, Spadaccini R, Cavella S,Picone D. Design of sweet protein based sweeteners: hints from structure-function relationships. Food Chemistry, 2015 April;(173)1179- 1186

Fiorini C, Gotte G, Donnarumma F, Picone D, Donadelli M. Bovine seminal ribonuclease triggers Beclin1–mediated autophagic cell death in pancreatic cancer cells. Biochim Biophys Acta, 2014 May;1843(5)976-84

Picone D, Donnarumma F, Ferraro G, Gotte G, Fagagnini A, Butera G, Donadelli M and Merlino A. A comparison study on RNase A oligomerization induced by cisplatin, carboplatin and oxaliplatin. J Inorg Biochem submitted.

Pica A, Donnarumma F, Emendato A, Leone S, Rega MF, Di Girolamo R, Merlino A, Picone D; Structure and aggregation propensity of the super-sweet protein Y65R-MNEI, Manuscript in preparation

Attended congresses/workshops/summer schools/contribution:

June 12-14, 2014: 14th Naples Workshop on Bioactive Peptides. POSTER SECTION on Industrial Peptides : F. Donnarumma, M. F. Rega, R. Di Monaco, S. Cavella and D. Picone, "Design, production and characterization of new protein sweeteners.

October 6-10, 2014: 1st European Summer School on Industrial Biotechnology (Milan) – "Stability, Folding and Misfolding of Recombinant Proteins"

February, 11-15, 2017: Biophysical Society 61th Annual Meeting, New Orleans, USA. Poster communication: Sweeter and stronger: structure-driven molecular design to enhance sweetness and stability of the single chain monellin MNEI.